Study of Inter-Protein Electron Transfer as Rate-Limiting Steps in Microbial Electron Conduction

（バイオフィルムの電子伝導における律速段階としてのタンパク質間電子移動に関する研究）

A Thesis

Submitted by

Xinxin WEN

In fulfillment for the award of the degree of

Doctor of Science

Graduate School of Chemical Sciences and Engineering,

Hokkaido University

2026

Abstract

Microbial biofilm, particularly that formed by electroactive bacteria, facilitates long-distance electron transfer (LDET) across spatially heterogeneous environments, enabling key applications in bioenergy, bioelectronics, and pathogenesis. Although substantial progress has been made in characterizing the structural components of these biofilms, the mechanistic bottlenecks that constrain their electron conduction remain poorly understood. This dissertation systematically investigates the molecular, biophysical, and thermodynamic principles governing two principal conduction pathways, inter-cytochrome electron transfer and vesicle-mediated electron transport, in both model electroactive and pathogenic biofilms. Special emphasis is placed on the role of extracellular redox-active flavins, which dynamically shuttle electrons as redox cofactors to regulate conduction efficiency and pathway selection in diverse biofilm systems.

Chapter 1 provides an overview of the research background.

Chapter 2 investigated the mechanism of electron conduction in *Shewanella oneidensis* MR-1 (*S.* MR-1) biofilms, a model electroactive bacterium, with particular emphasis on interprotein electron transfer. While previous studies proposed that electron hopping between hemes 5 and 10 in the outer membrane cytochrome MtrC is the rate-limiting step, the strong intramolecular coupling between hemes suggests that interprotein interactions may constitute the true bottleneck. To test this hypothesis, temperature-dependent conduction currents were measured using IDE in both wild-type and mutant strains. Deletion of periplasmic cytochromes had little effect on activation energy (E_a), whereas deletion of omcA or mtrC led to a threefold increase in E_a, indicating that electron transfer between OmcA and MtrC is critical for efficient conduction. Additionally, the reduction of outer membrane fluidity significantly increased E_a, while inter-heme exciton coupling remained unchanged, highlighting the importance of protein diffusion. Notably, flavin binding suppressed heme-based

conduction but enhanced flavin-mediated currents, likely by obstructing key interprotein transfer sites at hemes 2 and 7. These findings establish interprotein electron transfer and flavin modulation as key determinants of biofilm electron conduction, laying a foundation for engineering high-performance bioelectronic materials.

Chapter 3 explored the role of pathogen-derived outer membrane vesicles (OMVs) in mediating electron transfer within the oral biofilm of *Porphyromonas gingivalis* (PG), aiming to translate the principles established in **Chapter 2** into a pathogenic context by investigating the conductive properties of PG biofilm. While OMVs are known to support bacterial survival by promoting biofilm formation, densely packed microbial communities often experience metabolic inhibition under reductive stress. Evidence showed that OMVs facilitate extracellular electron transfer, thereby sustaining metabolic activity in reductive biofilm environments. Using interdigitated electrodes with 10 μm spacing, a fivefold increase in conduction current (I_{cond}) was observed when biofilms were incubated with isolated OMVs. These vesicles were enriched in peptidylarginine deiminase (PPAD), an enzyme with citrullination activity. Genetic knockout or chemical inhibition of PPAD significantly reduced the I_{cond} enhancement, whereas supplementation with FMN, the cofactor of PPAD, further amplified the conductive response. Moreover, PPAD-containing OMVs markedly promoted biofilm formation on calcium phosphate discs, indicating that vesicle-mediated electron conduction is a key factor in pathogenic biofilm development. These findings reveal a novel electrochemical role for pathogenic OMVs and suggest new targets for anti-biofilm strategies.

Chapter 4 investigated the functional implications of redox-active biofilms in antibiotic resistance, building on the novel electrochemical role and mechanism of pathogenic OMVs identified in **Chapter 3** to explore new targets for anti-biofilm strategies focused on disrupting bioenergetic pathways. Redox-active OMVs were shown to contribute to antibiotic resistance in PG biofilms by maintaining redox

homeostasis under drug-induced stress. While traditional antibiotics were less effective against OMVs-rich biofilms, metabolic inhibitors such as nitazoxanide remained broadly effective, suggesting that targeting bioenergetic pathways can circumvent redox-based antibiotic tolerance.

Chapter 5 presents the overall conclusions and prospects based on this body of work.

Collectively, these findings establish flavins and redox proteins as key mediators of biofilm electron transfer, with broad implications for microbial respiration, pathogenicity, and therapeutic intervention.

Keywords: Electroactive biofilm, Interprotein electron transfer, Flavin, Biofilm electron conduction, Activation energy.

CONTENTS

Chapter 1. General introduction

1.1 Microbial electric biofilm

Biofilms are complex, structured communities of bacteria that adhere to surfaces and are embedded within a self-produced extracellular matrix (Sharma et al., 2019; Schulze et al., 2021). These structures are of considerable biological and clinical significance, as they confer enhanced resilience to environmental stresses and enable microorganisms to persist under adverse conditions. In the context of human health, biofilms are recognized as major contributors to the pathogenesis of persistent and chronic infections. It has been widely reported that up to 80% of chronic diseases are biofilm-associated, particularly in cases involving implanted medical devices such as urinary catheters, orthopedic prostheses, heart valves, and chronic wound beds (Costerton et al., 1999; Hall-Stoodley et al., 2004). Prominent pathogens such as *Pseudomonas aeruginosa* (*P. aeruginosa*) and *Staphylococcus aureus* (*S. aureus*) are frequently implicated in these scenarios, exhibiting elevated tolerance to antimicrobial agents and evasion of host immune defenses within the biofilm niche (Ricciardi et al., 2018; Thi et al., 2020). From an environmental and industrial standpoint, biofilms also present substantial challenges. Their formation on surfaces in water systems, pipelines, and industrial equipment is a major cause of biofouling, material corrosion, and biocontamination, which can lead to decreased operational efficiency and significant economic losses (Flemming et al., 2002; Waqas et al., 2023).

Notably, not all biofilm systems are inherently harmful. A subset of biofilms formed by electroactive bacteria, such as *Shewanella oneidensis* MR-1 (*S.* MR-1) and *Geobacter sulfurreducens* (*G. sulfurreducens*), display highly specialized mechanisms for extracellular electron transfer (EET) (Reguera et al., 2005; Pirbadian et al., 2014; Shi et al., 2016). These microorganisms can utilize insoluble metal oxides or electrodes as terminal electron acceptors in anaerobic respiration, offering promising applications in bio-electrochemical systems, including microbial fuel cells (MFCs) and environmental bioremediation technologies (Logan et al., 2006; Lovley, 2008). Such

duality, biofilms as both pathological agents and biotechnological tools, has positioned them at the forefront of interdisciplinary research spanning microbiology, materials science, and biomedical engineering.

Considering their biological complexity and broad relevance, this part aims to systematically review microbial biofilms from three interrelated perspectives: microbial biofilm formation process, microbial biofilm dangers, and cell survival strategy in microbial biofilms.

1.1.1 Microbial biofilm formation process

Microbial biofilms are highly organized, three-dimensional cellular aggregates that form at the interface between liquid and solid phases (Herrling et al., 2019). These structures are the result of a dynamic and regulated developmental process involving surface attachment, cell proliferation, extracellular matrix production, and spatial organization (Sharma et al., 2023). The formation of a biofilm confers upon microorganisms the ability to establish long-term colonization, resist environmental fluctuations, and maintain a stable population under hostile conditions (Hall-Stoodley et al., 2004). The biofilm developmental process is generally divided into five distinct but interconnected stages (**Figure 1.1**):

1) Free-floating cells

In the initial phase, planktonic (free-living) bacterial cells approach the surface through weak physicochemical forces, such as van der Waals interactions, electrostatic attraction, and hydrophobic effects. This stage is characterized by transient contact that can still be reversed. For instance, *P. aeruginosa* utilizes type IV pili and adhesion-related proteins such as PilY1 to initiate weak yet directed surface binding (Orans et al., 2010; Beaussart et al., 2014; Guo et al., 2024). This preliminary interaction allows bacteria to sense surface properties and initiate downstream signaling cascades.

2) Adhesion

Following surface sensing, bacterial cells transition to an irreversible attachment phase, often mediated by the secretion of extracellular polymeric substances (EPS) that

anchor the cells more firmly to the substrate. A classic example is *Staphylococcus epidermidis*, which produces polysaccharide intercellular adhesin to reinforce attachment and initiate quorum sensing signals, thereby establishing the foundation for multilayered biofilm growth (Mack et al., 1996; Vuong et al., 2004).

3) Aggregation

After stable attachment, bacterial cells undergo rapid proliferation and secrete structured EPS, resulting in the formation of three-dimensional microcolonies interspersed with fluid-filled channels. This stage is critical for nutrient diffusion and waste removal. Vibrio cholerae, for example, regulates spatial heterogeneity within biofilms through a quorum-sensing network that governs matrix composition and cellular differentiation (Hammer & Bassler, 2003).

4) Maturation

As the biofilm matures, it develops chemical and physical gradients, such as oxygen, pH, and nutrient levels, which drive the emergence of metabolically stratified subpopulations. Outer-layer cells tend to perform aerobic respiration, whereas cells embedded deeper in the biofilm often switch to anaerobic pathways using alternative electron acceptors such as nitrate or ferric iron (Okabe et al., 1996). These gradients contribute to the resilience and heterogeneity of mature biofilms.

5) Dispersion

In the final stage, a subset of biofilm-embedded cells reactivates motility-related pathways or expresses specific enzymes to degrade components of the EPS matrix, enabling dispersal to new environments. *Bacillus subtilis*, for example, employs a regulated, signal-mediated detachment system involving the production of biofilm-degrading enzymes to initiate group dispersal (Boyd & O'Toole, 2012).

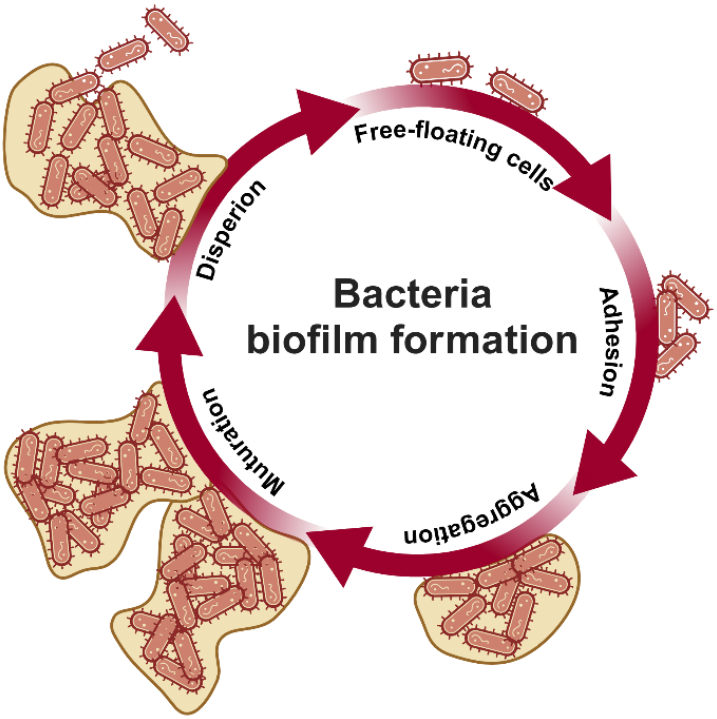

Figure 1.1. Developmental stages involved in microbial biofilm formation. the schematic illustration depicts the cyclic developmental stages of bacterial biofilm formation.

This progression from initial adhesion to eventual dispersion underscores the dynamic and adaptive nature of microbial biofilms. These characteristics are particularly pronounced in electrochemically active biofilms (EABs), which are specialized for electron transfer to solid-state acceptors. A representative model is *S.* MR-1, which forms biofilms on electrode surfaces or metal oxides. This species utilizes a multi-heme outer membrane cytochrome complex (e.g., MtrCAB) to export electrons across the cell envelope to external acceptors, thus thriving in redox-limited and anaerobic environments (Marsili et al., 2008; Pirbadian et al., 2014; Shi et al., 2016). Recent research has demonstrated that modular regulation of biofilm development at each stage, ranging from surface interaction to structural maturation, can significantly enhance both biofilm robustness and electron transfer efficiency. For example, Li et al., (2023) reported a bioengineered *S.* MR-1 strain that achieved a maximum power output

of 3.62 W/m², the highest reported to date for this species. This was accomplished through synthetic manipulation of cellular hydrophobicity, extracellular DNA accumulation, elevation of intracellular c-di-GMP levels, and heterologous expression of outer membrane cytochromes and electron shuttle biosynthesis genes. Additionally, integration of nanomaterials such as graphene oxide and carbon nanotubes enabled the construction of a three-dimensional artificial conductive network. This work provides a strategic framework for improving the performance of biofilms in energy conversion and bioelectronic applications (**Figure 1.2**).

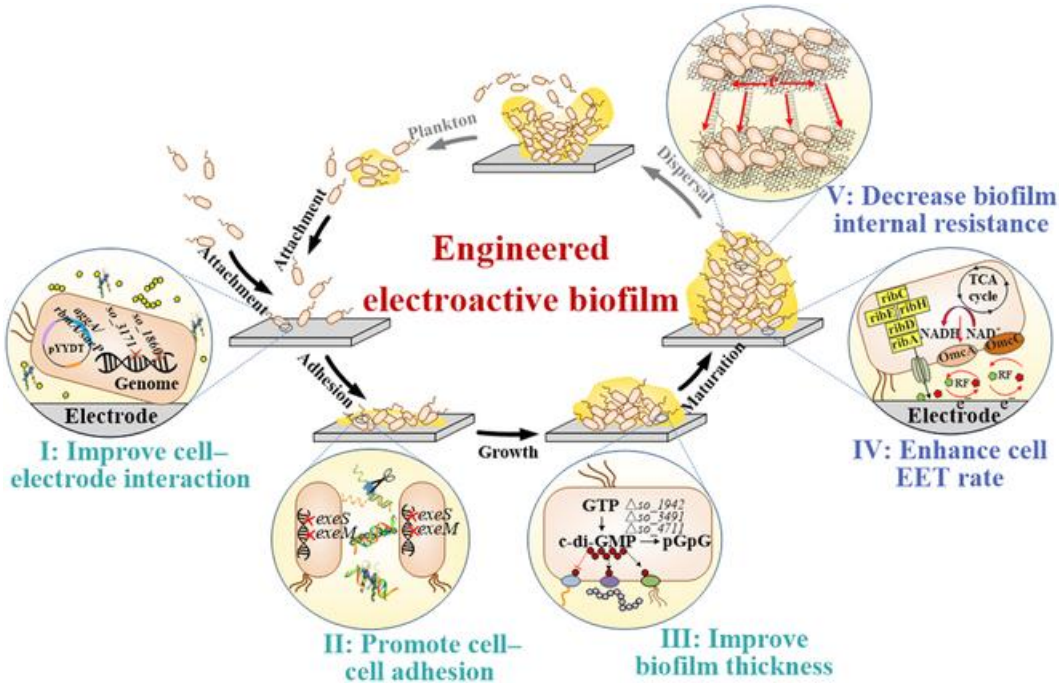

Figure 1.2. Schematic illustration of stage-specific biofilm engineering to enhance structural development and electron conductivity in *Shewanella oneidensis MR-1* (*S. MR-1*) (Li et al., 2023).

1.1.2 Microbial biofilm dangers

Microbial biofilms are ubiquitous in natural ecosystems, the human microbiota, and various industrial infrastructures. While their structural stability and metabolic versatility enable microorganisms to adapt to diverse environments, these features pose

significant threats to human health and engineered systems. The major categories of biofilm-associated risks are outlined below (**Figure 1.3**):

1) Pathogenic threats

Polymicrobial biofilms formed by anaerobic pathogens such as *Porphyromonas gingivalis* (PG) and *Fusobacterium nucleatum* (FUSO) play a central role in the etiology of periodontitis, systemic inflammatory responses, and have been increasingly linked to the progression of some cancers (Kostic et al., 2013; Gallimidi et al., 2015; Wang et al., 2024). These organisms utilize heme acquisition systems and putative EET pathways to sustain anaerobic respiration within the biofilm matrix. Recent findings suggest that such biofilms may exhibit electroactive behavior, contributing to redox homeostasis and interspecies interactions (Naradasu et al., 2020 and 2022). These properties not only enhance microbial survival but may also facilitate tissue invasion and immune evasion.

2) Clinical infections and antibiotic resistance

In healthcare settings, *P. aeruginosa* is a well-documented opportunistic pathogen known for forming resilient biofilms on the respiratory tract and the surfaces of medical devices such as endotracheal tubes, catheters, and stents. Biofilm-embedded cells exhibit markedly increased resistance to antibiotics, largely due to the presence of dormant "persister" subpopulations and the protective extracellular matrix (Mah et al., 2003; Høiby et al., 2015; Sultana et al., 2016). Furthermore, exposure to sub-inhibitory concentrations of antibiotics has been shown to upregulate genes associated with redox balance and potential conductive pathways, indicating a capacity for redox regulation within *P. aeruginosa* biofilms (Soares et al., 2020; Ciemniecki et al., 2024). Such findings suggest that microbial biofilms may dynamically respond to pharmacological pressure by modulating metabolic and electron transport activities.

3) Industrial and environmental corrosion

In engineered systems, EABs formed by bacteria such as *S.* MR-1 and *Desulfovibrio desulfuricans* are exploited in applications including wastewater treatment, MFCs, and

bioremediation due to their EET capabilities (Lovley, 2006b). However, these same electrochemical properties can lead to microbially influenced corrosion of metallic surfaces, including pipelines, electrodes, and marine infrastructure (Little et al., 2020). This form of corrosion is driven by the localized redox reactions mediated by biofilm-associated microorganisms, leading to material degradation and reduced system lifespan (Deng et al., 2015 and 2018). The duality of EABs, offering both technological utility and infrastructure risk, demands careful design and monitoring in industrial contexts.

Given the numerous dangers associated with biofilm formation, understanding the survival strategies and underlying mechanisms of cells within biofilms is essential for developing effective approaches to disrupt and mitigate biofilm-related infection and pollution.

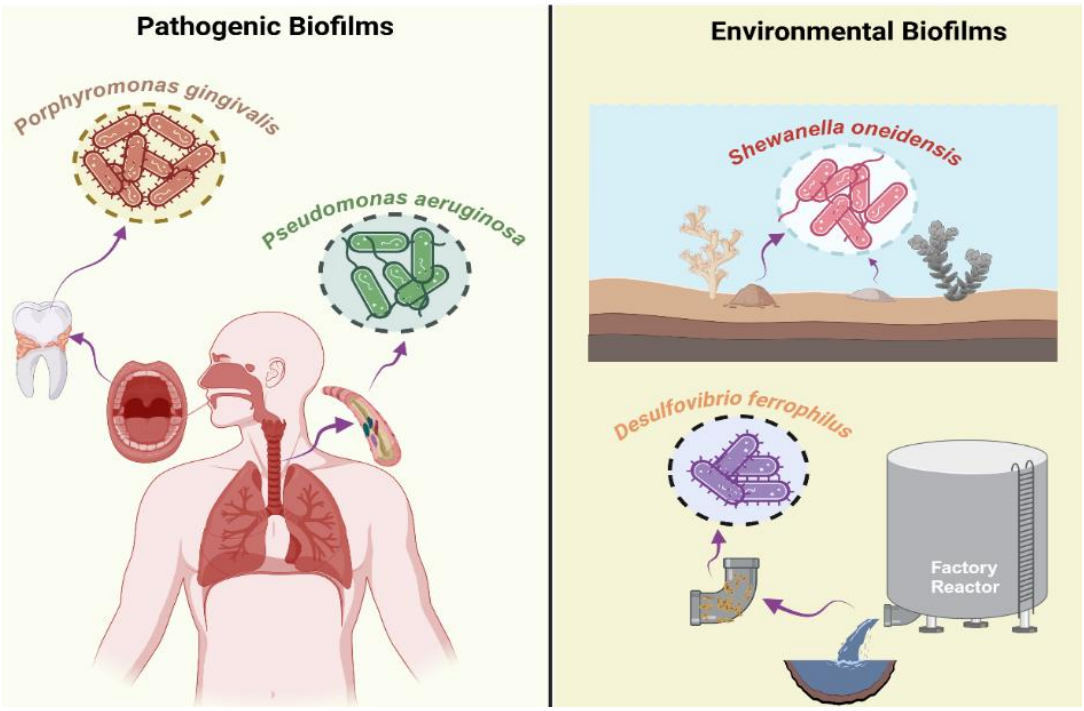

Figure 1.3. Representative electroactive microbial species involved in pathogenic and environmental biofilm formation. Pathogenic biofilms include *Porphyromonas gingivalis* (PG), commonly associated with oral infections, and *Pseudomonas aeruginosa*, linked to respiratory tract infections. Environmental biofilms feature electroactive bacteria such as *S.* MR-1, found in marine sediments, and *Desulfovibrio*

ferrophilus, often present in industrial settings such as factory reactors and pipelines.

1.2 Long-distance electron transfer (LDET)

1.2.1 Cell survival strategy in microbial biofilm

To sustain energy homeostasis under adverse environmental conditions, such as anoxia, electron acceptor scarcity, or metal-enriched niches, microorganisms have evolved specialized metabolic adaptations. Among these, EET is a pivotal mechanism that enables cells to discharge electrons from intracellular respiratory chains to external, non-traditional electron acceptors, including oxidized metal species or abiotic electrode surfaces (Lovley, 2006a). This process not only ensures continuity of respiration under redox-limited conditions but also fundamentally restructures intercellular energy interactions, facilitating cooperative metabolic networks within the biofilm (**Figure 1.4**).

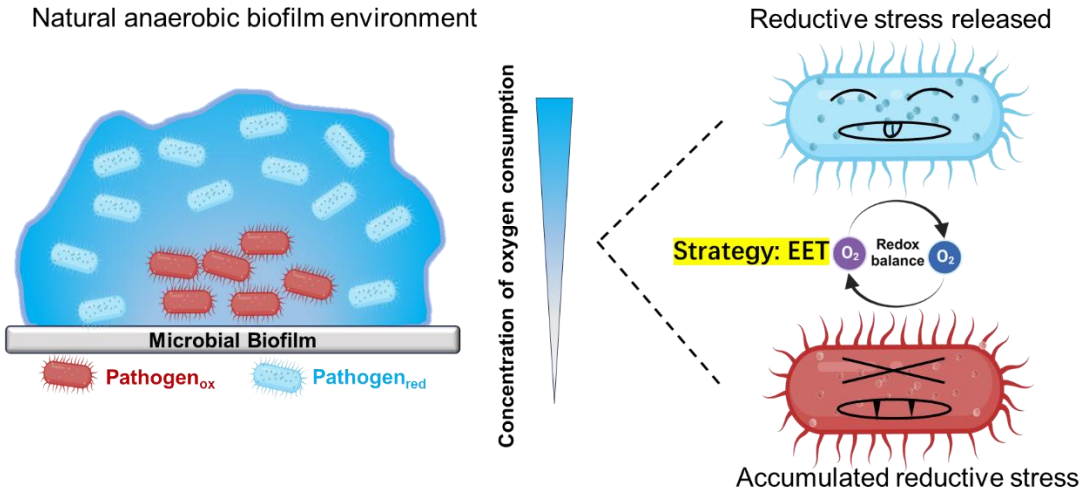

Figure 1.4. Oxygen gradient-driven metabolic differentiation within microbial biofilms. An oxygen concentration gradient across the biofilm leads to spatial metabolic differentiation among microbial populations. Surface-associated cell utilizes oxygen for aerobic respiration, while deeper-layer cell encounters oxygen limitation and adapt by employing extracellular electron transfer (EET) strategies to maintain energy production.

Emerging studies have revealed that certain microbial biofilms can support not only short-range electron exchange between neighboring cells but also long-distance electron transfer (LDET) across tens to hundreds of micrometers. This capacity is underpinned by the construction of transcellular conductive networks, which serve as biological equivalents to electrical circuits. Three primary mechanisms have been identified as contributors to LDET: Multi-heme cytochromes, often arrayed along outer membranes or periplasmic extensions, enable stepwise electron hopping across redox centers spanning multiple cells (**Figure 1.5. A**) (Reguera et al., 2005; Lovley, 2006a; Dahl et al., 2022). Conductive pili or protein nanowires enriched in aromatic residues facilitate electron delocalization via π-π stacking interactions, forming quasi-metallic conduction pathways analogous to organic semiconductors (**Figure 1.5. B**) (Malvankar et al., 2011). Diffusible redox mediators, such as flavin mononucleotide (FMN) or anthraquinone-2,6-disulfonate (AQDS), shuttle electrons through the extracellular matrix, enabling dynamic electron exchange across distant cells or species boundaries (**Figure 1.5. C**) (Newman & Kolter, 2000; Marsili et al., 2008; Von Canstein et al., 2008; Glasser et al., 2017)

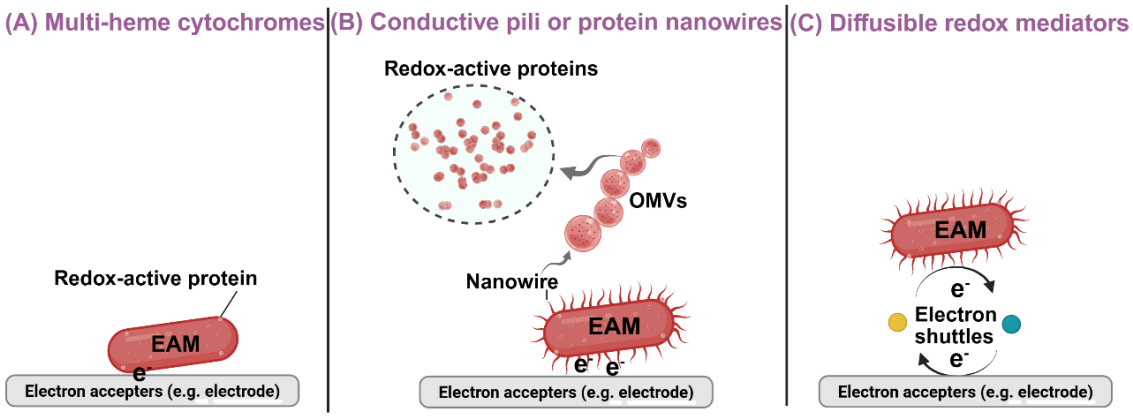

Figure 1.5. Representative mechanisms of LDET utilized by EAMs: (A) Multi-heme cytochrome-mediated direct electron transfer; (B) Conductive pili or protein nanowire-based long-range conduction; (C) Electron shuttling via diffusible redox mediators.

Collectively, these strategies reflect an evolutionary solution to metabolic challenges in redox-restricted environments. Beyond environmental electron transfer, LDET is increasingly recognized as a functional component of pathogenic biofilms, where it may contribute to oxidative stress resistance, interspecies metabolic cooperation, and persistence under immune pressure or antibiotic exposure. As the field advances, investigations have begun to focus on elucidating the structural, thermodynamic, and ecological foundations of LDET in electrochemically active biofilms. Such studies not only deepen our understanding of microbial energy metabolism but also provide a theoretical framework for exploring electron-sharing conduits in complex microbial communities, with implications for both microbial ecology and bioelectronic engineering.

1.2.2 LDET process

In both natural ecosystems and human-engineered environments, microorganisms frequently colonize interfacial habitats, where they optimize energy acquisition through the formation of biofilms. These biofilms are highly organized microbial consortia embedded within a self-produced extracellular matrix, typically adhering to solid or liquid-solid interfaces. They are characterized by pronounced spatial heterogeneity in metabolic activity, nutrient availability, and redox potential (Stewart & Franklin, 2008). High-resolution microelectrode analyses have revealed steep oxygen gradients within biofilms: while the dissolved oxygen concentration at the biofilm interface (0-50 μm) may reach up to 200 mM, it rapidly declines to less than 5 mM at depths beyond 100 μm, establishing distinct anaerobic microenvironments (Okabe et al., 1999). These sharp physicochemical gradients impose significant constraints on microbial respiration, necessitating the evolution of electron transfer mechanisms capable of bridging spatially separated redox zones (**Figure 1.6**).

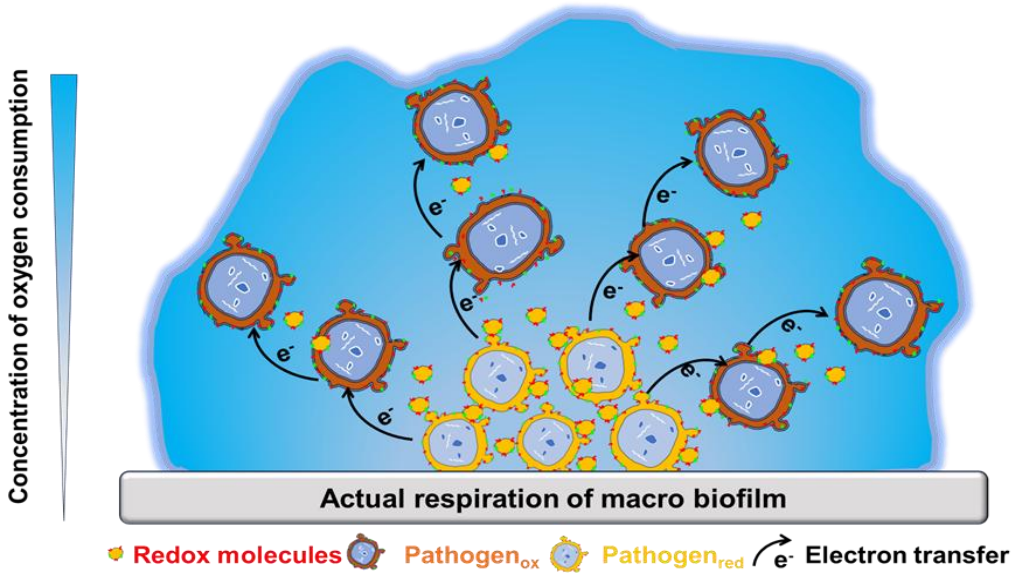

Figure 1.6. Redox gradient-driven LDET in microbial biofilm

LDET has emerged as a pivotal strategy enabling microbes to overcome such challenges. LDET encompasses a suite of mechanisms including the production of

conductive pili, the organization of outer membrane cytochrome networks, and the secretion of soluble redox mediators, that collectively facilitate electron transport from cells in deep anoxic layers to terminal electron acceptors located at or near the biofilm surface, such as oxygen, ferric iron (Fe^{3+}), or solid-state electrodes (Shi et al., 2016; Lovley, 2017). In *G. sulfurreducens*, for instance, cells located in the basal regions of the biofilm utilize conductive pili to relay electrons upward toward surface oxygen (Malvankar et al., 2014).

The distinctiveness of LDET lies in its multiscale integration of electron flow. At the nanometer scale, electron transfer between heme centers can proceed via quantum tunneling when their separation is within 2 nm (Page et al., 1999; Gray & Winkler, 2005; Winkler & Gray, 2015). At the micrometer scale, protein-based conductive networks enable electron propagation over distances of several hundred microns. This spatial coordination of redox activity not only underpins microbial survival under redox-stratified conditions but also represents a fundamental biophysical framework for cooperative metabolism in multicellular microbial communities (Pfeffer et al., 2012; Kato, 2015). Hence, LDET is not merely a metabolic adaptation, it is integral to the ecological success and biotechnological potential of electroactive microorganisms.

1.2.3 Molecular mechanism for LDET

Microbial biofilms are highly organized multicellular systems capable of sustaining efficient LDET, a feature crucial for maintaining redox homeostasis and energy metabolism across spatially stratified environments. This ability is primarily attributed to the development of diverse electron conduction architectures, enabling millimeter-scale electron transport across extracellular space. Representative electroactive bacteria, such as *S.* MR-1 and *G. sulfurreducens*, have evolved multiple strategies to overcome the intrinsic electronic barriers between intracellular donors and distant extracellular acceptors. These mechanisms encompass outer membrane-integrated multiheme cytochrome complexes, conductive protein nanostructures, and redox mediator-facilitated shuttle systems, together reflecting a high degree of structural and functional

coupling across biological and physical scales (**Figure 1.7**).

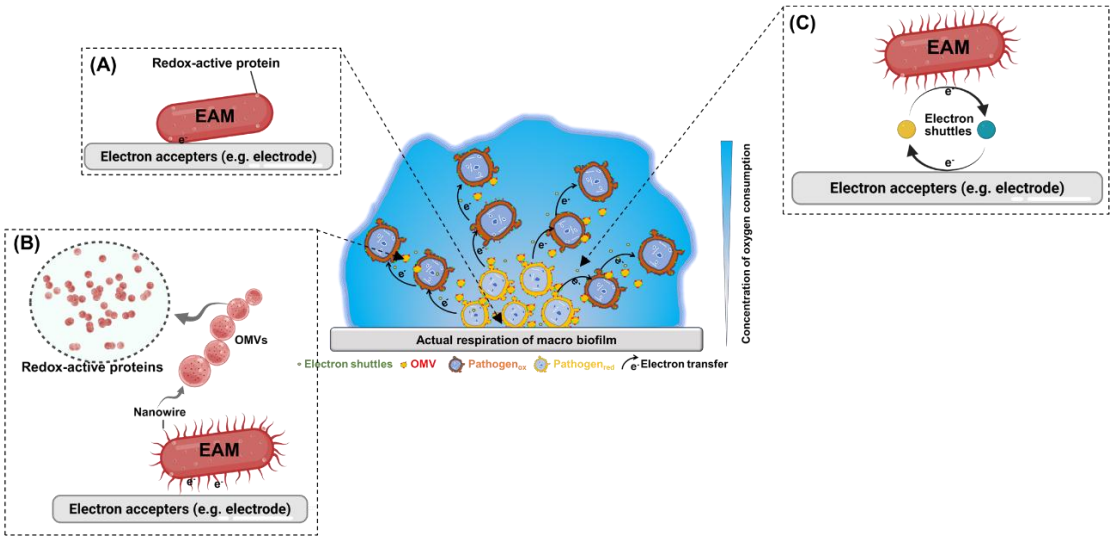

Figure 1.7. Microbial ecological mechanisms underlying LDET. Electroactive microorganisms within biofilms facilitate LDET by transferring electrons from inner, metabolically active cells to distant external electron acceptors such as electrodes. In a stratified biofilm, pathogens in oxygen-depleted zones utilize conductive extracellular structures or redox mediators to relay electrons outward, enabling collective respiration across spatially separated regions. This ecological cooperation supports sustained energy metabolism under redox-limited conditions.

1) Outer membrane cytochromes

In *S.* MR-1, transmembrane electron flow is primarily mediated by the MtrCAB complex, a tripartite assembly composed of the outer membrane cytochrome MtrC (10 hemes), the periplasmic cytochrome MtrA (10 hemes), and the β-barrel membrane protein MtrB (Richardson et al., 2012). This complex forms a contiguous electron orbital chain (Firer-Sherwood et al., 2008), in which electrons are transferred via stepwise hopping through closely spaced heme centers (~1.3 nm apart), consistent with Marcus theory for electron tunneling (El-Naggar et al., 2010; Edwards et al., 2018). These properties confer high adaptability and robustness to the electron transfer system in fluctuating environmental conditions.

2) Nanostructured protein conductors

Beyond membrane-associated complexes, certain metal-reducing bacteria utilize conductive nanostructures for extended-range electron conduction. Recent studies have demonstrated that *G. sulfurreducens.* Employs conductive pili (also known as e-pili), assembled from polymerized PilA protein subunits, to facilitate LDET beyond membrane-bound cytochrome systems. These pili exhibit exceptional electrical conductivity, with values reaching up to 5000 $S \cdot m^{-1}$, comparable to synthetic organic conductors (Shu et al., 2019). Structural and mutagenesis analyses have revealed that conserved aromatic residues, particularly tyrosine, such as Y32 and Y57, are axially aligned within the pilus filament, enabling π-π stacking interactions. This arrangement supports delocalized electron transport via a quasi-metallic π-electron cloud, forming a molecular wire architecture (Vargas et al., 2013; Shu et al., 2019). Although direct visualization of ~1.2 nm-spaced periodic positive charges remains elusive, cryo-electron microscopy and scanning probe studies have uncovered a helical structural organization of PilA monomers that correlates with thermally activated electron conduction and low activation energy barriers (Malvankar et al., 2015; Lampa-Pastirk et al., 2016). These findings underscore the significance of protein-based nanowires in microbial electron transport and suggest a critical role of aromatic amino acid composition and spatial arrangement in modulating pili conductivity.

In contrast, *S.* MR-1 produces nanowire-like structures not through PilA-based pili, but rather via the self-assembly of outer membrane cytochromes, including MtrC and OmcA. Although these structures exhibit electron-conductive properties, their conductivity appears to stem primarily from heme-heme coupling rather than through-protein backbone conduction (Pirbadian et al., 2014). Advanced imaging techniques such as cryo-electron tomography and photoelectron microscopy have demonstrated that the structural organization of these protein nanowires is dynamically regulated under oxidative stress or low-electron-acceptor conditions, maintaining redox balance within the biofilm matrix (El-Naggar et al., 2010; Subramanian et al., 2018).

3) Redox mediator

Redox mediator molecules play an essential role in facilitating electron transport over distances beyond the reach of physical conductive structures. In *S.* MR-1, secreted flavin derivatives such as FMN and flavin adenine dinucleotide (FAD) can form reversible coordination complexes with multiheme cytochromes like MtrC, thereby enhancing EET efficiency (Okamoto et al., 2013; Xu et al., 2016). Spectroscopic studies have confirmed directional non-covalent interactions between flavins and the iron centers of heme groups, which stabilize transient electron pathways and reduce energetic loss during redox transitions (Okamoto et al., 2013). In *G. sulfurreducens*, extracellular cytochromes such as OmcZ form conductive polymer-like filaments that integrate with pili to create a three-dimensional electron conduction network. This hierarchical system not only expands the effective conduction distance but also enhances the structural and metabolic resilience of the biofilm under environmental stress (Wang et al., 2019). Recent findings from *Desulfovibrio varians* GY32 have extended the phylogenetic distribution of LDET mechanisms, revealing the presence of 8 nm wide conductive filaments composed of phenylalanine-rich MtrA homologs with graphene-like electronic properties (Guo et al., 2024). These discoveries open new avenues for the design of biomolecular materials and redefine the evolutionary boundaries of microbial electron transfer capabilities.

In summary, LDET in bio-membranes is a multi-mechanism process achieved through the synergistic action of outer membrane cytochromes, conductive nanostructures, and soluble small molecules. These conduction pathways may be highly heterogeneous in bio-membranes of different species, environments, and developmental stages, and further analysis is urgently needed by combining structural biology, electrochemistry, and in vivo imaging techniques.

1.2.4 Applied perspectives for microbial LDET

1.3.1 Microbial fuel cells applications

Beyond its ecological relevance, LDET also holds considerable promise in

applications related to energy conversion and antimicrobial intervention. In MFCs, the upper limit of current density is fundamentally constrained by the efficiency of electron transport within biofilms (Malvankar et al., 2012). Genetic engineering approaches such as structure-guided mutagenesis and directed evolution have been employed to enhance the conductivity of microbial pili study has obtained a variant strain of *G. sulfurreducens* KN400, through selective cultivation. The current and power density of this strain in MFCs are significantly higher than those of the wild type. The enhanced current generation ability of KN400 is related to its higher conductivity and lower internal resistance, indicating that genetic engineering can improve the electron transfer efficiency of microorganisms, thereby improving the performance of MFCs (Yi et al., 2009).

1.3.2 Antimicrobial application

In the context of clinical biofilm-associated infections, EET has been increasingly recognized as a contributing factor to bacterial resistance against antimicrobial agents. For instance, in *P. aeruginosa*, components of the aerobic respiratory chain, including NADH dehydrogenases and flavodoxins, facilitate intracellular NADH oxidation, thereby attenuating reactive oxygen species (ROS) accumulation induced by antibiotics such as ciprofloxacin. This modulation of redox metabolism has been shown to enhance oxidative stress resistance and promote cellular survival (Moyano et al., 2014). *P. aeruginosa* is a gram-negative bacterium that causes serious infections clinically due to its complex antibiotic resistance mechanisms and biofilm-forming ability. The oxygen-terminated EET may enhance the resistance of biofilms to environmental stress, including antibiotic stress (Tokunou et al., 2022). The electron transport systems in its biofilm, such as outer membrane cytochromes, help maintain the cellular redox balance and reduce antibiotic-induced oxidative stress, thereby enhancing its resistance.

MRSA's ability to form biofilms makes it more challenging in clinical infections. Studies have shown that the biofilm structure of MRSA is closely related to its antibiotic resistance. For example, the resistance of MRSA to vancomycin in invasive

diseases in children emphasizes the role of exopolysaccharides in resistance (Pardo et al., 2024). The exopolysaccharide and protein network in MRSA biofilms may enhance its structural stability through electron transport mechanisms and hinder the penetration of antibiotics. Emerging evidence suggests that electron transfer processes within the biofilm matrix may influence its physical properties, thereby modulating antibiotic diffusivity. Moreover, using multiple particle tracking demonstrated the power of MPT to quantify changes in the diffusion behavior of tracer particles within AMR biofilms before and after antibiotic treatment (Powell et al., 2021).

Their findings revealed that antimicrobial exposure not only reduced the mobility of particles but also increased the stiffness of the EPS network, highlighting the dynamic interplay between antibiotic stress, biofilm mechanics, and transport properties.

1.3.3 Nanomaterial-based disruption of LDET for antimicrobial applications

Targeting LDET pathways has therefore emerged as a promising strategy in antimicrobial therapy. For example, Nanomaterials, particularly Fe_3O_4-based composites, have demonstrated synergistic antibacterial effects when used in conjunction with conventional antibiotics. Fe_3O_4@Ag nanocomposites can significantly enhance the antibacterial effect when used in combination with traditional antibiotics. The developed ciprofloxacin-loaded silver nanoparticles showed significant synergistic effects against multidrug-resistant strains such as Staphylococcus aureus and Escherichia coli, with an inhibition zone diameter of up to 34 mm, which exceeded the effect of using silver nanoparticles or ciprofloxacin alone. (Laib et al., 2025). In addition, T Graphene quantum dots (GQDs) can interact with aromatic residues in proteins and nucleic acids due to their unique electronic structure and π–π stacking ability, thereby regulating their structure and functional state. GQDs can induce cascade apoptosis of trypanosomes by interacting with antioxidant-related proteins, indicating that GQDs have potential in regulating the electronic environment of biomacromolecules (Xie et al., 2022). This lays the conceptual groundwork for the rational design of LDET-inhibiting nonintervention tools.

These studies provide mechanistic insights into the red oxygen-based antibacterial strategy and lay a conceptual foundation for designing non-interventional tools targeting LDET. By using nanomaterials to regulate the electron transport pathways of bacteria, it is expected that new antibacterial treatments will be developed to overcome the resistance challenges faced by traditional antibiotics.

1.3 Biofilm electron conduction

In electroactive biofilms, Electric biofilm conduction serves as a fundamental physical indicator of the efficiency of LDET. The ability of microorganisms to transport electrons over micron to millimeter scales varies substantially among species, reflecting diverse structural and biochemical adaptations (Ding et al., 2016). For instance, biofilms formed by *G. sulfurreducens.* Exhibit conductivities up to approximately 5,000 $\mu S \cdot cm^{-1}$, whereas *S.* MR-1 biofilms range between 10-100 $\mu S \cdot cm^{-1}$. In contrast, anaerobic granular sludge biofilms typically show values in the tens of $\mu S \cdot cm^{-1}$ (Malvankar et al., 2011; Snider et al., 2012). These differences, spanning several orders of magnitude, underscore the significance of conductivity as both a mechanistic marker and a performance-limiting parameter in microbial electrochemical systems. Biofilm conductivity arises from a combination of mechanisms, including: (i) redox cycling by small, diffusible electron shuttles such as flavins and quinones, and (ii) structural electron transport through extracellular conductive appendages, including multiheme cytochrome networks and microbial nanowires. The arrangement of redox-active centers, the density and spatial organization of conductive biomolecules, and external conditions, such as pH, ionic strength, and temperature, all strongly influence conductivity across the biofilm matrix (Okamoto et al., 2014).

1.3.1 Configuration of interdigitated electrode (IDE)

Interdigitated electrode (IDE) provides a high-resolution, non-destructive method for assessing the lateral conductivity of biofilms (Ding et al., 2016). A typical IDE consists of 130 parallel gold electrode fingers (2 mm × 10 μm × 90 nm) patterned onto a glass substrate, with an inter-finger spacing of 10 μm. The electrodes are grouped into two interleaved sets, source and drain, each containing 65 fingers. The total inter-electrode path length is 25.8 cm, the total electrode area is 0.026 cm², while the total biofilm coverage area is 0.039 cm² (**Figure 1.8**). This configuration allows for highly sensitive detection of in-plane current flow under controlled electrochemical conditions.

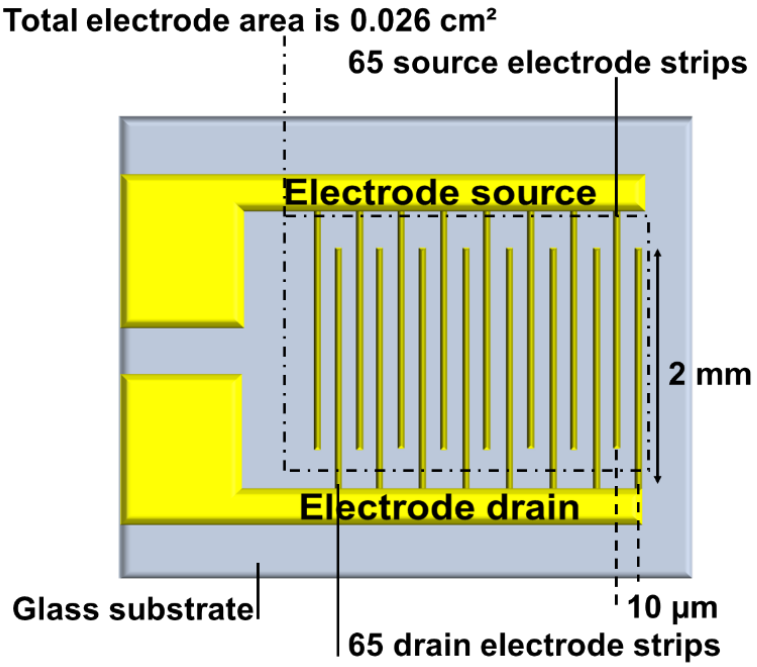

Figure 1.8. Configuration of an interdigitated electrode (IDE) for biofilm electron conduction measurement.

1.3.2 Electrochemical setup and gating measurement on IDE

For conductivity measurements, the IDE is incorporated into a single-chamber electrochemical cell. A platinum wire serves as the counter electrode, and a saturated Ag/AgCl (3 M KCl) electrode is used as the reference. The system contains 4.5 mL of defined growth medium. Dissolved oxygen is removed by bubbling N_2/CO_2 gas for 30 minutes. A low scan rate (1 mV·s^{1}) and a fixed source–drain potential difference (E_{SD} = 0.02 V) are applied, and the resulting current difference (I_{cond}) is recorded to quantify lateral electron transport.

Electrochemical gating measurement (EGM) is further employed to modulate the redox environment across the electrodes and probe the responsiveness of the biofilm. In single-electrode EGM, the IDE is polarized at E_{SD} = 0 V during biofilm growth. In dual-electrode EGM, after biofilm maturation, a small potential difference is applied (E_{SD} = 0.02 V), and the synchronized current response is measured to isolate conduction-dependent signals (**Figure 1.9**).

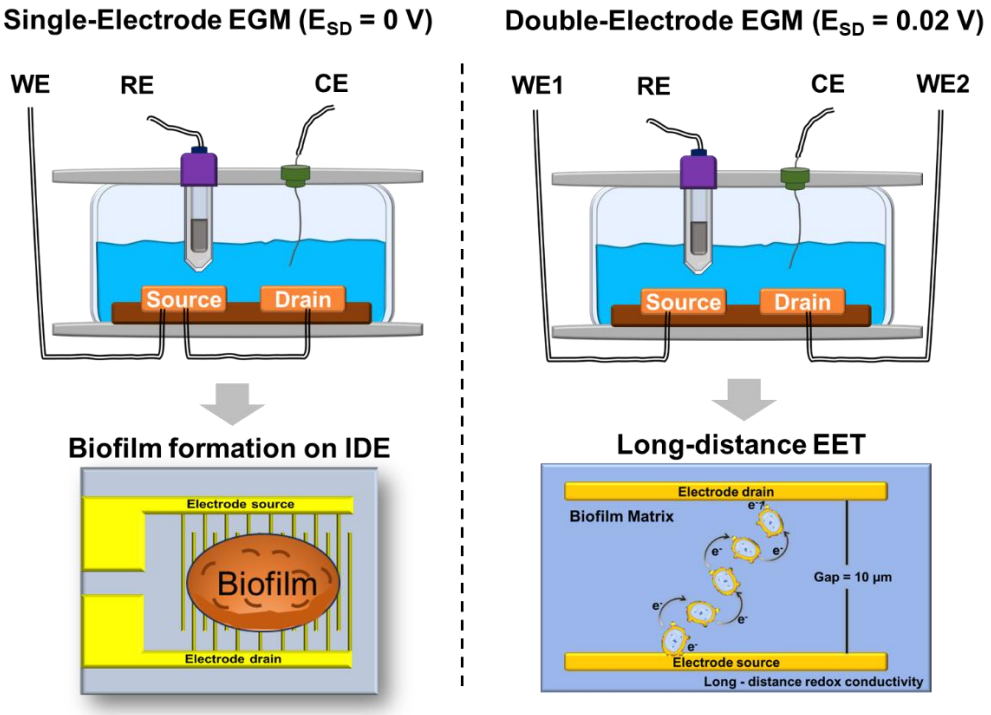

Figure 1.9. Electrochemical gating measurement of biofilm electron conduction using an IDE array. Left: IDE-based single-chamber electrochemical system for biofilm

growth. Right: an IDE-based double-chamber electrochemical system for electron conduction analysis and schematic representation of LDET between microbial cells across the 10 μm electrode gap.

1.3.3 Biofilm electron conduction current

The measured current (I_{total}) includes three components:

$$I_{total} = I_{redox} + I_{catalytic} + I_{cond} \quad (1)$$

- I_{redox}: arising from redox-active species at the interface.
- $I_{catalytic}$: due to metabolic oxidation of electron donors.
- I_{cond}: attributed to the true electronic conductivity of the biofilm matrix.

To extract I_{cond}, the method proposed by (Xu et al., 2018) is employed. The current at E_{SD} = 0 V (baseline) is subtracted from that at E_{SD} = 0.02 V (**Figure 1.10**), yielding:

$$I_{cond} = (I_{drain} - I_{source})/2 \quad (2)$$

This single-scan background subtraction minimizes biofilm disturbance and ensures accurate conductivity estimation.

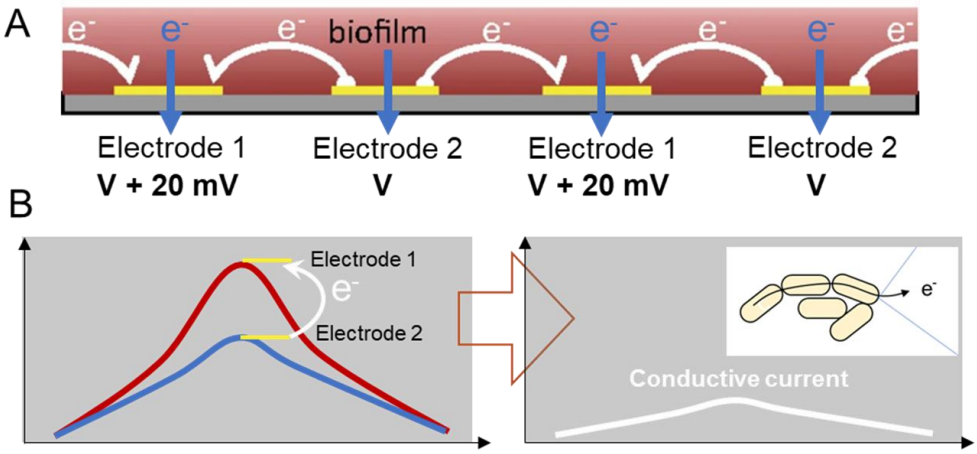

Figure 1.10. (A) Schematic cross-sectional view of a biofilm-coated IDE, illustrating electron transport across the biofilm. Adapted from the design by Snider, R. M. (2012). (B) Representative plots of source current, drain current, and calculated conductive

current derived from dual-electrode measurements, reflecting biofilm-mediated electron conduction.

1.4 Thermodynamic mechanism of LDET

1.4.1 Activation energy (E_a)

In electroactive microbial biofilms, LDET involves the movement of electrons from intracellular donors to extracellular acceptors through structurally and chemically diverse pathways. These pathways include quantum tunneling, thermally activated hopping, mediated electron transfer, and metal-like conduction. Studies have shown that electron transport in *G. sulfurreducens.* Biofilm is a thermally activated process with an activation energy of about 0.2 eV (about 19.3 kJ/mol). This suggests that electron transport occurs primarily through a thermally activated hopping mechanism (Yates et al., 2016). A crucial parameter for distinguishing between these mechanisms is the activation energy (E_a), which reflects the energy barrier that electrons must overcome during conduction. As a thermodynamic descriptor, E_a provides critical insight into the nature of the electron transport process. By measuring the temperature dependence of biofilm electron conduction or electron flux and applying the Arrhenius model, researchers can extract the apparent activation energy of the system. This parameter not only reveals the fundamental nature of the conduction mechanism but also allows comparative analysis across microbial species, genetic mutants, redox mediators, and environmental conditions, offering actionable guidance for optimizing bio-electrochemical systems and synthetic bioelectronics.

1.4.2 Arrhenius model

The rate of electron migration in the microbial conductive network is closely related to the ambient temperature. Under ideal conditions, the electron conduction behavior can be approximately obeyed by the Arrhenius thermodynamic model, and its mathematical expression is as follows (Xu et al., 2018):

$$\ln (I_{cond}) = A - 1000/T \times (E_a/1000k) \qquad (3)$$

Where A was the pre-exponential factor, T was absolute temperature (K), and k was the Boltzmann constant.

In practice, researchers usually use IDEs to record transverse electron currents at multiple temperature points and perform a logarithmic transformation (ln σ) to fit the relationship between ln (I_{cond}) and 1000/T by linear regression. The slope of the straight line is, and E_a is obtained. In contrast, other non-Arrhenius behaviors (such as variable range transitions, Coulomb blockade, and band deformation) may also occur in some proteins or disordered conductors. However, in most bacterial conductive systems, the Arrhenius model has been widely verified as the main thermodynamic framework for estimating electron migration processes (Malvankar et al., 2011). In addition, by analyzing the linearity of the temperature response curve of conductivity (R^2 value), it can also help determine whether the electron migration path is dominated by a single mechanism.

1.4.3 Application in E_a

Activation energy analysis, grounded in the Arrhenius model, serves as a critical thermodynamic framework for dissecting microbial electron transfer mechanisms (Xu et al., 2018). It enables the identification of conduction modes, the evaluation of mutant phenotypes, and the optimization of synthetic bioelectronic designs. As instrument resolution and environmental control improve, E_a will become a core performance metric in biofilm electrochemistry, energy bioconversion, and redox-driven microbial technologies.

1.5 Outline of the thesis

This dissertation is structured into five chapters, each contributing to a comprehensive and systematic investigation of microbial LDET within biofilm environments. The central objective of this work is to elucidate the roles of membrane-associated cytochromes, outer membrane extension complexes and electron shuttles in mediating LDET, and to assess how these elements mutually influence biofilm conductivity, structural integrity, and functional adaptability. Through mechanistic analyses in model electroactive bacteria and translational perspectives on pathogenic biofilms, this thesis aims to establish a foundational understanding that informs the development of both advanced bioelectronic systems and innovative antimicrobial strategies.

Chapter 1 provides the theoretical foundation and contextual background for the subsequent chapters. It introduces the concept of electron conduction in microbial biofilms, with a particular focus on LDET pathways mediated by multiheme c-type cytochromes embedded in the outer membrane, extended membrane-derived structures (such as nanowires and vesicles), and diffusible redox mediators, including flavins and quinones (Reguera et al., 2005; Okamoto et al., 2013). The structural architecture of electroactive biofilms is described in detail, emphasizing the spatial arrangement of redox centers and the critical role of percolation pathways in facilitating efficient electron transport over micrometer-scale distances (Malvankar et al., 2011; Yates et al., 2016). This chapter also contextualizes microbial LDET within broader biomedical and bioengineering frameworks. This includes its application in enhancing power output in MFCs, its influence on redox signaling and antibiotic tolerance in chronic biofilm-associated infections, and its potential as a therapeutic target for anti-biofilm interventions (PYi et al., 2009; Owell et al., 2021). In addition, the concept of E_a is introduced as a thermodynamic parameter for evaluating electron transfer kinetics. By quantifying the temperature dependence of biofilm conductive current via the Arrhenius

model, E_a serves as a diagnostic indicator to distinguish between different rate-limiting factors and conduction mechanisms involved in LDET. Collectively, this framework underscores the interdisciplinary relevance of microbial LDET and provides a coherent rationale for the multi-level investigations presented in the subsequent chapters.

Chapter 2 investigates the molecular determinants of electron conduction within *S.* MR-1 biofilms. Utilizing a custom-built IDE platform under variable temperature conditions, this chapter reveals that the rate-limiting step in biofilm LDET lies in interprotein electron transfer between the outer membrane cytochromes MtrC and OmcA. The study employs mutant strains, electrochemical measurements, circular dichroism spectroscopy, and fluorescence recovery after photobleaching to demonstrate that lateral diffusion and dynamic collision of OMCs on the cell surface critically dictate E_a of biofilm conduction. These results underscore interprotein electron transfer and flavin modulation as key determinants of biofilm electron conduction, laying a foundation for engineering high-performance bioelectronic materials.

Chapter 3 builds upon the mechanistic insights gained in *S.* MR-1 and applies them to the biofilm-forming human oral pathogen PG. Through detailed electrochemical and proteomic analyses, this chapter demonstrates that OMVs secreted by PG serve not only as structural agents in biofilm development but also as active redox mediators. It identifies peptidylarginine deiminase (PPAD) as an OMVs-associated enzyme that, in the presence of FMN, catalyzes redox reactions facilitating electron conduction across the biofilm matrix. The synergistic interaction between PPAD and FMN is shown to lower E_a of conduction and significantly enhance biofilm conductivity and biomass accumulation. This chapter highlights an unorthodox function of PPAD, extending its role beyond immunopathology into microbial electron metabolism.

Chapter 4 investigates the implications of redox-enabled biofilm architectures for antimicrobial resistance. It reveals that OMVs-enriched PG biofilms exhibit markedly enhanced tolerance to conventional antibiotics such as amoxicillin, clindamycin, and metronidazole, likely due to the redox buffering capacity and structural protection

provided by OMVs and PPAD. In contrast, energy metabolism-targeting agents such as nitazoxanide and tizoxanide maintain efficacy even under these conditions, suggesting that disruption of anaerobic electron flow and ATP synthesis bypasses the resistance mechanisms conferred by redox-active biofilms. The chapter emphasizes a paradigm shift toward targeting microbial energetics as a strategy for controlling recalcitrant biofilm infection.

Chapter 5 synthesizes the major findings of this dissertation and discusses their broader implications for the fields of microbial bioelectrochemistry, pathogenesis, and biofilm-targeted therapy. It outlines prospective research directions, including structural resolution of OMVs redox assemblies, synthetic modulation of membrane electron transfer systems, and therapeutic targeting of flavin-cytochrome interactions. This chapter positions the dissertation within a growing scientific effort to integrate systems biology, bioengineering, and clinical microbiology toward understanding and manipulating biofilm-based microbial survival strategies.

Collectively, this dissertation advances a unified model of biofilm electron conduction and its regulatory principles by exploring cross-kingdom conservation and divergence of LDET mechanisms. Through the dual lens of environmental electroactive bacteria and clinically significant pathogens, the thesis bridges the gap between fundamental redox biology and translational biofilm research, contributing to both theoretical frameworks and practical innovations in energy and health sciences.

1.6 References

Beaussart, A., Baker, A. E., Kuchma, S. L., El-Kirat-Chatel, S., O'Toole, G. A., & Dufrêne, Y. F. (2014). Nanoscale adhesion forces of *Pseudomonas aeruginosa* type IV pili. *ACS nano*, *8*(10), 10723-10733.

Boyd, C. D., & O'Toole, G. A. (2012). Second messenger regulation of biofilm formation: breakthroughs in understanding c-di-GMP effector systems. *Annual review of cell and developmental biology*, *28*(1), 439-462.

Ciemniecki, J. A., Ho, C.-L., Horak, R. D., Okamoto, A., & Newman, D. K. (2024). Mechanistic study of a low-power bacterial maintenance state using high-throughput electrochemistry. *Cell*, *187*(24), 6882-6895. e6888.

Costerton, J. W., Stewart, P. S., & Greenberg, E. P. (1999). Bacterial biofilms: a common cause of persistent infections. *Science*, *284*(5418), 1318-1322.

Dahl, P. J., Yi, S. M., Gu, Y., Acharya, A., Shipps, C., Neu, J., O'Brien, J. P., Morzan, U. N., Chaudhuri, S., & Guberman-Pfeffer, M. J. (2022). A 300-fold conductivity increase in microbial cytochrome nanowires due to temperature-induced restructuring of hydrogen bonding networks. *Science Advances*, *8*(19), eabm7193.

Deng, X., Dohmae, N., Nealson, K. H., Hashimoto, K., & Okamoto, A. (2018). Multi-heme cytochromes provide a pathway for survival in energy-limited environments. *Science Advances*, *4*(2), eaao5682.

Deng, X., Nakamura, R., Hashimoto, K., & Okamoto, A. (2015). Electron extraction from an extracellular electrode by *Desulfovibrio ferrophilus* strain IS5 without using hydrogen as an electron carrier. *Electrochemistry*, *83*(7), 529-531.

Ding, M., Shiu, H.-Y., Li, S.-L., Lee, C. K., Wang, G., Wu, H., Weiss, N. O., Young, T. D., Weiss, P. S., & Wong, G. C. (2016). Nanoelectronic investigation reveals the electrochemical basis of electrical conductivity in *Shewanella* and *Geobacter. ACS nano*, *10*(11), 9919-9926.

Edwards, M. J., White, G. F., Lockwood, C. W., Lawes, M. C., Martel, A., Harris, G.,

Scott, D. J., Richardson, D. J., Butt, J. N., & Clarke, T. A. (2018). Structural modeling of an outer membrane electron conduit from a metal-reducing bacterium suggests electron transfer via periplasmic redox partners. *Journal of Biological Chemistry*, *293*(21), 8103-8112.

El-Naggar, M. Y., Wanger, G., Leung, K. M., Yuzvinsky, T. D., Southam, G., Yang, J., Lau, W. M., Nealson, K. H., & Gorby, Y. A. (2010). Electrical transport along bacterial nanowires from *Shewanella oneidensis* MR-1. *Proceedings of the National Academy of Sciences*, *107*(42), 18127-18131.

Firer-Sherwood, M., Pulcu, G. S., & Elliott, S. J. (2008). Electrochemical interrogations of the Mtr cytochromes from *Shewanella*: opening a potential window. *JBIC Journal of Biological Inorganic Chemistry*, *13*, 849-854.

Flemming, H.-C. (2002). Biofouling in water systems–cases, causes and countermeasures. *Applied microbiology and biotechnology*, *59*(6), 629-640.

Gallimidi, A. B., Fischman, S., Revach, B., Bulvik, R., Maliutina, A., Rubinstein, A. M., Nussbaum, G., & Elkin, M. (2015). Periodontal pathogens *Porphyromonas gingivalis* and *Fusobacterium nucleatum* promote tumor progression in an oral-specific chemical carcinogenesis model. *Oncotarget*, *6*(26), 22613.

Glasser, N. R., Saunders, S. H., & Newman, D. K. (2017). The colorful world of extracellular electron shuttles. *Annual review of microbiology*, *71*, 731-751.

Gray, H. B., & Winkler, J. R. (2005). Long-range electron transfer. *Proceedings of the National Academy of Sciences*, *102*(10), 3534-3539.

Guo, S., Chang, Y., Brun, Y. V., Howell, P. L., Burrows, L. L., & Liu, J. (2024). PilY1 regulates the dynamic architecture of the type IV pilus machine in *Pseudomonas aeruginosa*. *Nature Communications*, *15*(1), 9382.

Hall-Stoodley, L., Costerton, J. W., & Stoodley, P. (2004). Bacterial biofilms: from the natural environment to infectious diseases. *Nature Reviews Microbiology*, *2*(2), 95-108.

Hammer, B. K., & Bassler, B. L. (2003). Quorum sensing controls biofilm formation in

Vibrio cholerae. *Molecular microbiology*, *50*(1), 101-104.

Herrling, M. P., Lackner, S., Nirschl, H., Horn, H., & Guthausen, G. (2019). Recent NMR/MRI studies of biofilm structures and dynamics. *Annual reports on NMR spectroscopy*, *97*, 163-213.

Høiby, N., Bjarnsholt, T., Moser, C., Bassi, G., Coenye, T., Donelli, G., Hall-Stoodley, L., Holá, V., Imbert, C., & Kirketerp-Møller, K. (2015). ESCMID guideline for the diagnosis and treatment of biofilm infections 2014. *Clinical microbiology and infection*, *21*, S1-S25.

Kato, S. (2015). Biotechnological aspects of microbial extracellular electron transfer. *Microbes and environments*, *30*(2), 133-139.

Kostic, A. D., Chun, E., Robertson, L., Glickman, J. N., Gallini, C. A., Michaud, M., Clancy, T. E., Chung, D. C., Lochhead, P., & Hold, G. L. (2013). *Fusobacterium nucleatum* potentiates intestinal tumorigenesis and modulates the tumor-immune microenvironment. *Cell host & microbe*, *14*(2), 207-215.

Laib, I., Mohammed, H. A., Laouini, S. E., Bouafia, A., Abdullah, M. M. S., Al-Lohedan, H. A., Al-Essa, Q., & Trzepieciński, T. (2025). Cutting-edge nanotherapeutics: silver nanoparticles loaded with ciprofloxacin for powerful antidiabetic, antioxidant, anti-inflammatory, and antibiotic action against resistant pathogenic bacteria. *International Journal of Food Science and Technology*, *60*(1).

Lampa-Pastirk, S., Veazey, J. P., Walsh, K. A., Feliciano, G. T., Steidl, R. J., Tessmer, S. H., & Reguera, G. (2016). Thermally activated charge transport in microbial protein nanowires. *Scientific Reports*, *6*(1), 23517.

Li, F., Tang, R., Zhang, B., Qiao, C., Yu, H., Liu, Q., Zhang, J., Shi, L., & Song, H. (2023). Systematic full-cycle engineering microbial biofilms to boost electricity production in *Shewanella oneidensis*. *Research*, *6*, 0081.

Little, B., Blackwood, D., Hinks, J., Lauro, F., Marsili, E., Okamoto, A., Rice, S., Wade, S., & Flemming, H.-C. (2020). Microbially influenced corrosion—Any progress? *Corrosion Science*, *170*, 108641.

Logan, B. E., Hamelers, B., Rozendal, R., Schröder, U., Keller, J., Freguia, S., Aelterman, P., Verstraete, W., & Rabaey, K. (2006). Microbial fuel cells: methodology and technology. *Environmental Science & Technology*, *40*(17), 5181-5192.

Lovley, D. R. (2006a). Bug juice: harvesting electricity with microorganisms. *Nature Reviews Microbiology*, *4*(7), 497-508.

Lovley, D. R. (2006b). Microbial fuel cells: novel microbial physiologies and engineering approaches. *Current opinion in Biotechnology*, *17*(3), 327-332.

Lovley, D. R. (2008). The microbe electric: conversion of organic matter to electricity. *Current opinion in Biotechnology*, *19*(6), 564-571.

Lovley, D. R. (2017). Electrically conductive pili: biological function and potential applications in electronics. *Current Opinion in Electrochemistry*, *4*(1), 190-198.

Mack, D., Haeder, M., Siemssen, N., & Laufs, R. (1996). Association of biofilm production of coagulase-negative *staphylococci* with expression of a specific polysaccharide intercellular adhesin. *Journal of Infectious Diseases*, *174*(4), 881-883.

Mah, T.-F., Pitts, B., Pellock, B., Walker, G. C., Stewart, P. S., & O'Toole, G. A. (2003). A genetic basis for *Pseudomonas aeruginosa* biofilm antibiotic resistance. *Nature*, *426*(6964), 306-310.

Malvankar, N. S., Tuominen, M. T., & Lovley, D. R. (2012). Biofilm conductivity is a decisive variable for high-current-density *Geobacter sulfurreducens* microbial fuel cells. *Energy & Environmental Science*, *5*(2), 5790-5797.

Malvankar, N. S., Vargas, M., Nevin, K., Tremblay, P.-L., Evans-Lutterodt, K., Nykypanchuk, D., Martz, E., Tuominen, M. T., & Lovley, D. R. (2015). Structural basis for metallic-like conductivity in microbial nanowires. *MBio*, *6*(2), 10.1128/mbio. 00084-00015.

Malvankar, N. S., Vargas, M., Nevin, K. P., Franks, A. E., Leang, C., Kim, B.-C., Inoue, K., Mester, T., Covalla, S. F., & Johnson, J. P. (2011). Tunable metallic-like

conductivity in microbial nanowire networks. *Nature nanotechnology*, *6*(9), 573-579.

Malvankar, N. S., Yalcin, S. E., Tuominen, M. T., & Lovley, D. R. (2014). Visualization of charge propagation along individual pili proteins using ambient electrostatic force microscopy. *Nature nanotechnology*, *9*(12), 1012-1017.

Marsili, E., Baron, D. B., Shikhare, I. D., Coursolle, D., Gralnick, J. A., & Bond, D. R. (2008). *Shewanella* secretes flavins that mediate extracellular electron transfer. *Proceedings of the National Academy of Sciences*, *105*(10), 3968-3973.

Moyano, A., Tobares, R., Rizzi, Y., Krapp, A., & Mondotte, J. (2014). A Long-Chain Flavodoxin Protects *Pseudomonas aeruginosa* from Oxidative Stress.

Naradasu, D. (2022). Extracellular electron transfer capability of oral pathogens *Aggregatibacter actinomycetemcomitans* and *Porphyromonas gingivalis*. In: Microbiology Society.

Naradasu, D., Guionet, A., Okinaga, T., Nishihara, T., & Okamoto, A. (2020). Electrochemical characterization of current-producing human oral pathogens by whole-cell electrochemistry. *ChemElectroChem*, *7*(9), 2012-2019.

Newman, D. K., & Kolter, R. (2000). A role for excreted quinones in extracellular electron transfer. *Nature*, *405*(6782), 94-97.

Okabe, S., Hiratia, K., Ozawa, Y., & Watanabe, Y. (1996). Spatial microbial distributions of nitrifiers and heterotrophs in mixed-population biofilms. *Biotechnology and Bioengineering*, *50*(1), 24-35.

Okabe, S., Itoh, T., Satoh, H., & Watanabe, Y. (1999). Analyses of spatial distributions of sulfate-reducing bacteria and their activity in aerobic wastewater biofilms. *Applied and Environmental Microbiology*, *65*(11), 5107-5116.

Okamoto, A., Hashimoto, K., Nealson, K. H., & Nakamura, R. (2013). Rate enhancement of bacterial extracellular electron transport involves bound flavin semiquinones. *Proceedings of the National Academy of Sciences*, *110*(19), 7856-7861.

Okamoto, A., Nakamura, R., Nealson, K. H., & Hashimoto, K. (2014). Bound flavin model suggests similar electron-transfer mechanisms in *Shewanella* and *Geobacter*. *ChemElectroChem*, *1*(11), 1808-1812.

Orans, J., Johnson, M. D., Coggan, K. A., Sperlazza, J. R., Heiniger, R. W., Wolfgang, M. C., & Redinbo, M. R. (2010). Crystal structure analysis reveals *Pseudomonas* PilY1 as an essential calcium-dependent regulator of bacterial surface motility. *Proceedings of the National Academy of Sciences*, *107*(3), 1065-1070.

Page, C. C., Moser, C. C., Chen, X., & Dutton, P. L. (1999). Natural engineering principles of electron tunnelling in biological oxidation–reduction. *Nature*, *402*(6757), 47-52.

Pardo, L., Mota, M. I., Parnizari, A., Varela, A., Algorta, G., & Varela, G. (2024). Detection of Vancomycin Resistance among Methicillin-Resistant *Staphylococcus aureus* Strains Recovered from Children with Invasive Diseases in a Reference Pediatric Hospital. *Antibiotics*, *13*(4), 298.

Pfeffer, C., Larsen, S., Song, J., Dong, M., Besenbacher, F., Meyer, R. L., Kjeldsen, K. U., Schreiber, L., Gorby, Y. A., & El-Naggar, M. Y. (2012). Filamentous bacteria transport electrons over centimetre distances. *Nature*, *491*(7423), 218-221.

Pirbadian, S., Barchinger, S. E., Leung, K. M., Byun, H. S., Jangir, Y., Bouhenni, R. A., Reed, S. B., Romine, M. F., Saffarini, D. A., & Shi, L. (2014). *Shewanella oneidensis* MR-1 nanowires are outer membrane and periplasmic extensions of the extracellular electron transport components. *Proceedings of the National Academy of Sciences*, *111*(35), 12883-12888.

Powell, L. C., Abdulkarim, M. F., Stokniene, J., Yang, Q. E., Walsh, T. R., Hill, K. E., Gumbleton, M., & Thomas, D. W. (2021). Quantifying the effects of antibiotic treatment on the extracellular polymer network of antimicrobial resistant and sensitive biofilms using multiple particle tracking. *NPJ biofilms and microbiomes*, *7*.

Reguera, G., McCarthy, K. D., Mehta, T., Nicoll, J. S., Tuominen, M. T., & Lovley, D. R.

(2005). Extracellular electron transfer via microbial nanowires. *Nature*, *435*(7045), 1098-1101.

Ricciardi, B. F., Muthukrishnan, G., Masters, E., Ninomiya, M., Lee, C. C., & Schwarz, E. M. (2018). *Staphylococcus aureus* evasion of host immunity in the setting of prosthetic joint infection: biofilm and beyond. *Current reviews in musculoskeletal medicine*, *11*, 389-400.

Richardson, D. J., Butt, J. N., Fredrickson, J. K., Zachara, J. M., Shi, L., Edwards, M. J., White, G., Baiden, N., Gates, A. J., & Marritt, S. J. (2012). The 'porin–cytochrome'model for microbe-to-mineral electron transfer. *Molecular microbiology*, *85*(2), 201-212.

Schulze, A., Mitterer, F., Pombo, J. P., & Schild, S. (2021). Biofilms by bacterial human pathogens: Clinical relevance-development, composition and regulation-therapeutical strategies. *Microbial Cell*, *8*(2), 28.

Sharma, D., Misba, L., & Khan, A. U. (2019). Antibiotics versus biofilm: an emerging battleground in microbial communities. *Antimicrobial Resistance & Infection Control*, *8*, 1-10.

Sharma, S., Mohler, J., Mahajan, S. D., Schwartz, S. A., Bruggemann, L., & Aalinkeel, R. (2023). Microbial biofilm: a review on formation, infection, antibiotic resistance, control measures, and innovative treatment. *Microorganisms*, *11*(6), 1614.

Shi, L., Dong, H., Reguera, G., Beyenal, H., Lu, A., Liu, J., Yu, H.-Q., & Fredrickson, J. K. (2016). Extracellular electron transfer mechanisms between microorganisms and minerals. *Nature Reviews Microbiology*, *14*(10), 651-662.

Shu, C., Zhu, Q., Xiao, K., Hou, Y., Ma, H., Ma, J., & Sun, X. (2019). Direct extracellular electron transfer of the *Geobacter sulfurreducens* pili relevant to interaromatic distances. *BioMed research international*, *2019*(1), 6151587.

Snider, R. M., Strycharz-Glaven, S. M., Tsoi, S. D., Erickson, J. S., & Tender, L. M. (2012). Long-range electron transport in *Geobacter sulfurreducens* biofilms is redox gradient-driven. *Proceedings of the National Academy of Sciences*, *109*(38),

15467-15472.

Soares, A., Alexandre, K., & Etienne, M. (2020). Tolerance and persistence of *Pseudomonas aeruginosa* in biofilms exposed to antibiotics: Molecular mechanisms, antibiotic strategies and therapeutic perspectives. *Frontiers in Microbiology*, *11*, 2057.

Stewart, P. S., & Franklin, M. J. (2008). Physiological heterogeneity in biofilms. *Nature Reviews Microbiology*, *6*(3), 199-210.

Subramanian, P., Pirbadian, S., El-Naggar, M. Y., & Jensen, G. J. (2018). Ultrastructure of *Shewanella oneidensis* MR-1 nanowires revealed by electron cryotomography. *Proceedings of the National Academy of Sciences*, *115*(14), E3246-E3255.

Sultana, S. T., Call, D. R., & Beyenal, H. (2016). Eradication of Pseudomonas aeruginosa biofilms and persister cells using an electrochemical scaffold and enhanced antibiotic susceptibility. *NPJ biofilms and microbiomes*, *2*(1), 2.

Thi, M. T. T., Wibowo, D., & Rehm, B. H. (2020). *Pseudomonas aeruginosa* biofilms. *International Journal of Molecular Sciences*, *21*(22), 8671.

Tokunou, Y., Toyofuku, M., & Nomura, N. (2022). Physiological Benefits of Oxygen-Terminating Extracellular Electron Transfer. *MBio*, *13*(6), e01957-01922.

Vargas, M., Malvankar, N. S., Tremblay, P.-L., Leang, C., Smith, J. A., Patel, P., Synoeyenbos-West, O., Nevin, K. P., & Lovley, D. R. (2013). Aromatic amino acids required for pili conductivity and long-range extracellular electron transport in *Geobacter sulfurreducens*. *MBio*, *4*(2), 10.1128/mbio. 00105-00113.

Von Canstein, H., Ogawa, J., Shimizu, S., & Lloyd, J. R. (2008). Secretion of flavins by *Shewanella* species and their role in extracellular electron transfer. *Applied and Environmental Microbiology*, *74*(3), 615-623.

Vuong, C., Voyich, J. M., Fischer, E. R., Braughton, K. R., Whitney, A. R., DeLeo, F. R., & Otto, M. (2004). Polysaccharide intercellular adhesin (PIA) protects *Staphylococcus epidermidis* against major components of the human innate immune system. *Cellular microbiology*, *6*(3), 269-275.

Wang, B., Deng, J., Donati, V., Merali, N., Frampton, A. E., Giovannetti, E., & Deng, D. (2024). The roles and interactions of P*orphyromonas gingivalis* and *Fusobacterium nucleatum* in oral and gastrointestinal carcinogenesis: A narrative review. *Pathogens*, *13*(1), 93.

Wang, F., Gu, Y., O'Brien, J. P., Yi, S. M., Yalcin, S. E., Srikanth, V., Shen, C., Vu, D., Ing, N. L., & Hochbaum, A. I. (2019). Structure of microbial nanowires reveals stacked hemes that transport electrons over micrometers. *Cell*, *177*(2), 361-369. e310.

Waqas, U., Farhan, A., Haider, A., Qumar, U., & Raza, A. (2023). Advancements in biofilm formation and control in potable water distribution systems: A comprehensive review and analysis of chloramine decay in water systems. *Journal of Environmental Chemical Engineering*, *11*(6), 111377.

Winkler, J. R., & Gray, H. B. (2015). Electron flow through biological molecules: does hole hopping protect proteins from oxidative damage? *Quarterly reviews of biophysics*, *48*(4), 411-420.

Xie, Y., Liang, H., Jiang, N., Liu, D., Zhang, N., Li, Q., Zhang, K., Sang, X., Feng, Y.-k., Chen, R., Zhang, Y., & Chen, Q. (2022). Graphene quantum dots induce cascadic apoptosis via interaction with proteins associated with anti-oxidation after endocytosis by *Trypanosoma brucei*. *Frontiers in Immunology*, *13*.

Xu, S., Barrozo, A., Tender, L. M., Krylov, A. I., & El-Naggar, M. Y. (2018). Multiheme cytochrome mediated redox conduction through *Shewanella oneidensis* MR-1 cells. *Journal of the American Chemical Society*, *140*(32), 10085-10089.

Xu, S., Jangir, Y., & El-Naggar, M. Y. (2016). Disentangling the roles of free and cytochrome-bound flavins in extracellular electron transport from *Shewanella oneidensis* MR-1. *Electrochimica Acta*, *198*, 49-55.

Yates, M. D., Strycharz-Glaven, S. M., Golden, J. P., Roy, J., Tsoi, S., Erickson, J. S., El-Naggar, M. Y., Barton, S. C., & Tender, L. M. (2016). Measuring conductivity of living *Geobacter sulfurreducens* biofilms. *Nature nanotechnology*, *11*(11), 910-

913.

Yi, H., Nevin, K. P., Kim, B.-C., Franks, A. E., Klimes, A., Tender, L. M., & Lovley, D. R. (2009). Selection of a variant of *Geobacter sulfurreducens* with enhanced capacity for current production in microbial fuel cells. *Biosensors and Bioelectronics*, *24*(12), 3498-3503.

Chapter 2. Cell-surface inter-cytochrome electron transfer limits biofilm electron conduction kinetics in *Shewanella oneidensis* MR-1

2.1 Introduction

Electrochemically active bacteria, with the ability to form electrically conductive biofilm matrices for bioenergy conversion and bioelectronics (Chen et al., 2020), have engendered much interest in the scientific community, thereby, understanding the flow of electrons inside the biofilm is crucial to achieving high current density in microbial electrochemical systems (Logan et al., 2019). Significant progress has been made in elucidating the molecular structures of redox-active proteins within the extracellular matrix (Shi et al., 2016; Kumar et al., 2017), yet the kinetic bottlenecks in long-distance electron transfer (LDET) across the densely packed, multi-layered biofilms remain poorly understood.

Among electrogenic organisms, *Shewanella oneidensis* MR-1 (*S.* MR-1) stands out, known for facilitating robust extracellular electron transfer (EET) to both electrodes and minerals via its intricate outer membrane cytochrome complexes (OMCs), including MtrC, MtrA, and OmcA. These complexes, which function akin to biological wires, are equipped with extensive networks of heme reaction centers that efficiently channel electrons from the cellular interior to the exterior (Edwards et al., 2020). Previous studies have inferred the role of OMCs in mediating LDET within biofilms through detailed analyses of redox signal (Okamoto et al., 2012). The unique configuration of heme centers along the surface of MtrC and OmcA enables multiple electron ingress and egress points (**Figure 2.1.A**), thereby facilitating the formation of expansive electron transport routes through diffusion and intermolecular collisions on the membrane's surface (Subramanian et al., 2018; Chong et al., 2022). However, defining the rate-limiting steps in electron transfer, whether intra- or inter-OMCs, challenges researchers. Recent work by Xu et al., (2018) highlighted the potential rate-limiting pathways by employing an interdigitated electrode (IDE) system to ascertain the temperature-dependence of biofilm conductivity, revealing insights into the activation energy (E_a) associated with the rate-limiting step of the biofilm electron conduction (Yates et al., 2015; Xu et al., 2018). Their analysis suggests that the electron routes hemes 5-10 pathway of MtrC, characterized by E_a values comparable to a kinetic Monte Carlo model simulation and higher than those of alternate routes, are likely critical. This

approach, however, did not explore other potential electron transfer pathways involving periplasmic cytochromes or inter-OMCs interactions comprehensively (**Figure 2.1.B**).

Our investigation builds on this foundation by contrasting gene knockout mutant strains to examine the impact of inter-cytochrome interactions on the rate-limiting step energy barrier, E_a, for biofilm electron dynamics. We also probe the effects of OMCs diffusion and collision dynamics with cholesterol(Eaton et al., 1981) and the interaction of non-covalently attached flavin with OMCs on the biofilm electron conduction, associated with whole-cell circular dichroism (CD) spectroscopy to explore inter-heme exciton coupling in OMCs (Tokunou et al., 2018). By pinpointing and clarifying these bottlenecks, our research aims to develop strategies that significantly enhance electron transfer within biofilms, thereby augmenting the operational efficacy of bioelectronic devices.

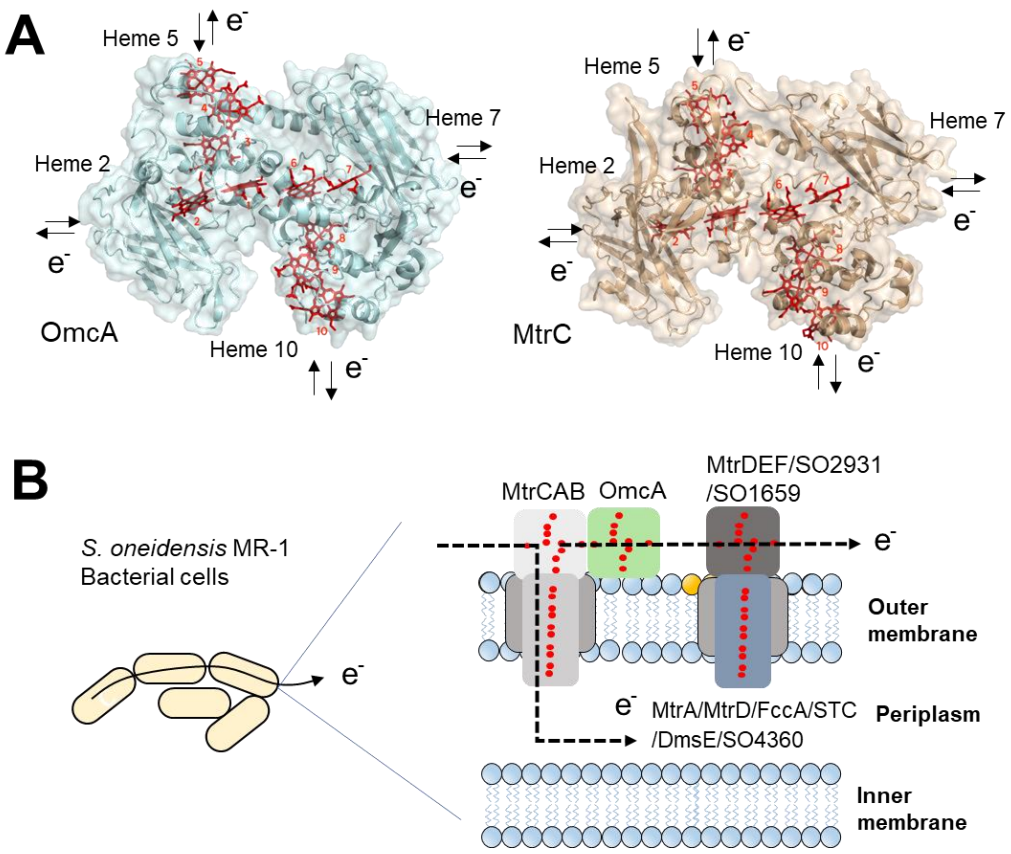

Figure 2.1. (A) The crystal structure of OmcA (PDB: 4LMH) and MtrC (PDB: 4LM8). Heme centers for electron ingress and egress points were highlighted. (B) The schematic model for potential intercellular electron pathways through the outer membrane (OM) or the periplasm cytochromes.

2.2 Methods

2.2.1 The microbe culture conditions

S. MR-1 wild type (WT) and mutant strains were inoculated from our lab storage and precultured in a 50 Ml Falcon tube with Luria-Bertani (LB) medium (shaking at 180 rpm, 30°C). Then, cell suspensions were washed two times with a defined medium (DM). Cells were harvested after washing twice with DM medium. The compositions of DM are $NaHCO_3$ 2.5 g/L, $CaCl_2 \cdot 2H_2O$ 0.08 g/L, NH_4Cl 1.0 g/L, $MgCl_2 \cdot 6H_2O$ 0.2 g/L, NaCl 10 g/L, and HEPES 7.2 g/L. The method to construct *ΔomcAll* (lacking the genes encoding the outer-membrane cytochrome C: mtrA, mtrB, mtrC, mtrD, mtrE, mtrF, and omcA), ΔPEC (lacking the genes encoding the periplasmic cytochrome C genes: mtrA, mtrD, dmsE, SO4360, and cctA), *ΔomcA*, and *ΔmtrC* was described in previous studies.

2.2.2 Electrochemistry measurements

A single-chamber cell was used for electrochemical linear sweep voltammetry under bipotential states. The working electrode IDE of indium tin oxide (ITO) sputter deposited on a glass with a 10 μm gap between the source and drain electrodes (10 μm in width) (**Figure 2.2.A**). The reference was Ag/AgCl electrode (3M KCl saturated), and the counter electrode was a Pt wire. The 6 Ml washed cell suspensions were redissolved in DM to an OD_{600} of 1.0 and were purged with nitrogen for 30 min to remove the oxygen. The S.MR-1 biofilm was electrochemically incubated for 24 hours by the poising potential at 0.4 V (vs. standard hydrogen electrode [SHE]) to form the biofilm on an IDE electrode (VMP3: Biologic SAS, Seyssinet-Pariset, France). Then, the conducting current (I_{cond}) was obtained by setting the source and drain potentials, ES and ED, respectively, in a constant offset voltage of 20 Mv. The current was subtracted by the equation below:

$$I_{cond} = (I_{drain} - I_{source})/2 \qquad (1)$$

I_{drain} and I_{source} were the current profiles of the cyclic voltammetry (CV) from IDE with higher and lower potential, respectively.

The E_a accounting for the redox-mediated electron transport of *S.* MR-1 wild type and mutant strains *ΔomcAll*, *ΔPEC*, *ΔomcA*, and *ΔmtrC* were acquired by conducting the temperature-linked Arrhenius equation examinations. Temperatures were step-controlled from 30°C to 9°C by circulating water in the jacket of the single-chamber

reactor. After stabilizing the temperature for 15 to 20 minutes, the gate measurements were conducted. The E_a was obtained by fitting the data to the empirical Arrhenius equation:

$$\ln (I_{cond}) = A - 1000/T \times (E_a/1000k) \quad (2)$$

Where A was the pre-exponential factor, T was the temperature (K), and k was the Boltzmann constant.

2.2.3 Scanning electron microscopy

The biofilm incubated on the electrode was fixed with 2.5% glutaraldehyde for 5 days at 4°C. Then, samples were dehydrated in 25, 50, 75, 90, and 100% ethanol and freeze-dried under a vacuum before scanning electron microscopy (SEM). The dried samples were coated with evaporated platinum for 30 seconds and were then checked by Keyence VE-9800 microscope at 10 kV.

2.2.4 Cellular cholesterol quantification

S. MR-1 cells were treated with 0, 20, 100, or 200 mg/L cholesterol and incubated in an electrochemical reactor at 0.4 V and 30°C for 20 h. Cells were harvested by centrifugation at 7,800 rpm for 5 min at 4°C both before and after the electrochemical assay. The resulting pellets were lysed by resuspension in cold ethanol: isopropanol (1:1, v/v), followed by vortexing for 30 s and incubation at -20°C for 1 h. Lysates were centrifuged at 12,000 rpm for 10 min, and supernatants were collected. After vacuum drying, the residues were resuspended in 1 mL of Assay Buffer II and used for subsequent analysis. Cellular cholesterol levels were measured using the Total Cholesterol & Cholesteryl Ester Colorimetric Assay Kit (ab282928, Abcam) according to the manufacturer's instructions. Cellular cholesterol concentrations were calculated based on a standard curve using the following equation:

$$C = (B / V) \times D \quad (3)$$

where B was the amount of cholesterol determined from the standard curve, V was the sample volume (μL), and D was the dilution factor.

2.2.5 Fluorescence recovery after photobleaching

S. MR-1 cells were treated with 0, 20, 100, or 200 mg/L cholesterol and incubated in an electrochemical reactor at 0.4 V and 30°C for 20 hours. After incubation, the entire

culture was harvested and resuspended in 1×phosphate-buffered saline (PBS) to an OD_{600} of 1.0. The outer membrane was stained by adding FM^{TM}4-64FX dye to a final concentration of 30 μg/mL, followed by incubation in the dark for 20 minutes. A 30 μL aliquot of the stained suspension was placed on a glass slide for imaging. Fluorescence imaging was performed using a Nikon A1 confocal microscope equipped with a 60×objective lens. The dye was visualized using 488 nm excitation light and an emission filter with a bandwidth of 663-738 nm. A defined region of interest (ROI) on the outer membrane was photobleached using a 488 nm laser at full power for 0.5 seconds. Fluorescence recovery within the ROI was recorded over 80 seconds post-bleaching. Fluorescence intensity in the bleached area was normalized to that of an adjacent unbleached control region. Recovery kinetics were fitted to a single-exponential function to determine the characteristic recovery time constant (τ), as described previously (Ginez et al., 2022):

$$F(t) = A \times (1 – e\text{-}t/\tau) \qquad (4)$$

2.2.6 Circular Dichroism spectroscopy measurement

The CD spectra of OMCs in an intact cell were measured by the Jasco spectropolarimeter (JASCO CD, J-1500: Tokyo, Japan). Cell suspensions of *S.* MR-1 and mutant strains *ΔomcAll*, *ΔomcA*, and *ΔmtrC* were prepared by washing and resuspending in DM to an OD_{600} of 1.32. To further enhance the signal, we increased the cell density and used an integrating sphere (IS) to alleviate the scattering light of the cell suspension in front of the CD detector. Briefly, the parameters were set as: 200 nm min-1, 0.1 nm data pitch, 5.0 nm bandwidth. Then, 3 mL of cell suspension was added to a quartz cuvette and purged with nitrogen for 10 min after adding 30 mM sodium lactate as an electron donor to reduce the OMCs. In contrast, to oxidize heme centers in OMCs, the cell suspension was incubated in the presence of oxygen and fumarate (50 mM). The temperature of the suspensions was controlled at 36°C, 31°C, 26°C, 21°C, 16°C and 11°C by the accessory equipped with the Peltier-type temperature controller (PTC-517: JASCO, Tokyo, Japan) with a temperature sensor. Upon reaching the setting temperature, the scanning of the suspensions was conducted. Then, their ellipticities were normalized at 440 (Long et al., 2023).

2.3 Results

2.3.1 The outer membrane cytochrome complexes (OMCs) mediate the biofilm electron conduction

To examine the contribution of the outer membrane or the periplasmic cytochromes on LDET inside the biofilm of *S.* MR-1, we first compared the biofilm conduction current among WT of *S.* MR-1, mutant strains *ΔomcAll* and *ΔPEC* by biopotentially controlled by the source and drain potentials (E_S and E_D). A single-chamber four-electrode system with a 10 μm gap indium tin-doped oxide (ITO) IDE was used to monitor the I_{cond} from the *S.* MR-1 biofilm (**Figure 2.2.A and B**). Followed by incubation poising at 0.4 V (vs. SHE) at 30°C, 10 μm thick biofilm formation on the electrode was observed as reported (**Figure 2.2.C**) (Okamoto et al., 2012). We washed the electrode surface twice to diminish the interference of metabolic current toward I_{cond}, resulting in the low current production **(Figure 2.2.D**).

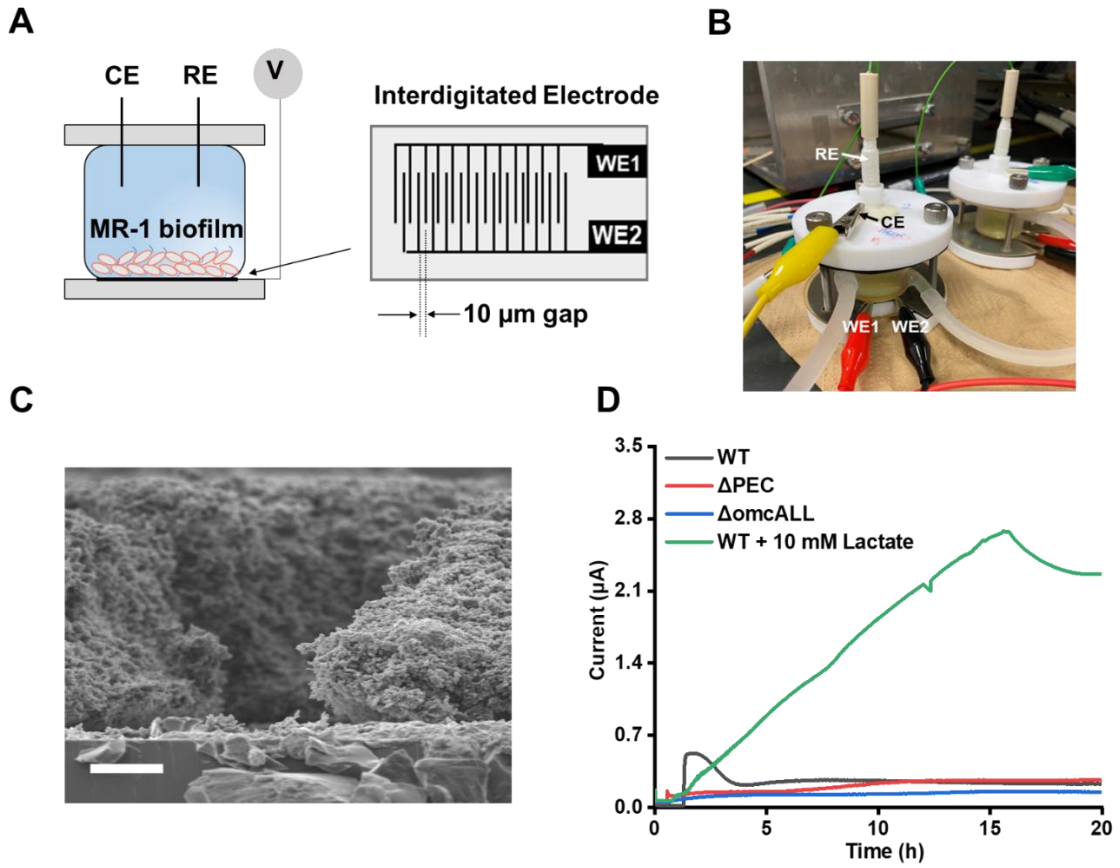

Figure 2.2. (A) *Shewanella oneidensis* MR-1 (*S.* MR-1) biofilm was electrically cultured for 24 hours to form the biofilm bridging the ITO interdigitated electrode (IDE)

with 10 μm gaps. (B) Photograph of the experimental four-electrode system. The reference electrode (RE) is Ag/AgCl (3M KCl saturated). The counter electrode (CE) is a Pt wire. Working electrode 1 (WE1) and 2 (WE2) are Indium ITO on glass. (C) Scanning electron microscope images of biofilm grown and remaining on the ITO electrodes after washing processes. The white bar is 10 μm. (D) Single-Potential Amperogram of *S.* MR-1 WT and mutant strains. This figure shows the time-dependent current profiles (30°C, 0.4 V vs. SHE) for *S.* MR-1 WT and mutant strains, recorded after washing the IDE with DM. The green profile represents positive control, showing the current profile measured under identical conditions but with 10 mM lactate present as the electron donor.

We then measured the I_{drain} and I_{source} by sweeping the voltammetry to calculate the I_{cond} by Equation 1. As shown in **Figure 2.3.A and B,** the oxidative peak of gate potential E_G ($E_G = [E_S + E_D]/2$) at around 200 Mv from the I_{cond} of *S.* MR-1 WT was observed. Upon altering the reactor temperature from 30°C to 9°C, we confirmed the linear correlation between ln (I_{cond}) and 1000/T (**Figure 2.3.C**). The magnitude of the energy barrier derived from the Arrhenius equation was estimated as previously reported (Equation 2), resulting in the semi-empirical thermal activation energy (E_a) of 0.34 ± 0.02 eV (**Figure 2.6.B**), consistent with electron transfer reactions involving hemes of *S.* MR-1 OMCs (Xu et al., 2018).

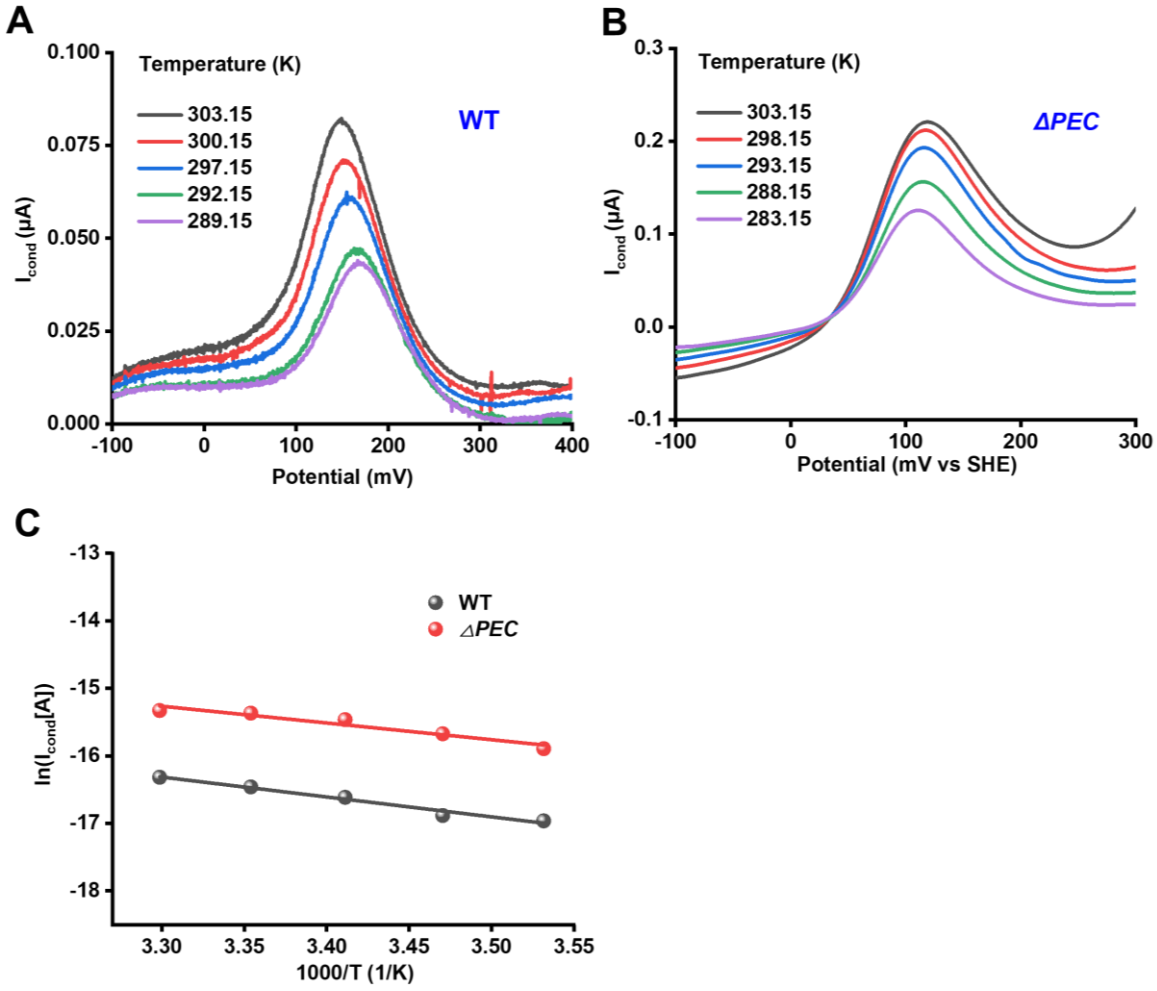

Figure 2.3. (A) Both of representative *S.* MR-1 WT biofilm conduction current (I_{cond}) (A) and *ΔPEC* I_{cond} (B) versus the gate potential under each temperature, calculated by subtracting the source from the drain current in the absence of an electron donor (offset

voltage = 20 mV, scan rate and ν = 1 mV·s^{-1}). The same tendency was observed in three independent assays. (C) Representative Arrhenius-style plots of WT, *ΔPEC*.

The I_{cond} profile and temperature dependency were distinct in *ΔomcAll* but similar in *ΔPEC* compared with WT (**Figure 2.3.C and Figure 2.4**). I_{cond} of *ΔomcAll* strain was disordered, lacking the clear Arrhenius behavior observed in the wild-type and single-knockout strains. Specifically, no systematic change in current was observed upon shifting the reactor temperature (**Figure 2.4.B)**, which makes it infeasible to derive a reliable E_a. In contrast, *ΔPEC* showed almost identical peak positions and E_a with WT (**Figure 2.3.C and 2.6.B**). These results suggest that OMCs, rather than the cytochromes in the periplasm, mediate the biofilm conduction current in WT.

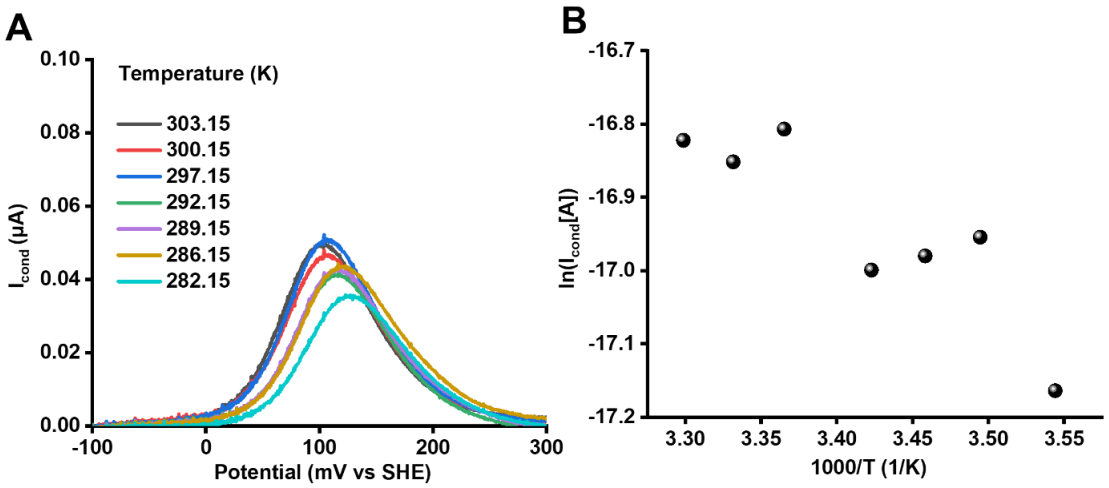

Figure 2.4. (A) The representative *S.* MR-1 *ΔOmcALL* I_{cond} versus the gate potential under each temperature, calculated by subtracting the source from the drain current in the absence of an electron donor (offset voltage = 20 mV, scan rate and ν = 1 mV·s^{-1}). The same tendency was observed in three independent assays. (B) Representative Arrhenius-style plots of *ΔOmcALL*.

2.3.2 The OmcA and MtrC interaction facilitates the biofilm electron conduction

Given the expression of MtrDEF is limited compared with OMCs in WT (Barchinger et al., 2016), the observed I_{cond} is most likely attributable to OmcA and MtrC on the cell surface (**Figure 2.1**). To elaborate the inter-protein electron transport between OmcA and MtrC, we measured the I_{cond} of strains *ΔomcA* and *ΔmtrC*. At 30°C, the I_{cond} was comparable to that of the WT (**Figure 2.3.A and 2.5**). However, at reduced temperatures, the conductivity of *ΔomcA* and *ΔmtrC* strains decreased sharply, corresponding to an increase in the E_a to 1.04 ± 0.14 eV (*ΔomcA*) and 1.48 ± 0.23 eV (*ΔmtrC*), respectively (**Figure 2.6.B**), indicating that the absence of OmcA or MtrC suppressed the interprotein electron transfer happening in the WT biofilm.

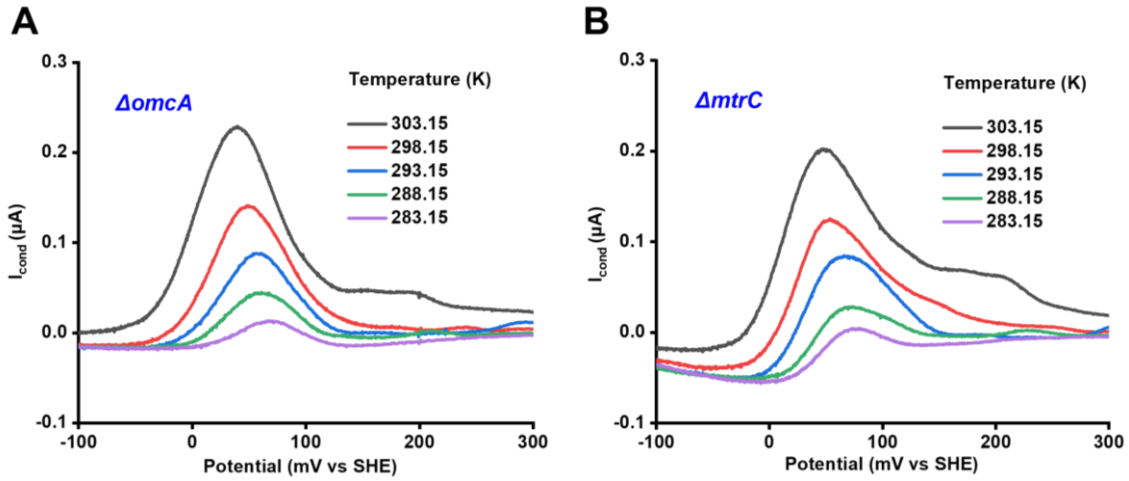

Figure 2.5. Temperature Dependency of I_{cond} in *ΔomcA* (A) and *ΔmtrC* (B). Representative plot of I_{cond} at various temperatures as a function of gate potential after 24 hours of incubation on an ITO electrode at varying temperatures.

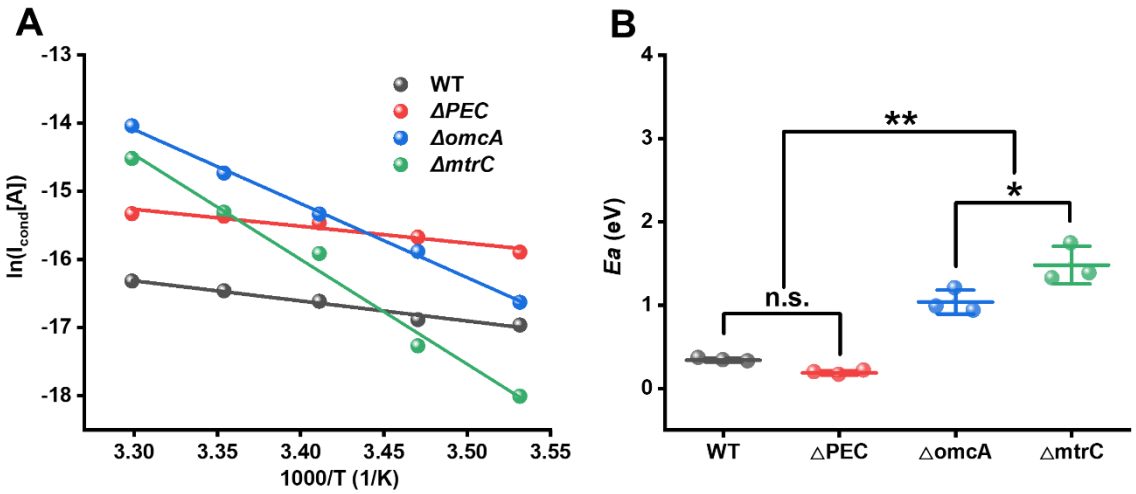

Figure 2.6. (A) Representative Arrhenius-style plots of WT, *ΔPEC*, *ΔomcA* and *ΔmtrC*. (B) The semi-empirical thermal E_a of WT, *ΔPEC*, *ΔomcA* and *ΔmtrC*. The activation energy (E_a) was calculated according to Equation 2 in the supporting information. Data in panel B are presented as means ± s.d. (n = 3). n.s., not significant, *, $p < 0.05$, and **, $p < 0.01$ (n = 3).

Since these measurements were conducted using the same differential two-electrode CV system described above (**Figure 1.9**), the changes in I_{cond} and E_a reflect alterations in lateral electron transport through the biofilm rather than direct cytochrome to electrode interactions. Given that these mutations of OMCs do not impact heme alignment in MtrC and OmcA (Tokunou et al., 2018), the significantly higher E_a of *ΔomcA* and *ΔmtrC* than WT is likely due to the loss of protein-protein interactions between OmcA and MtrC in the mutant strains. This indicates that electron transport between proteins (OmcA-OmcA and MtrC-MtrC) requires higher activation energy than OmcA-MtrC electron transfer. The near-identical concentration of heme centers on the cell surface, quantified by cyclic voltammetry (**Figure 2.7**), further supports our idea, as a concentration-dependent effect, such as mechanical pressure loss, can be neglected in the mutant strains (Long et al., 2023).

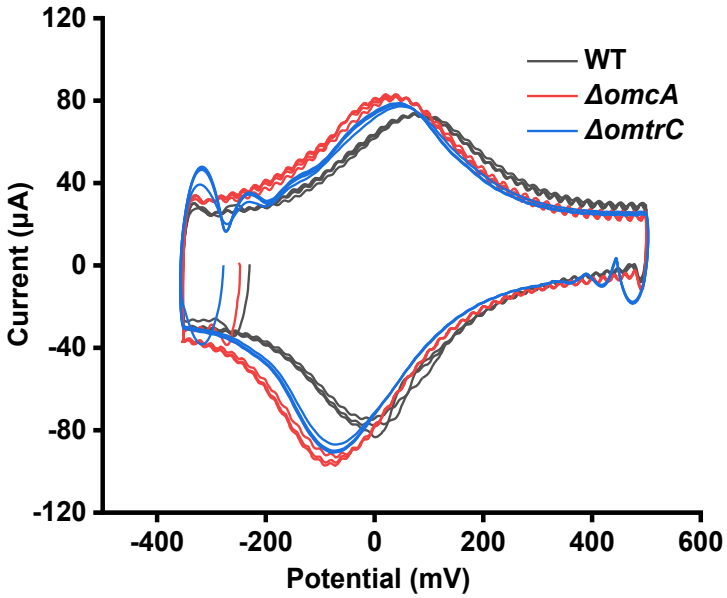

Figure 2.7. Representative cyclic voltammogram of *S.* MR-1 WT, *ΔomcA* and *ΔmtrC* after 24 hours of incubation on an ITO electrode (vs. SHE). The scan rate is 1000 $mV \cdot s^{-1}$.

2.3.3 Contribution of diffusion and collision among OMCs on the biofilm electron conduction

To confirm that the interprotein interaction via the diffusion and collision of OMCs dictates the E_a, we decreased membrane fluidity with cholesterol that specifically interacts with the lipid membrane (**Figure 2.8**) (Eaton et al., 1981).

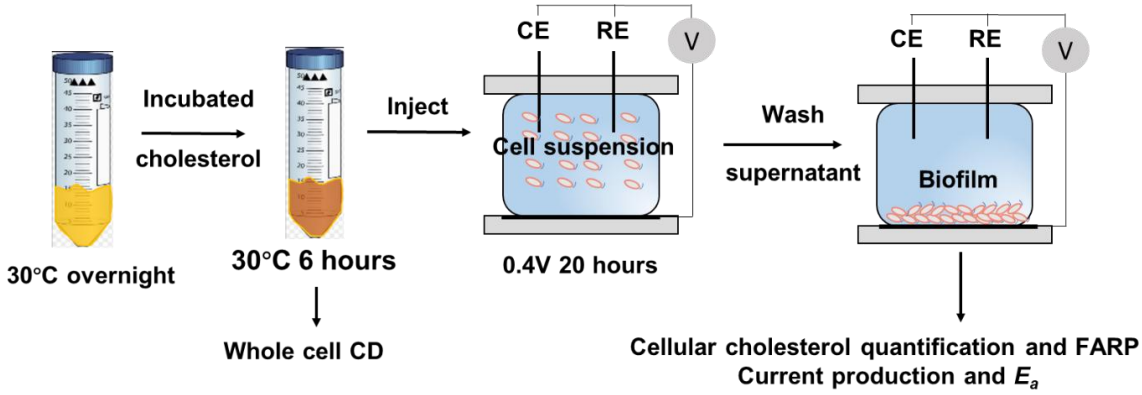

Figure 2.8. Scheme steps of electrochemical assays after preculturing with cholesterol.

Cholesterol incorporation into *S.* MR-1 cells was confirmed by quantifying intracellular cholesterol levels following cell lysis using a cholesterol assay kit. A dose-dependent increase in intracellular cholesterol was observed, with significant accumulation at concentrations of 100 and 200 mg/L relative to untreated controls (**Figure 2.9**).

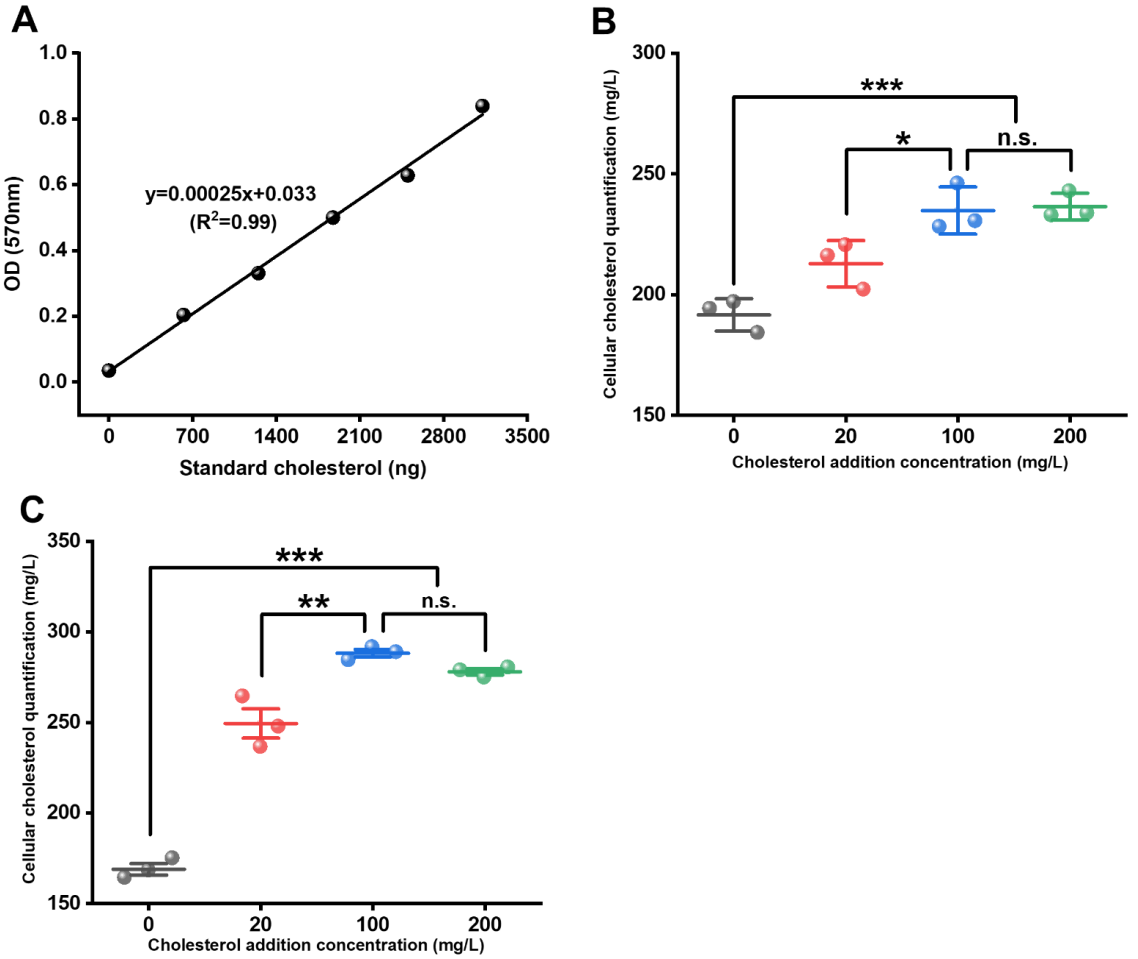

Figure 2.9. (A) Standard calibration curve for cholesterol. Quantification of intracellular cholesterol levels using the standard curve before (B) and after E_a measurement (C). Data are presented as mean ± s.d. (n = 3). n.s., not significant; *p < 0.05; **p < 0.01; ***p < 0.001.

We then evaluated the impact of altered membrane fluidity on protein dynamics by performing fluorescence recovery after photobleaching (FRAP) experiments (**Figure 2.10.A**) across a range of cholesterol concentrations. In cholesterol-free cells, full fluorescence recovery occurred within 9.6 s, whereas cells treated with 200 mg/L

cholesterol exhibited significantly slower recovery, reaching completion at approximately 23.0 s (**Figure 2.10.B**). Similarly, intermediate cholesterol concentrations (20 and 100 mg/L) also delayed recovery relative to the control (**Figure 2.10.B**). Quantitative analysis confirmed significant differences in fluorescence recovery times and diffusion time constants (τ) between the 0 and 200 mg/L groups ($p < 0.05$), while no significant difference was observed between the 100 and 200 mg/L groups (**Figure 2.10.C**), indicating that cholesterol incorporation significantly reduced the lateral mobility of membrane proteins.

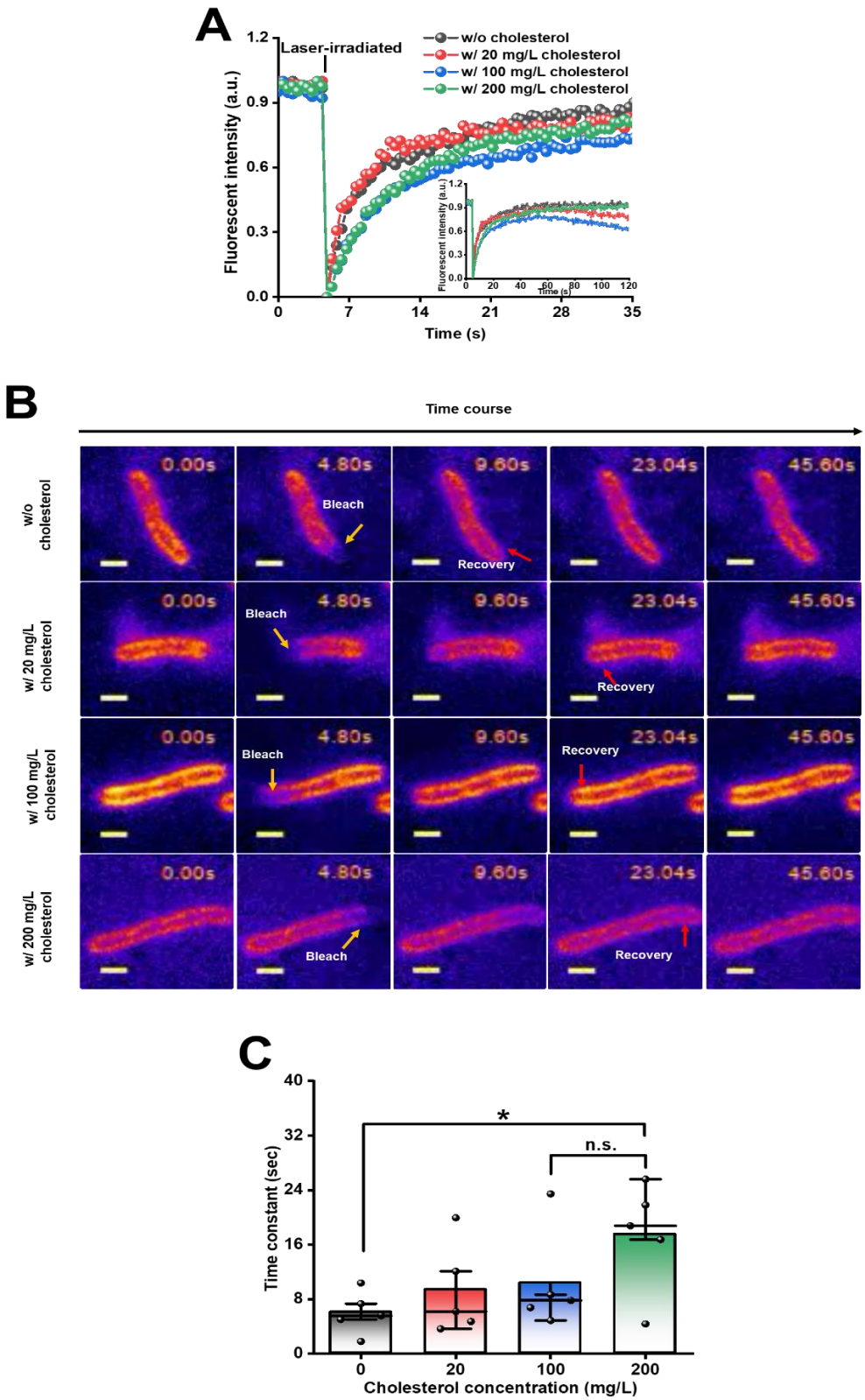

Figure 2.10. (A) Fluorescence recovery curves of *S.* MR-1 cells treated with 0, 20, 100 and 200 mg/L cholesterol concentrations. The scattered symbols show the recovery data,

and the continuous lines show the adjustments of the data to a single exponential equation for bidimensional diffusion. (B) Representative images of *S.* MR-1 stained with FM4-64FX showing different recovery speeds after bleaching. (C) Quantification of fluorescence recovery time and diffusion time constants (τ) at a varying cholesterol concentration. Data are presented as mean ± s.d. (n = 5). n.s., not significant, *p < 0.05.

Notably, the preincubation with cholesterol had a negligible effect on the microbial current production from lactate oxidation in *S.* MR-1 cells (**Figure 2.11**), indicating that the electron transfer capability to the electrode via OMCs was unaffected.

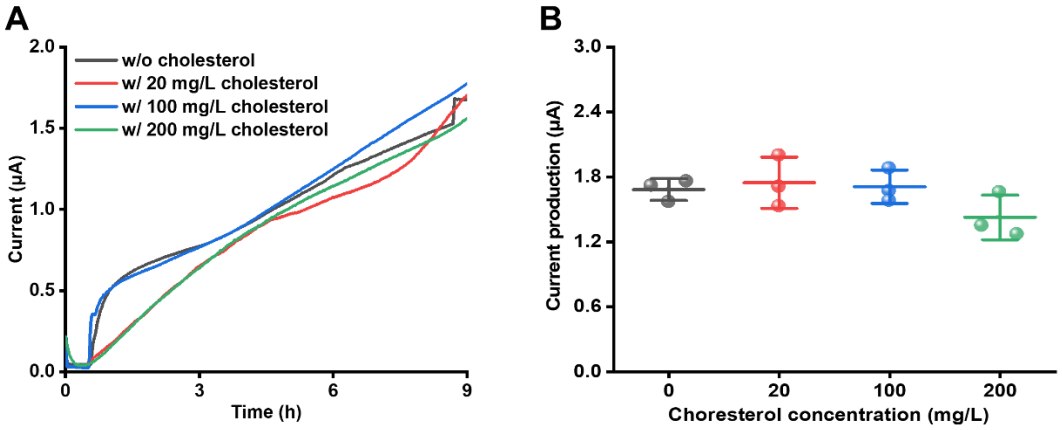

Figure 2.11. Single-potential amperometric measurements of *S.* MR-1 wild-type cells treated with varying concentrations of cholesterol were recorded at 30 °C. Representative current production is shown in (A), and results from three independent replicates are shown in (B).

However, the estimated E_a markedly increased following cholesterol treatment. Specifically, E_a increased from 0.34 ± 0.03 eV in the control group to 1.10 ± 0.10 eV at 20 mg/L cholesterol and further to approximately 2.07 ± 0.21 eV at 100 mg/L cholesterol (**Figure 2.12**). No significant difference in E_a was observed between the 100 mg/L and 200 mg/L (2.17 ± 0.39 eV) cholesterol treatments (**Figure 2.12**). Such a significant increase in activation energy is unlikely to be attributable to reduced lipid diffusion, as the E_a for lipid diffusion typically falls within two orders of magnitude lower (Venable et al., 2017). Furthermore, intracellular cholesterol levels in *S.* MR-1 cells remained unchanged following electrochemical measurements, consistent with

pre-activation levels (**Figure 2.9.C**). These findings strongly suggest that the lateral diffusion and transient collision of OMCs play a critical role in mediating efficient inter-protein electron transfer within the biofilm matrix.

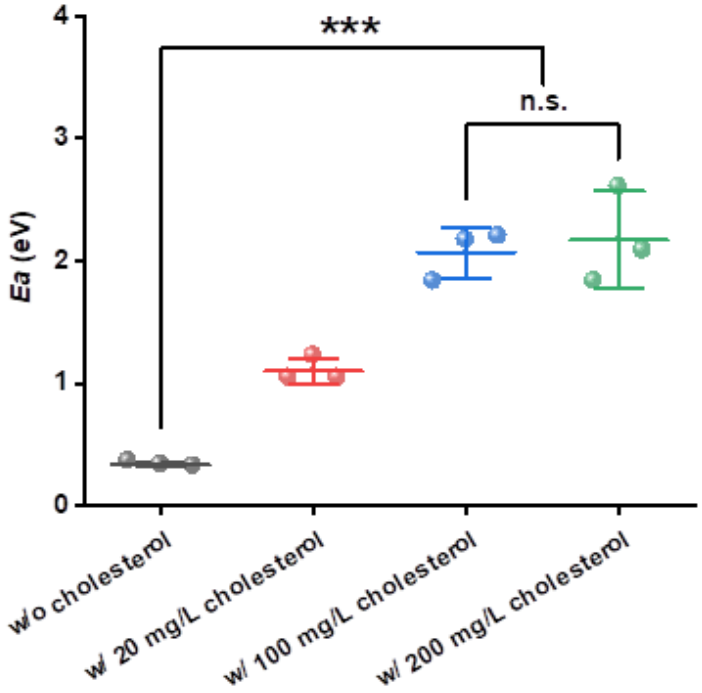

Figure 2.12. E_a in the absence and presence of cholesterol is presented as means ± s.d. (n = 3). n.s., not significant, ***p < 0.001.

Additionally, we validated that the cholesterol does not impact the inter-heme coupling in OMCs with the CD spectroscopy (Berova et al., 2007). To assess whether cholesterol or flavins impact the structural configuration of OMCs, we employed whole-cell CD difference spectroscopy focused on the Soret region (~420 nm), which selectively reports on inter-heme excitonic coupling. Unlike conventional UV CD spectroscopy, this method is highly specific to c-type cytochromes and is not significantly affected by non-heme proteins at the cell surface. The absence of notable spectral changes in the presence of cholesterol or flavins indicates that the alignment and electronic environment of hemes in MtrC and OmcA remain largely unaltered. These results support our conclusion that neither cholesterol nor flavins significantly perturb the inter-heme coupling within OMCs under the conditions tested. Given that the stacked ten ferrous porphyrin inside the OMCs has strong Soret absorption of CD

spectra based on the strong exciton coupling effect from the heme coupling, the variation of CD signal reflects the tiny changes of inter-heme distance and spatial orientation (Tokunou et al., 2018). Strong Soret absorption (at ~400-550 nm) observed in CD spectra of WT and OMCs mutants remained unchanged upon incubation in the presence of cholesterol (**Figure 2.13**). These results indicate that cholesterol did not affect the inter-heme coupling within OMCs, strongly supporting our idea that E_a is largely relying on the interprotein electron transfer via diffusion and collision among OMCs.

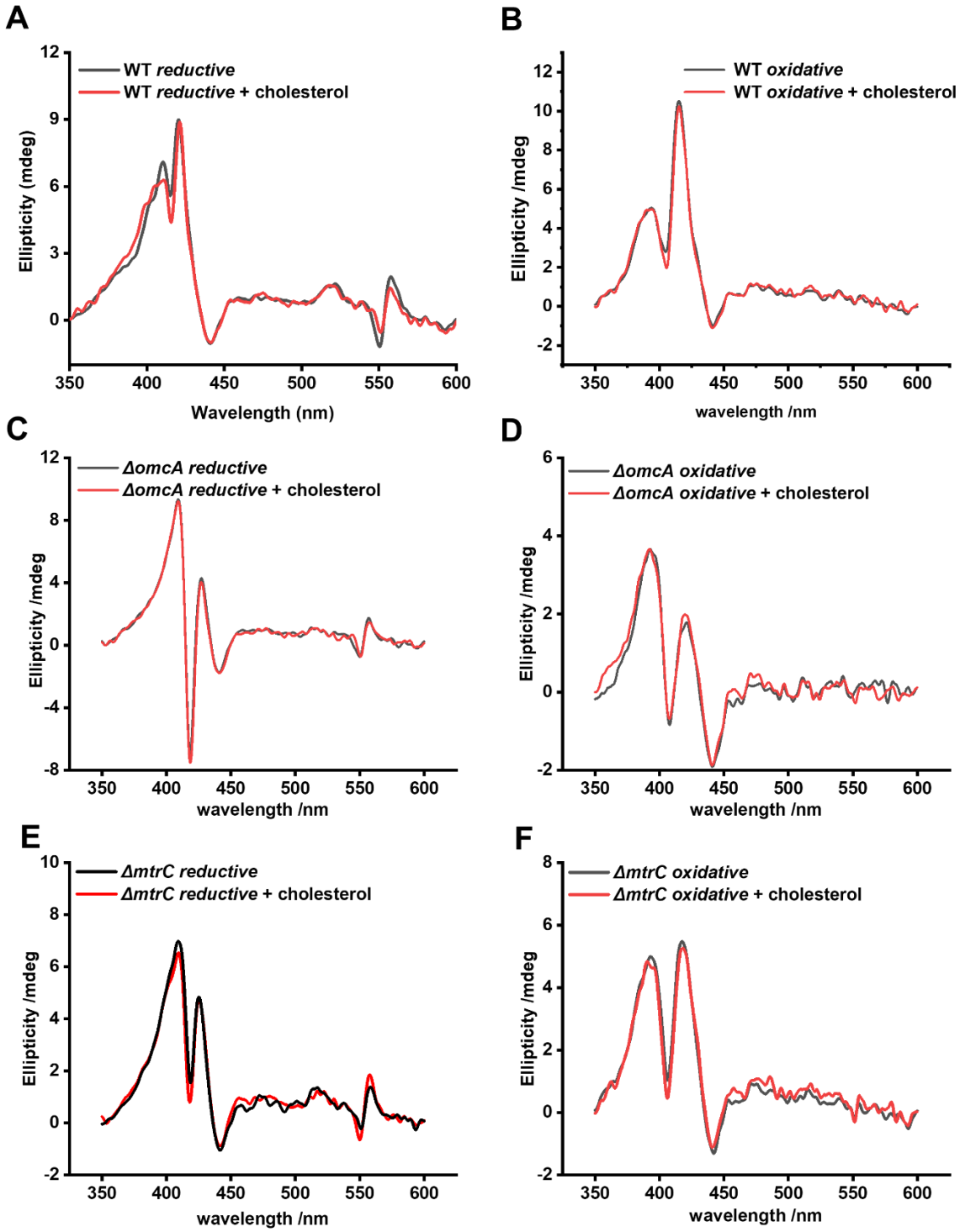

Figure 2.13. CD spectra of *S.* MR-1 WT and mutant strains *ΔomcA* and *ΔmtrC*, measured under oxidative/reductive conditions. An integrating sphere is used here.

2.3.4 Flavin binding reveals the electron transfer pathway in OMCs

To investigate the heme responsible for the interfacial electron transfer in OMCs in biofilm electron conduction, we examined the impact of flavin binding to OMCs. The staggered-cross structure of MtrC and OmcA suggests that four terminal hemes (2, 5, 7, and 10) serve as potential ingress/egress sites (**Figure 2.1.A**). Among these, hemes 2 and 7, being more buried under the barrel motif, selectively bind with non-covalently bound cofactors such as flavins (Hong & Pachter, 2016; Edwards et al., 2020). We hypothesized that flavin binding would block these hemes, reducing electron transfer through them while leaving hemes 5 and 10 open.

Upon increasing riboflavin (RF) to S. MR-1 biofilms on IDE, we observed a decrease in the I_{cond} peak associated with heme-mediated conduction, while the peak current at -150 mV increased in a concentration-dependent manner (**Figure 2.14**). The -150 mV peak potential aligns closely with the redox potential of non-covalently bound RF in OmcA, mediating the oxidized/semiquinone redox reaction (Huang et al., 2023). This suggests that the formation of bound flavin diminishes the I_{cond} contribution from heme redox centers.

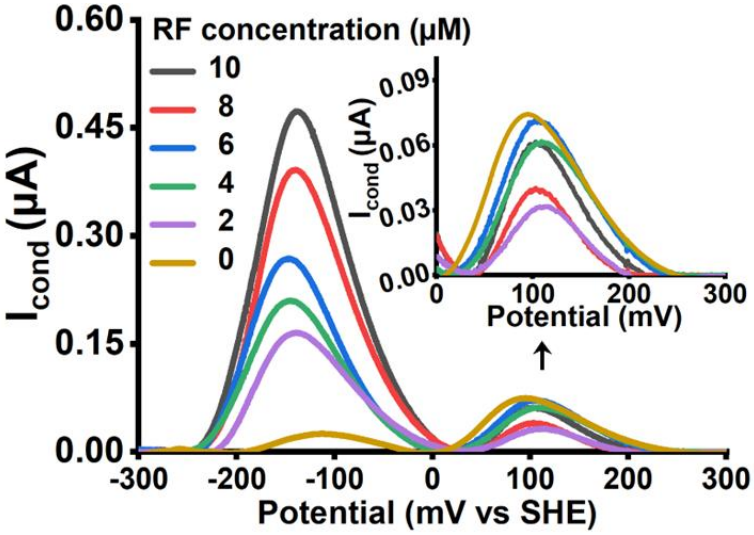

Figure 2.14. I_{cond} of *S.* MR-1 biofilm versus the gate potential at different concentrations of riboflavin (RF).

Supporting this, cell-free RF solutions exhibited I_{cond} peaks at -220 mV, consistent with the oxidized/hydroquinone 2-electron redox reaction (**Figure 2.15.A**). Additionally, treatment with 50 μM carbonyl cyanide m-chlorophenylhydrazone (CCCP) abolished

this peak (**Figure 2.16**), consistent with that RF binding to OMCs is stabilized by active microbial respiration (Pirbadian et al., 2020) and reduced heme center (Okamoto et al., 2013; Edwards et al., 2015; Huang et al., 2023). These findings indicate that the I_{cond} at -150 mV is predominantly mediated by bound RF within OmcA, rather than by free flavin diffusing through the biofilm. Moreover, the bound RF appears to suppress interprotein electron transfer via hemes 2 and 7, redirecting electron conduction through the flavin instead.

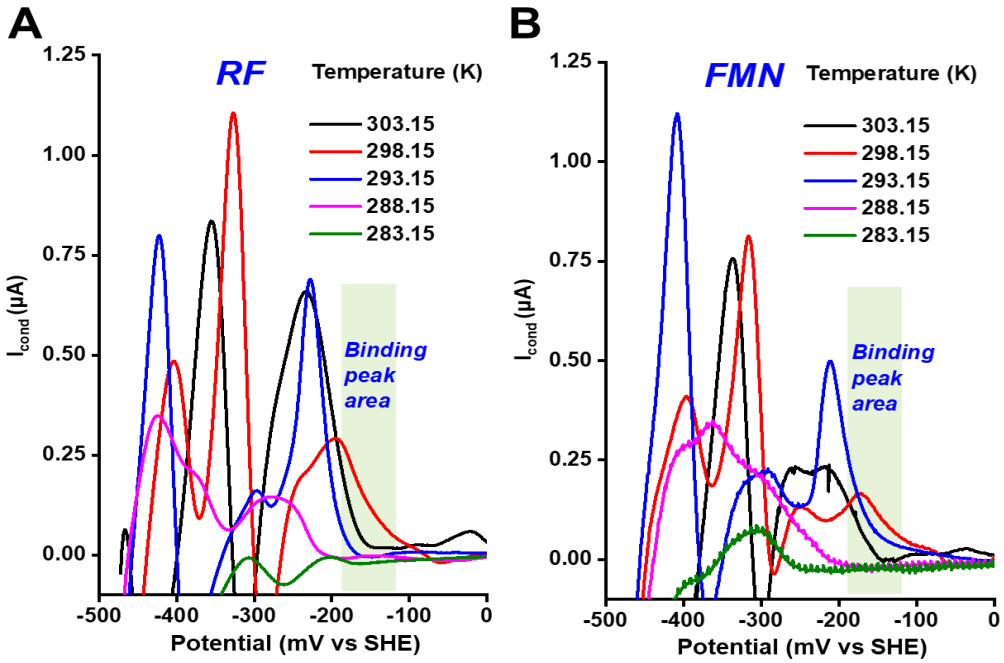

Figure 2.15. Conduction current of (A) 10 μM free RF and (B) 10 μM free flavin mononucleotide (FMN) under different gate potentials and temperatures.

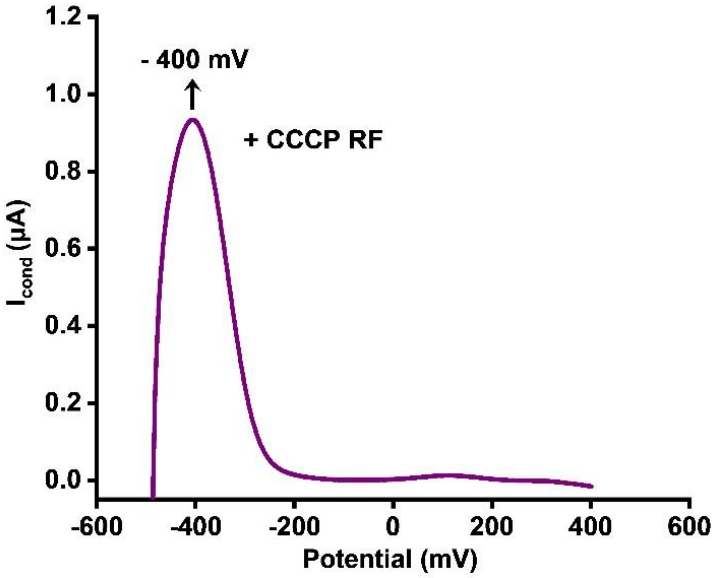

Figure 2.16. Conduction currents of S.MR-1 when adding 50 μM carbonyl cyanide m-chlorophenylhydrazone (CCCP) under 30 °C.

Flavin mononucleotide (FMN) exhibited similar effects, decreasing heme-mediated currents while increasing the −150 mV peak (**Figure 2.17**). FMN specifically binds MtrC, and its dissociation constant (Kd) of ~10 μM is comparable to RF (Okamoto et al., 2014). However, FMN caused a greater reduction in I_{cond} at 2 μM than RF, indicating it may additionally alter inter-OMC interactions, suppressing inter-heme electron transfer.

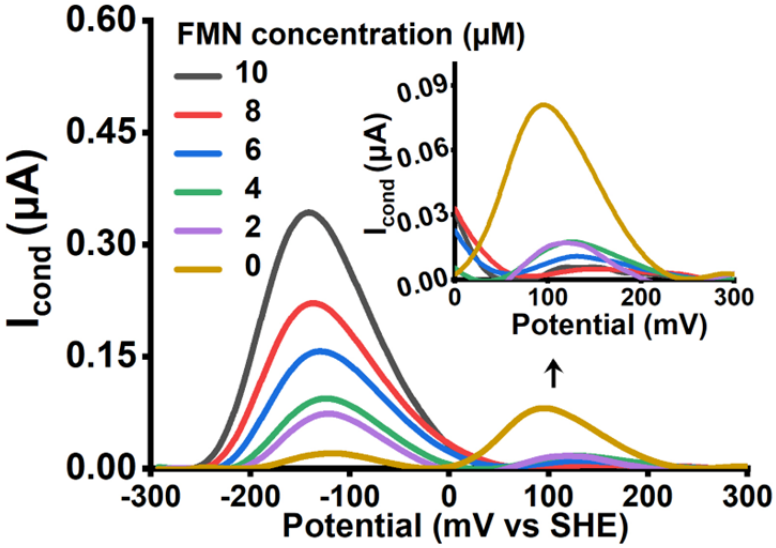

Figure 2.17. I_{cond} of *S.* MR-1 biofilm versus the gate potential at different concentrations of FMN.

Non-covalently bound flavins are unlikely to alter the overall protein structure, as demonstrated in previous studies (Breuer et al., 2015; Edwards et al., 2020). Consequently, hemes 5 and 10 are not expected to be influenced by flavin binding. To validate this hypothesis, we performed CD spectroscopy to assess the heme alignment in MtrC and OmcA using ΔomcA and ΔmtrC cell suspensions, respectively. Under reductive conditions, the CD spectra in the presence of 10 μM FMN and RF were nearly identical to those obtained for *ΔomcA* and *ΔmtrC* in the absence of flavins (**Figure 2.18**). These results confirm that non-covalently bound flavins do not impact the alignment of hemes 5 and 10. Instead, the data strongly suggest that hemes 2 and 7 play a dominant role in electron transfer at the interface between OMCs.

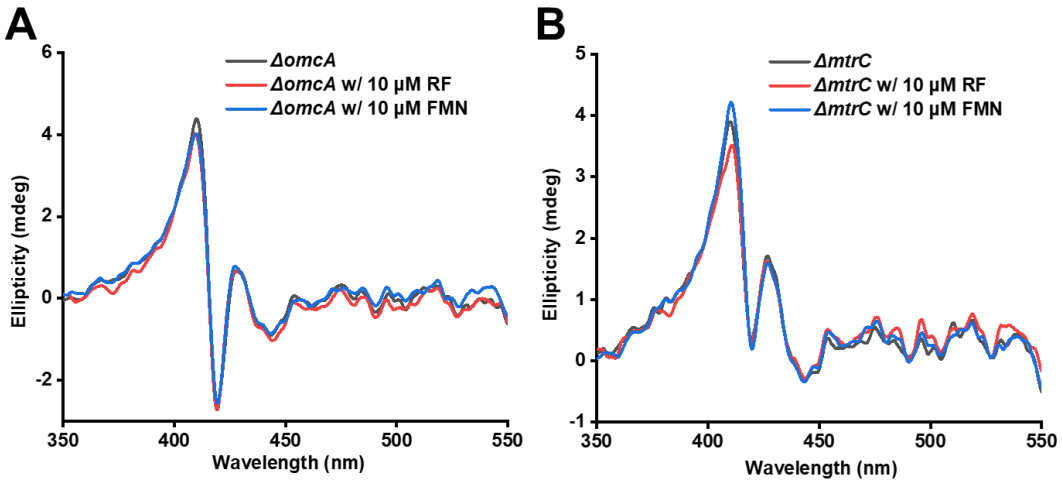

Figure 2.18. CD spectra of *S.*MR-1 mutant strains *ΔomcA* and *ΔmtrC* with flavins addition.

2.3.5 Non-covalently bound flavins decrease the energy barrier among monoclonal OMCs

Post-flavin binding, heme-mediated conduction no longer correlated linearly with temperature, indicating heterogeneity or instability in interprotein interactions (**Figures 2.19 and 2.20**). To distinguish between signals from free flavins and those arising from flavin-bound OMCs, we performed control experiments using RF in the absence of OMCs (**Figure 2.15**). Similarly, no linear correlation was observed in cell-free flavin solutions. These measurements showed irregular, non-specific redox features and lacked a peak at -150 mV, indicating that the well-defined signal observed under experimental conditions is not attributable to free RF alone. Based on this result, and consistent with previous studies reporting RF-heme binding as a dominant electron transfer pathway in OmcA, we attribute the -150 mV peak to RF bound at the heme sites of OmcA. This interpretation supports the conclusion that the enhanced conductivity arises from specific RF-OMC interactions rather than non-specific mediation by free flavins. In contrast, RF- and FMN-mediated conduction maintained linear temperature dependence, with E_a of ~0.3 eV, slightly lower than that in WT in the absence of flavins. These findings highlight that flavin cofactors act as efficient mediators of electron conduction with lower potential barriers than heme cofactors.

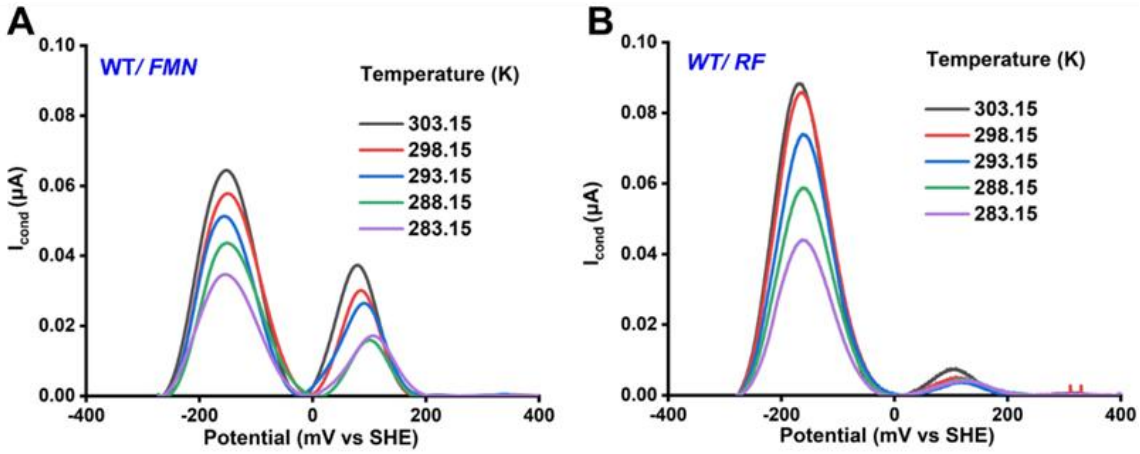

Figure 2.19. Representative temperature dependency of I_{cond} versus the gate potential of WT in the presence of 10 μM RF (A) and FMN (B). Notes: for RF and FMN-mediated conductions, the baseline subtraction was performed using Origin's Peak Analyzer tool with the "User Defined" mode. Points within ±100 mV of the conduction peak potential at each temperature were selected to isolate conduction currents assignable to flavin or

heme-mediated pathways. This method minimizes contributions from freely diffusing flavins or background noise, enabling precise quantification of bound flavin effects on electron conduction.

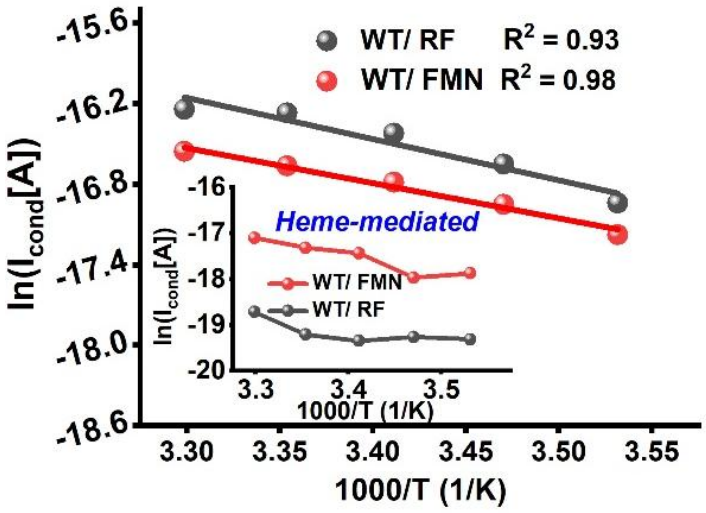

Figure 2.20. Arrhenius-style plots of I_{cond} assignable for heme and flavin peaks in the presence of 10 μM RF and FMN.

In *ΔomcA* or *ΔmtrC* biofilms, E_a significantly increased for clonal interprotein interactions in the absence of flavins (**Figure 2.6.B**). However, the addition of FMN to *ΔomcA* or RF to *ΔmtrC* restored E_a to ~0.3 eV (**Figures 2.21, 2.22 and 2.23**). In contrast, RF to *ΔomcA* or FMN to *ΔmtrC* had no such effect, consistent with the specific binding of RF to OmcA and FMN to MtrC (Huang et al., 2023). These results suggest that flavins thermodynamically enhance interprotein electron transfer between OMCs.

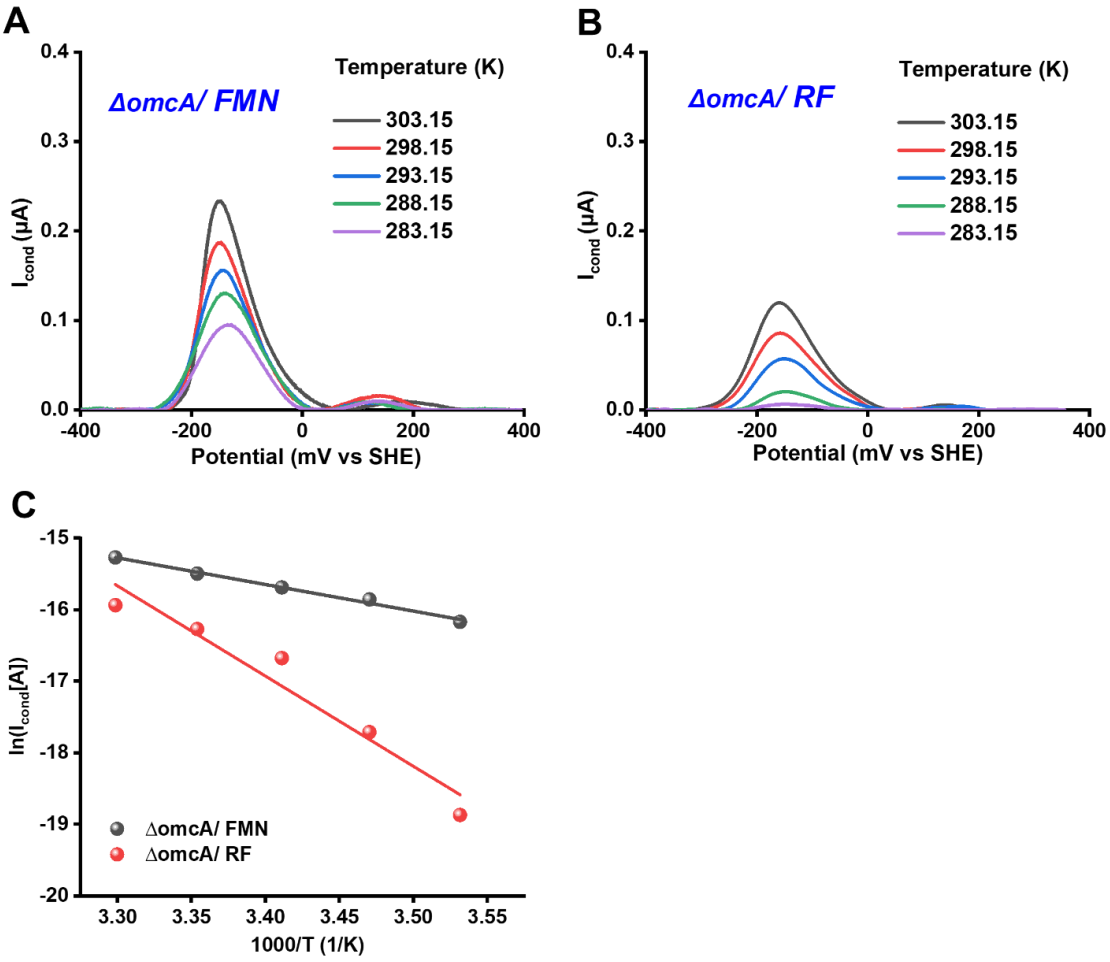

Figure 2.21. Representative temperature dependency of I_{cond} versus the gate potential of *ΔomcA* in the presence of 10 μM FMN (A) and RF (B). Notes: for FMN and RF-mediated conductions, the baseline subtraction was performed using Origin's Peak Analyzer tool with the "User Defined" mode. Points within ±100 mV of the conduction peak potential at each temperature were selected to isolate conduction currents assignable to flavin or heme-mediated pathways. This method minimizes contributions from freely diffusing flavins or background noise, enabling precise quantification of bound flavin effects on electron conduction. (C) Representative Arrhenius-style plots of *ΔomcA* in the presence of 10 μM RF and FMN.

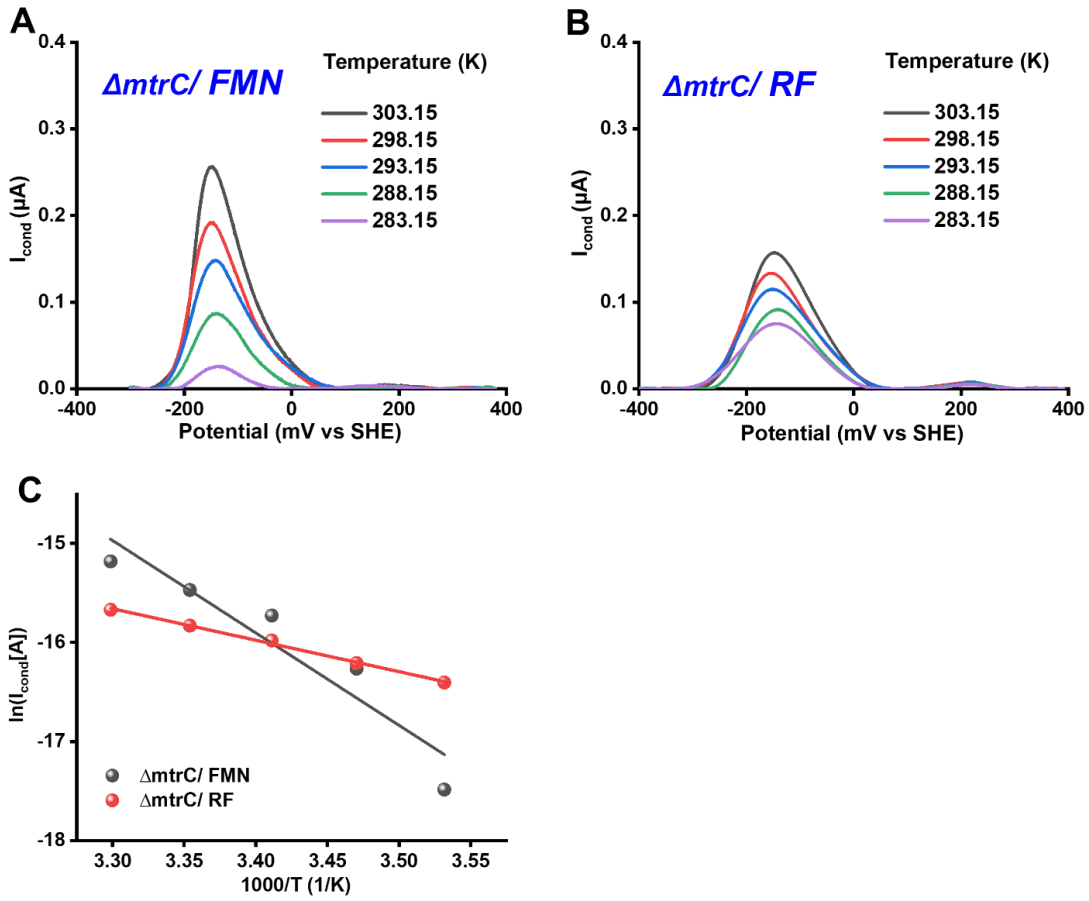

Figure 2.22. Representative temperature dependency of I_{cond} versus the gate potential of *ΔmtrC* in the presence of 10 μM FMN (A) and RF (B). Notes: for FMN and RF-mediated conductions, the baseline subtraction was performed using Origin's Peak Analyzer tool with the "User Defined" mode. Points within ±100 mV of the conduction peak potential at each temperature were selected to isolate conduction currents assignable to flavin or heme-mediated pathways. This method minimizes contributions from freely diffusing flavins or background noise, enabling precise quantification of bound flavin effects on electron conduction. (C) Representative Arrhenius-style plots of *ΔmtrC* in the presence of 10 μM RF and FMN.

Favorable interprotein interactions (WT with RF and FMN, *ΔomcA* with FMN, and *ΔmtrC* with RF) demonstrated high reproducibility with minimal standard error in E_a values (**Figure 2.23**). In contrast, the significant variation observed under other conditions likely reflects lower interprotein affinities. High-affinity interactions

contribute to greater stability, whereas low-affinity interactions, such as those mediated by short linear motifs, are more susceptible to minor changes in environmental conditions, particularly in diffusion- and collision-dominated systems (Benz et al., 2020). These results further support that direct electron transfer among OMCs mediates LDET.

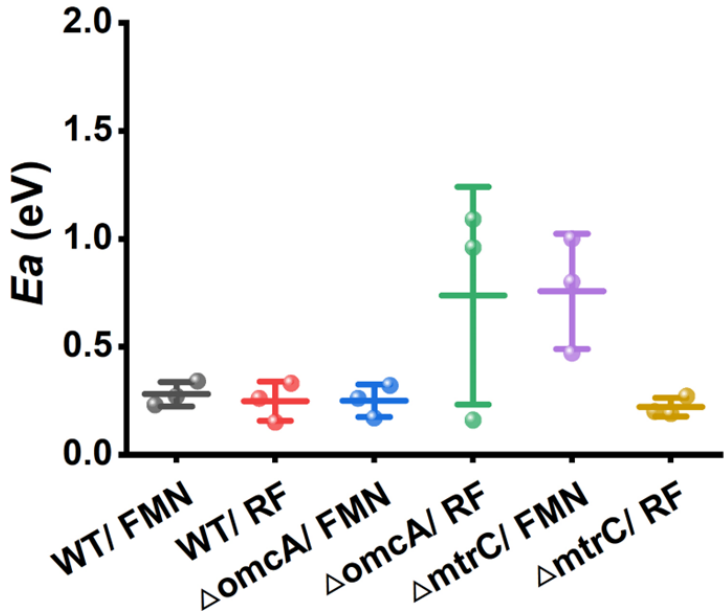

Figure 2.23. E_a and its standard error means (n =3) for I_{cond} assignable to flavin peaks with WT and mutant strains, *ΔmtrC* and Δ*omcA*, in the presence of 10 μM RF and FMN.

2.3.6 Effect of temperature sweeping on the heme alignment in OMCs

Additionally, we confirmed that the temperature dependency of inter-heme coupling in OMCs is negligible using CD spectroscopy. Given that interprotein electron transfer is the rate-limiting step, the heme oxidation state is expected to be more reduced under in vivo conditions. Under reductive conditions, the CD ellipticity of *S*.MR-1 changed by less than 6% across a temperature range of 36°C to 11°C (**Figure 2.24.A**). A similar trend was observed in Δ*omcAll*, which represents the background CD signal for OMCs in the WT (**Figures 2.24.B, 2.24.C and 2.24.D**). This minimal temperature dependency in CD signals indicates that heme alignment within OMCs is not a primary determinant of the temperature dependency of I_{cond}. These findings suggest that inter-heme electron coupling has a negligible impact on E_a, further supporting the conclusion that interprotein interactions between OMCs on the cell surface dominate biofilm electron conduction.

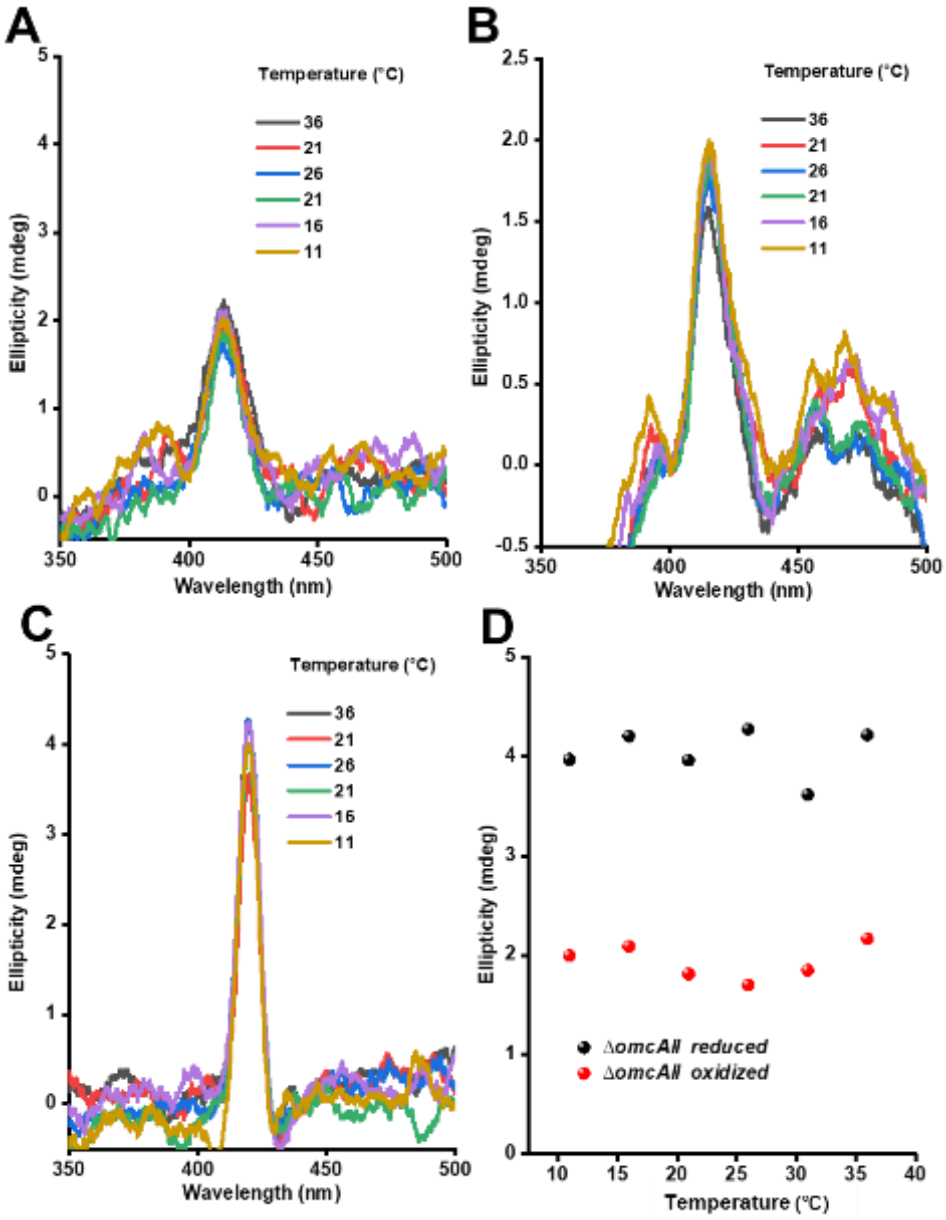

Figure 2.24. (A) CD spectra of *S.* MR-1 measured under reductive condition. The CD spectra from Δ*omcAll* on the cell surface under (B) oxidative and (C) reductive conditions. (D) The ellipticity from Δ*omcAll* on the cell surface under oxidative and reductive conditions across temperature variations.

2.4 Discussion

While LDET through biofilms has been extensively studied at both microbial population and molecular levels, identifying the rate-limiting step has remained a significant challenge (Okamoto et al., 2012; Yates et al., 2015; Xu et al., 2018). Because

the molecular structures of electron-mediating proteins have been resolved, most studies have focused on intraprotein electron transfer processes, often overlooking the critical role of interprotein electron transfer. In this study, we employed consistent growth conditions and preparation protocols for both wild-type and mutant strains and obtained highly reproducible electrochemical data. These results indicate that the observed differences in I_{cond} and E_a arise from intrinsic variations in protein-mediated electron transfer, rather than from differences in extracellular matrix components (e.g., eDNA, protein composition) or indirect conduction pathways. To isolate the contribution of interprotein electron transfer within *S.* MR-1 biofilms, we minimized the influence of indirect EET pathways by thoroughly washing cells before measurement, thereby reducing flavin-mediated background currents. While other components, such as eDNA or redox-active non-cytochrome proteins may be present, the pronounced decrease in conductivity observed in *ΔmtrC*, *ΔomcA*, and *ΔomcAll* mutants strongly supports that OMCs are essential for long-range conduction. Additionally, cholesterol treatment, used to reduce membrane fluidity, further impaired conductivity, underscoring the importance of lateral protein diffusion and cytochrome-cytochrome interactions in facilitating electron transfer.

Although other outer-membrane cytochromes and porin-cytochrome complexes have been proposed to participate in EET, our data support that MtrC and OmcA are the primary contributors under our experimental conditions. The *ΔomcAll* mutant exhibited disordered and non-temperature-responsive conductive behavior (**Figure 2.4**), preventing reliable E_a extraction and indicating a breakdown of thermally activated electron conduction in the absence of outer-membrane cytochromes. Additionally, the expression level of MtrDEF is minimal in the wild type (**Figure 2.1**) (Barchinger et al., 2016), and its deletion does not affect conduction (Myers et al., 2002), unlike the complete current loss observed in mtrA knockouts (Long et al., 2021). Together, these findings confirm that the MtrCAB-OmcA pathway dominates interprotein electron transfer in *S.* MR-1 biofilms.

We provide the first direct evidence that the diffusion and collision of OMCs on the outer membrane mediate electron transfer through a rate-limiting interprotein interaction in biofilms, by genetically deleting OMCs and modulating membrane fluidity. Furthermore, hemes 2 and 7 serve as key interfaces for interprotein electron

transfer among OMCs (**Figures 2.1.A and 2.23**). This finding aligns with the crystal structure of the MtrCAB complex, where heme 10 receives electrons from MtrA (Edwards et al., 2020).

Additionally, lateral electron transfer pathways involving hemes 2 and 7 have been demonstrated in gene-engineered *E. coli*, where enhanced inter-heme coupling at these sites significantly improved lateral electron conduction (Long et al., 2023). These insights provide a stronger foundation for understanding the cross-dagger structure of deca-heme cytochromes, which appear to be evolutionarily optimized for both lateral and vertical electron transfer against the outer membrane, facilitating biofilm development on electron acceptor surfaces.

The present study also demonstrates that the affinity between OmcA and MtrC facilitates LDET in biofilms, providing insight into mechanisms that regulate electron transfer pathways and kinetics on the outer membrane (**Figure 2.6**). While the diffusion of OMCs on the membrane of *S.* MR-1 has been previously observed using quantum dot-based imaging techniques (Okamoto et al., 2014), stoichiometric electron hopping among OMCs has been generally assumed. Our findings suggest that the affinity between OmcA and MtrC likely originates from structural compatibility near hemes 2 and 7. Given that interprotein interactions often involve conformational changes, validating and elucidating this interaction will require advanced protein docking analyses or co-crystallization studies of OmcA and MtrC (Dobbins et al., 2008; Edwards et al., 2020; Tsuchiya et al., 2022). This novel insight could significantly advance our understanding of the dynamic alignment of heme groups within the unique deca-heme cytochrome complexes in vivo (Louro et al., 2001; Okamoto et al., 2012; Gu et al., 2021).

Flavin binding to OMCs thermodynamically enhances electron exchange and increases the interprotein affinity between clonal protein pairs, such as OmcA and MtrC, interactions that are otherwise less favorable in the absence of flavins (**Figure 2.23**). By increasing interprotein affinity, flavin binding improves the efficiency of electron exchange via diffusion and collision. In addition to the above-mentioned interest in interprotein interaction, these findings suggest that the presence of flavins enhances electron transfer within biofilms both qualitatively and quantitatively, underscoring the importance of optimizing protein interfaces. Given the natural accumulation of secreted

flavins, such as RF and FMN (Edel et al., 2021), within *S.* MR-1 biofilms, the organism appears to utilize a low-barrier, high-stability electron conduction mechanism for biofilm maturation. Spectroscopy in the Soret region further confirmed that neither flavin binding nor cholesterol altered inter-heme excitonic coupling, validating that changes in E_a arise from dynamic protein interactions rather than structural perturbations.

These findings open new avenues for leveraging synthetic biology to integrate flavin biosynthetic pathways, enabling the creation of highly conductive biofilms for biocatalysis. Furthermore, targeted genetic modifications to MtrC or OmcA, coupled with the identification of more effective bound cofactors than flavins, could further enhance electron transfer rates in biofilm systems by optimizing interprotein electron transfer (Edwards et al., 2015; Tokunou et al., 2019). The significance of protein interfaces in mediating efficient electron transfer is also evident in other LDET systems, such as the protein nanowires in *G. sulfurreducens.* species (Okamoto et al., 2012), suggesting a potentially universal mechanism for LDET kinetics in biofilms.

In conclusion, while significant progress has been made in elucidating the roles of MtrC and OmcA in EET, our study challenges the long-standing assumption that intraprotein electron transfer within OMCs is the rate-limiting step for biofilm electron conduction. Instead, we identified key heme centers facilitating dominant inter-OMC electron transfer pathways, providing a new perspective on the mechanisms governing biofilm conductivity. These findings enhance our understanding of biofilm electron conduction and pave the way for engineering highly conductive biofilms through targeted protein interface modifications. Such advancements hold great promise for the development of next-generation bioelectric devices, including organic electronic transistors, poised to drive future innovations.

2.5 References

Barchinger, S. E., Pirbadian, S., Sambles, C., Baker, C. S., Leung, K. M., Burroughs, N. J., El-Naggar, M. Y., & Golbeck, J. H. (2016). Regulation of gene expression in *Shewanella oneidensis* MR-1 during electron acceptor limitation and bacterial nanowire formation. *Applied and Environmental Microbiology*, *82*(17), 5428-5443.

Benz, C., Kassa, E., Tjärnhage, E., Lind, S. B., & Ivarsson, Y. (2020). Identification of Cellular Protein–Protein Interactions. In A. Tavassoli (Ed.), *Inhibitors of Protein–Protein Interactions* (pp. 0). The Royal Society of Chemistry.

Berova, N., Di Bari, L., & Pescitelli, G. (2007). Application of electronic circular dichroism in configurational and conformational analysis of organic compounds. *Chemical Society Reviews*, *36*(6), 914-931.

Breuer, M., Rosso, K. M., & Blumberger, J. (2015). Flavin binding to the deca-heme cytochrome mtrc: insights from computational molecular simulation. *Biophysical journal*, *109*(12), 2614-2624.

Chen, H., Simoska, O., Lim, K., Grattieri, M., Yuan, M., Dong, F., Lee, Y. S., Beaver, K., Weliwatte, S., & Gaffney, E. M. (2020). Fundamentals, applications, and future directions of bioelectrocatalysis. *Chemical Reviews*, *120*(23), 12903-12993.

Chong, G. W., Pirbadian, S., Zhao, Y., Zacharoff, L. A., Pinaud, F., & El-Naggar, M. Y. (2022). Single molecule tracking of bacterial cell surface cytochromes reveals dynamics that impact long-distance electron transport. *Proceedings of the National Academy of Sciences*, *119*(19), e2119964119.

Dobbins, S. E., Lesk, V. I., & Sternberg, M. J. (2008). Insights into protein flexibility: the relationship between normal modes and conformational change upon protein–protein docking. *Proceedings of the National Academy of Sciences*, *105*(30), 10390-10395.

Eaton, L., Erdos, G., Vreeland, N., & Ingram, L. (1981). Failure of *Escherichia coli* to alter its fatty acid composition in response to cholesterol-induced changes in membrane fluidity. *Journal of bacteriology*, *146*(3), 1151-1153.

Edel, M., Sturm, G., Sturm-Richter, K., Wagner, M., Ducassou, J. N., Couté, Y., Horn, H., & Gescher, J. (2021). Extracellular riboflavin induces anaerobic biofilm formation in *Shewanella oneidensis*. *Biotechnology for biofuels*, *14*(1), 130.

Edwards, M. J., White, G. F., Butt, J. N., Richardson, D. J., & Clarke, T. A. (2020). The crystal structure of a biological insulated transmembrane molecular wire. *Cell*, *181*(3), 665-673. e610.

Edwards, M. J., White, G. F., Norman, M., Tome-Fernandez, A., Ainsworth, E., Shi, L., Fredrickson, J. K., Zachara, J. M., Butt, J. N., & Richardson, D. J. (2015). Redox linked flavin sites in extracellular decaheme proteins involved in microbe-mineral electron transfer. *Scientific Reports*, *5*(1), 11677.

Ginez, L. D., Osorio, A., Vázquez-Ramírez, R., Arenas, T., Mendoza, L., Camarena, L., & Poggio, S. (2022). Changes in fluidity of the *E. Coli* outer membrane in response to temperature, divalent cations and polymyxin-B show two different mechanisms of membrane fluidity adaptation. *The FEBS Journal*, *289*(12), 3550-3567.

Gu, Y., Srikanth, V., Salazar-Morales, A. I., Jain, R., O'Brien, J. P., Yi, S. M., Soni, R. K., Samatey, F. A., Yalcin, S. E., & Malvankar, N. S. (2021). Structure of *Geobacter* pili reveals secretory rather than nanowire behaviour. *Nature*, *597*(7876), 430-434.

Hong, G., & Pachter, R. (2016). Bound flavin–cytochrome model of extracellular electron transfer in *Shewanella oneidensis*: analysis by free energy molecular dynamics simulations. *The Journal of Physical Chemistry B*, *120*(25), 5617-5624.

Huang, W., Long, X., & Okamoto, A. (2023). Enhancement of microbial current production by riboflavin requires the reduced heme centers in outer membrane cytochromes in *Shewanella oneidensis* MR-1. *Electrochimica Acta*, *464*, 142860.

Kumar, A., Hsu, L. H.-H., Kavanagh, P., Barrière, F., Lens, P. N., Lapinsonnière, L., Lienhard V, J. H., Schroeder, U., Jiang, X., & Leech, D. (2017). The ins and outs of microorganism-electrode electron transfer reactions. *Nature Reviews Chemistry*, *1*(3), 0024.

Logan, B. E., Rossi, R., Ragab, A. a., & Saikaly, P. E. (2019). Electroactive microorganisms in bioelectrochemical systems. *Nature Reviews Microbiology*, *17*(5), 307-319.

Long, X., & Okamoto, A. (2021). Outer membrane compositions enhance the rate of extracellular electron transport via cell-surface MtrC protein in *Shewanella oneidensis* MR-1. *Bioresource Technology*, *320*, 124290.

Long, X., Tokunou, Y., & Okamoto, A. (2023). Mechano-control of Extracellular Electron Transport Rate via Modification of Inter-heme Coupling in Bacterial Surface Cytochrome. *Environmental Science & Technology*, *57*(19), 7421-7430.

Louro, R. O., Catarino, T., LeGall, J., Turner, D. L., & Xavier, A. V. (2001). Cooperativity between electrons and protons in a monomeric cytochrome c3: the importance of mechano-chemical coupling for energy transduction. *ChemBioChem*, *2*(11), 831-837.

Myers, C. R., & Myers, J. M. (2002). MtrB is required for proper incorporation of the cytochromes OmcA and OmcB into the outer membrane of *Shewanella putrefaciens* MR-1. *Applied and Environmental Microbiology*, *68*(11), 5585-5594.

Okamoto, A., Hashimoto, K., & Nakamura, R. (2012). Long-range electron conduction of *Shewanella* biofilms mediated by outer membrane C-type cytochromes. *Bioelectrochemistry*, *85*, 61-65.

Okamoto, A., Hashimoto, K., Nealson, K. H., & Nakamura, R. (2013). Rate enhancement of bacterial extracellular electron transport involves bound flavin semiquinones. *Proceedings of the National Academy of Sciences*, *110*(19), 7856-7861.

Okamoto, A., Nakamura, R., Nealson, K. H., & Hashimoto, K. (2014). Bound flavin model suggests similar electron-transfer mechanisms in *Shewanella* and *Geobacter*. *ChemElectroChem*, *1*(11), 1808-1812.

Pirbadian, S., Chavez, M. S., & El-Naggar, M. Y. (2020). Spatiotemporal mapping of bacterial membrane potential responses to extracellular electron transfer. *Proceedings of the National Academy of Sciences*, *117*(33), 20171-20179.

Shi, L., Dong, H., Reguera, G., Beyenal, H., Lu, A., Liu, J., Yu, H.-Q., & Fredrickson, J. K. (2016). Extracellular electron transfer mechanisms between microorganisms and minerals. *Nature Reviews Microbiology*, *14*(10), 651-662.

Subramanian, P., Pirbadian, S., El-Naggar, M. Y., & Jensen, G. J. (2018). Ultrastructure of *Shewanella oneidensis* MR-1 nanowires revealed by electron cryotomography. *Proceedings of the National Academy of Sciences*, *115*(14), E3246-E3255.

Tokunou, Y., Chinotaikul, P., Hattori, S., Clarke, T. A., Shi, L., Hashimoto, K., Ishii, K., & Okamoto, A. (2018). Whole-cell circular dichroism difference spectroscopy reveals an in vivo-specific deca-heme conformation in bacterial surface cytochromes. *Chemical Communications*, *54*(99), 13933-13936.

Tokunou, Y., Saito, K., Hasegawa, R., Nealson, K., Hashimoto, K., Ishikita, H., & Okamoto, A. (2019). Basicity of N5 in semiquinone enhances the rate of respiratory electron outflow in. *Shewanella oneidensis*, 68-93.

Tsuchiya, Y., Yamamori, Y., & Tomii, K. (2022). Protein–protein interaction prediction methods: from docking-based to AI-based approaches. *Biophysical Reviews*, *14*(6), 1341-1348.

Venable, R. M., Ingólfsson, H. I., Lerner, M. G., Perrin, B. S., Jr., Camley, B. A., Marrink, S. J., Brown, F. L. H., & Pastor, R. W. (2017). Lipid and Peptide Diffusion in Bilayers: The Saffman–Delbrück Model and Periodic Boundary Conditions. *The Journal of Physical Chemistry B*, *121*(15), 3443-3457.

Xu, S., Barrozo, A., Tender, L. M., Krylov, A. I., & El-Naggar, M. Y. (2018). Multiheme cytochrome mediated redox conduction through *Shewanella oneidensis* MR-1 cells. *Journal of the American Chemical Society*, *140*(32), 10085-10089.

Yates, M. D., Golden, J. P., Roy, J., Strycharz-Glaven, S. M., Tsoi, S., Erickson, J. S., El-Naggar, M. Y., Barton, S. C., & Tender, L. M. (2015). Thermally activated long range electron transport in living biofilms. *Physical Chemistry Chemical Physics*, *17*(48), 32564-32570.

Chapter 3. Outer membrane vesicles facilitate biofilm development by enhancing electron conduction in *Porphyromonas gingivalis* biofilm

3.1 Introduction

The formation of bacterial aggregates provides significant survival advantages (Hall-Stoodley et al., 2004), such as the concentration of substrates and enhanced resistance to antimicrobial agents (Flemming et al., 2002; Stewart et al., 2008; Poole et al., 2012). To achieve these survival benefits, microorganisms actively produce adhesive factors, including polymers and membrane vesicles (MVs), to facilitate aggregation and biofilm formation (Schooling et al., 2006; Wang et al., 2015). However, in oral biofilm environments, pathogenic bacteria are known to experience accumulated reductive stress (Marquis et al., 1995; Steeves et al., 2011; Kesarwala et al., 2016; Džunková et al., 2018), which can shift the redox balance of substrates like NADH, thereby impeding metabolic activity. Paradoxically, studies using meta-transcriptomic analysis have shown that obligate anaerobic bacteria residing within biofilms often maintain high metabolic activity (Walters et al., 2003; Stewart et al., 2008).

Understanding how bacteria sustain metabolic activity within biofilms has been a long-standing focus, especially in medical fields where biofilm control is crucial. Recently, extracellular electron transfer (EET) has emerged as a potential strategy microorganisms use to address this fundamental challenge (Gray et al., 2005; Shi et al., 2016; Glasser et al., 2017). By expelling reductive power to the oxidative environment outside the biofilm, certain bacteria can maintain metabolic activity; for instance, they may utilize conductive protein nanowires (Reguera et al., 2005) or small molecules (Okamoto et al., 2014; Light et al., 2018), like phenazines, to make long-distance extracellular electron (LDET), thereby alleviating intracellular reductive stress (Saunders et al., 2020).

Environmental bacteria have been observed to form conductive chains of MVs via membrane-bound redox enzymes, acting as nanowires that facilitate intercellular and LDET (Okamoto et al., 2012; Schwechheimer et al., 2015; Deng et al., 2018; Naradasu et al., 2021; Dahl et al., 2022). While this phenomenon has only been documented in

environmental species, pathogenic bacteria that rely on MVs for biofilm formation remain unexplored in this context (Begić et al., 2020; Jeong et al., 2024). Given that MVs promote cell-to-cell adhesion (Camussi et al., 2010; Hasegawa et al., 2015), they may also serve as a suitable pathway for intercellular electron transfer (Liu et al., 2019; Yu et al., 2023). If MVs, which are ubiquitous in pathogenic biofilms, facilitate biofilm activation via inter-enzyme electron transfer, then inhibiting the specific process could offer a novel biofilm control strategy.

Porphyromonas gingivalis (PG), a keystone pathogen in biofilm-related diseases, is capable of sustaining metabolic activity through EET (Naradasu et al., 2019 and 2022). Moreover, PG vesicles are not simply by-products of cell lysis but are actively produced through membrane blebbing (Naradasu et al., 2021). This study aims to elucidate the role of these proactively produced MVs in biofilm electron conduction and to explore the possibility of biofilm control by targeting this process. Using an interdigitated electrode (IDE) with 10 μm gap, we will measure biofilm electron conduction and the impact of OMVs addition, identify key proteins within the vesicles, and investigate biofilm formation on calcium discs. By revisiting the connection between MVs, biofilm formation, and metabolic activity, this study will open potential avenues for biofilm management.

3.2 Methods

3.2.1 The microbe culture conditions

PG grew anaerobically in 20 mL Gifu Anaerobic Medium (GAM) for 48 hours at 37 °C. To maintain microbial circumstances anaerobically, GAM was purged with CO_2: N_2 (20:80 v/v) mixed gas for 30 min before cell cultivation. Cell suspensions were centrifuged at 7500 rpm and 4°C for 5 min, then cells were washed two times with a defined medium (DM) under the same centrifugal conditions, resulting in an OD_{600} of 0.5. The components of DM (per liter) are $NaHCO_3$ 2.5 g, $CaCl_2 \cdot 2H_2O$ 0.08 g, NH_4Cl 1.0 g, $MgCl_2 \cdot 6H_2O$ 0.2 g, NaCl 10 g, HEPES 7.2 g and yeast extract 0.5 g.

3.2.2 Outer membrane vesicles (OMVs) preparation and quantification

PG solution was cultured using the method previously described. Cell suspensions were centrifuged at 7800 rpm and 4°C for 10 min, then the cell supernatants were filtered through a 0.22 μm filter to remove cell debris. The filtrates were ultracentrifuged at 210,000 × g and 4°C for 2 h. After the ultracentrifugation, the supernatants gradually drained away, and the inner surface of the tube was softly cleansed using 1×phosphate-buffered saline (1×PBS). Subsequently, the aggregated pellets adhered to the tube were collected using 1×PBS through pipetting, resulting in OMVs solutions, and stored at 4°C until further use. OMVs solutions underwent a fourfold dilution, following which the dimensions and concentration of the nanoparticles were quantified utilizing the nanoparticle flow cytometry (Nano Analyzer, NanoFCM Co. Ltd.).

3.2.3 Transmission electron microscopy

OMVs samples were placed onto formvar-coated copper grids and negatively stained with 2% phosphotungstate acid solution (pH = 7.0) for 60 sec. The grids were analyzed and visualized using a JEM-1400 microscope (JEOL Ltd.) operated at an acceleration voltage of 100 kV and imaged by an EM-14830RUBY2 CCD camera (JEOL Ltd.).

3.2.4 Integrated detection of OMVs redox activity and protein identification using TMBZ staining, SDS-PAGE, and LC-MS

To assess the redox activity of OMVs, a combination of TMBZ staining, SDS-PAGE and LC-MS were utilized. For redox protein detection, 10 μL of OMVs solution was first denatured by boiling with 10 μL of 2×SDS sample buffer at 95°C for 10 minutes. Additionally, 15 μL of OMVs solution was mixed with 5 μL of 4×heme buffer for redox protein detection. Samples (10 μL) were then mixed with 2 μL of PageRuler™ Plus Prestained Protein Ladder, loaded into polyacrylamide gel wells, and electrophoresis was performed at 120 V for 100 minutes. The gel was stained with freshly prepared TMBZ solution (0.6% TMBZ in 0.25 M sodium acetate buffer, pH 5.0) for 30 minutes, followed by the addition of 0.2% H_2O_2. Redox proteins catalyzed TMB oxidation, forming blue bands. The reaction was stopped after 10-15 minutes with distilled water, and the absorbance at 595 nm was measured to quantify redox activity. The gel was subsequently analyzed for protein presence.

For further identification of redox proteins, digested peptides from OMVs were analyzed using nano-liquid chromatography coupled with tandem mass spectrometry (LC-MS) on a Q-exactive mass spectrometer. Peptide separation was achieved using a C18 analytical column with a linear gradient of 0–35% buffer B (100% acetonitrile and 0.1% formic acid) at a flow rate of 300 nL/min for 10 minutes. MS and MS/MS spectra were acquired in a data-dependent TOP10 method, and the resulting MS/MS data were searched against an in-house PG database using the MASCOT server (v2.5), with peptide mass tolerance of ±15 ppm, fragment mass tolerance of ±20 mmu, up to three missed cleavages, and ESI-TRAP as the instrument type.

Additionally, Functional analysis of all identified potential redox proteins detected from the UniProt database (https://www.uniprot.org/).

3.2.5 Electrochemical and thermal activation energy (E_a) measurements in an interdigitated electrode (IDE) system

These were conducted using an IDE configuration with both source and drain electrodes separated by 10 μm gaps in a single-chamber bioreactor. Platinum wire served as the counter electrode, while Ag/AgCl (saturated with 3M KCl) was utilized as the reference electrode. The bioreactor contained 4.5 mL DM, adding 0.5 mL of 100 mM histidine and was sparged with N_2 gas for 30 minutes to exhaust O_2. The I_{cond} in the IDE array was determined by computing the difference between the source (E_S) currents and drain (E_D) currents under a voltage difference condition ($E_{SD} = E_D - E_S = 0.02$ V), within the electrochemical measurements at the stable current scanning rate of 1 $mV \cdot s^{-1}$. The range of potential voltage scanning was from - 0.48 V to 0.5 V and - 0.50 V to 0.48 V, respectively. The I_{cond} was calculated by the following equation (E1): (17)

$$I_{cond} = (I_{drain} - I_{source}) / 2 \qquad (1)$$

I_{drain} and I_{source} were expressed by the current profile of CV, subtracting I_{source} from I_{drain} under a voltage difference condition.

Thermal activation energy was determined by measuring the temperature dependence of I_{cond}. The I_{cond} was tested for the efficacy of six dependent temperatures: 37, 32, 27, 22, 17 and 12 ℃ in the water bath, respectively. Between CV tests under different temperature conditions, conducting a water bath for approximately fifteen minutes was necessary to ensure the stability of the required solution temperature within the bioreactor. The activation energy was calculated with the classical equation (E2):

$$\ln (I_{cond}) = A - 1000/T \times (E_a/1000k) \qquad (2)$$

where A was a temperature-independent factor, T was the Kelvin temperature (K) and k was the Boltzmann constant.

3.2.6 Citrullination assay

Citrullination assay is based on a homocitrulline/Citrulline Assay Kit (ab242292;

Abcam plc.) for citrullination analysis. First, samples are prepared according to the kit's instructions, followed by the addition of reagent A and reagent B. These reagents allow citrulline or homocitrulline in the samples to react with the chromogenic reagent, forming a blue-green product. The reaction mixture is incubated at 37°C for 1 hour, and absorbance is measured using a colorimetric method at a wavelength of 540 nm. To ensure accuracy, a standard curve is generated using known concentrations of citrulline standards. The absorbance of the samples is compared to the standard curve to calculate the concentration of citrulline. This assay is used to evaluate the citrullination levels of specific proteins, aiming to explore their potential role in cellular signal transduction and biofilm electrical conduction.

3.2.7 Colony Forming Units (CFUs) measurement after IDE assay

1×PBS was used for diluting cell cultures before plating for colony-forming units (CFUs) measurement. Dilutions spanning 6-7 orders of magnitude were plated on BHI agar using 5 μL spots and incubated at 37˚C overnight in an anaerobic culture tank. Colonies were counted with dilution spots containing at least 10 colonies. Then samples for CFU counting were diluted anaerobically in Brain Heart Infusion (BHI) agar plates supplemented with 0.5 mL sterile sheep blood. The plates were incubated at 37˚C anoxically for more than 3 days and then counted.

3.2.8 Biofilm formation assay

The calcium discs, as human teeth, were soaked in 1×PBS for 2 hours, then replaced the GAM culture medium with cell or OMVs suspension and incubated for 24 hours to simulate bacterial attachment to human teeth. The calcium discs are gently washed twice with 1×PBS, added 0.1% crystal violet staining solution, and incubated at 4°C for 1 hours. After that, the stained cells were eluted from the calcium discs using ethanol and acetone (4:1). The biofilm formation on the discs was determined by the absorbance at 590 nm.

3.2.9 Scanning electron microscopy

The calcium discs were removed from the cell suspension and washed twice with 1×PBS, treated with 2.5% glutaraldehyde for 2 hours at 4°C. Following this, the calcium discs were washed three times with double-distilled water. The washed samples were dehydrated using a series of ethanol gradients (25%, 50%, 75%, and 100%) in the same buffer, followed by two exchanges with t-butanol. The samples were then freeze-dried under vacuum. The dried samples were coated with evaporated platinum and observed using a Keyence VE-9800 microscope.

3.3 Results

3.3.1 Biofilm electron conduction generation within *Porphyromonas gingivalis* (PG) biofilm

We first established the electrochemical system for measuring electron conduction in PG biofilms. In a single-chamber, four-electrode system equipped with interdigitated ITO electrodes (Xu et al., 2018) with a 10 μm gap to study electron conduction (**Figure 3.1.A**), I_{cond} between E_S and E_D electrodes was monitored using a potentiostat, upon the incubation of biofilm for 24 h of incubation at + 0.2 V vs SHE (Figure 1A).

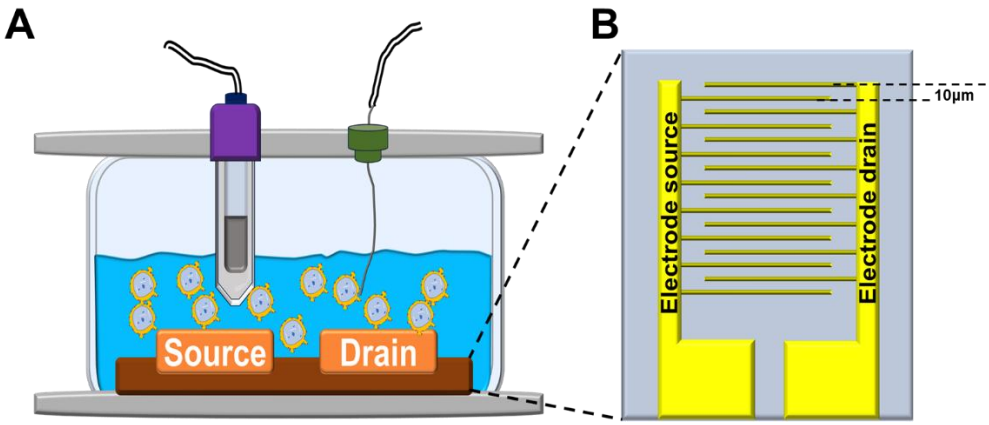

Figure 3.1. Schematic illustration of the electrochemical system for measuring electrical conduction in *Porphyromonas gingivalis* (PG) biofilm. (A) Diagram of the experimental setup; (B) Top view of the interdigitated ITO electrode (IDE) array. Yellow regions indicate conductive electrodes, with the left side labeled as the source and the right as the drain. The interdigitated fingers between them enable high-resolution measurement of lateral electron transfer through the biofilm formed by PG cells connecting the two electrodes.

Fluorescence microscopy showed a monolayer biofilm formation on the electrode, bridging the E_D and E_S (**Figure 3.2.A**). Scanning electron microscopy (SEM) showed that abundant nano-sized particles, MVs, were attaching and connecting PG cells in the biofilm incubated on the electrode (**Figure 3.2.B(a)**).

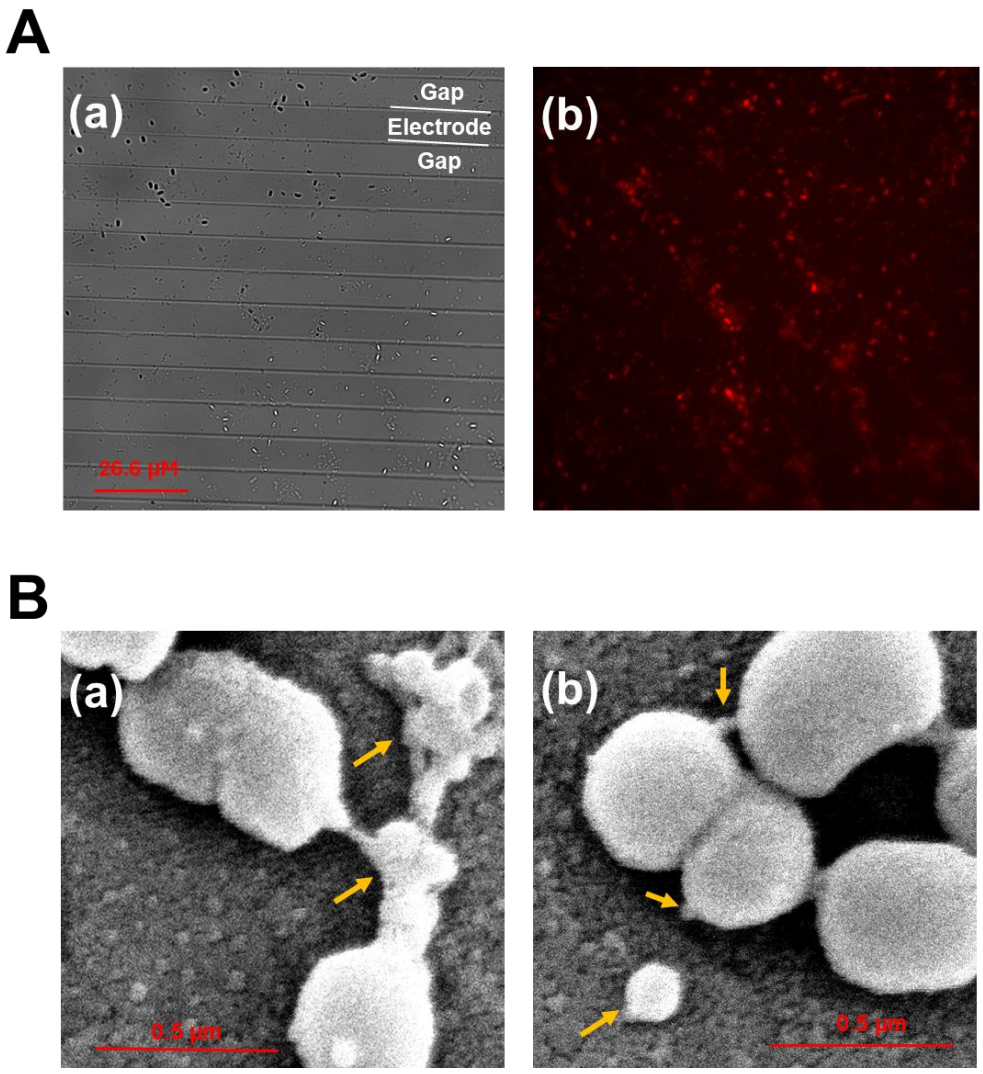

Figure 3.2. Microscopic characterization of PG biofilm formation on interdigitated electrodes (IDE). A (a) Bright-field image showing PG cells distributed along IDE. The labeled electrode and gap regions demonstrate the spatial configuration for biofilm formation and subsequent electron transport measurements. Scale bar: 26.6 μm. A (b) Fluorescence microscopy image of PG cells stained with FM4-64FX, a membrane-selective dye, highlighting the outer membrane structures. The red fluorescence signal confirms widespread cell attachment and biofilm development across the electrode surface. (C). Scanning electron microscopy (SEM) image showing high-resolution morphology of PG cells adhered to the electrode surface before (a) and after (b) changing fresh electrolyte. Scale bar: 0.5 μm. Yellow regions indicate MVs.

We then performed double-electrode measurements using voltammetry, applying a 20-millivolt potential difference (E_D - E_S = 0.02 V) to drive electron movement from the source to the drain electrode. As illustrated in **Figure 3.1**, the oxidation peak for the gate potential (E_G = [E_S + E_D] / 2) was observed at approximately 0 V (vs. Ag/AgCl) in the I_{cond} measurements, with a conduction current of 4.23 ± 0.14 nA (**Figure 3.3.A**), which is a similar extent of current observed in *S.* MR-1, model environmental electrogenic bacteria (Xu et al., 2018). We next examined the contribution of soluble substrate and membrane-bound enzyme to the I_{cond}. We first preincubate the PG cells with 100 mg/L of cholesterol to increase membrane rigidity by embedding cholesterol between the phospholipids before the electrochemical incubation. Upon twenty-four hours of electrochemical incubation, I_{cond} reduced to 0.91 ± 0.35 nA (**Figures 3.3.B and 3.3.D**). In contrast, before and after replacing the supernatant solution to fresh electrolyte, I_{cond} did not show a significant difference (**Figures 3.3.C and 3.3.D**). We observed abundant nano-sized particles that remained in the biofilm after washing (**Figure 3.2.B(b)**). These results indicate that the electron carrier is not a soluble small molecule but a membrane-associated redox enzyme.

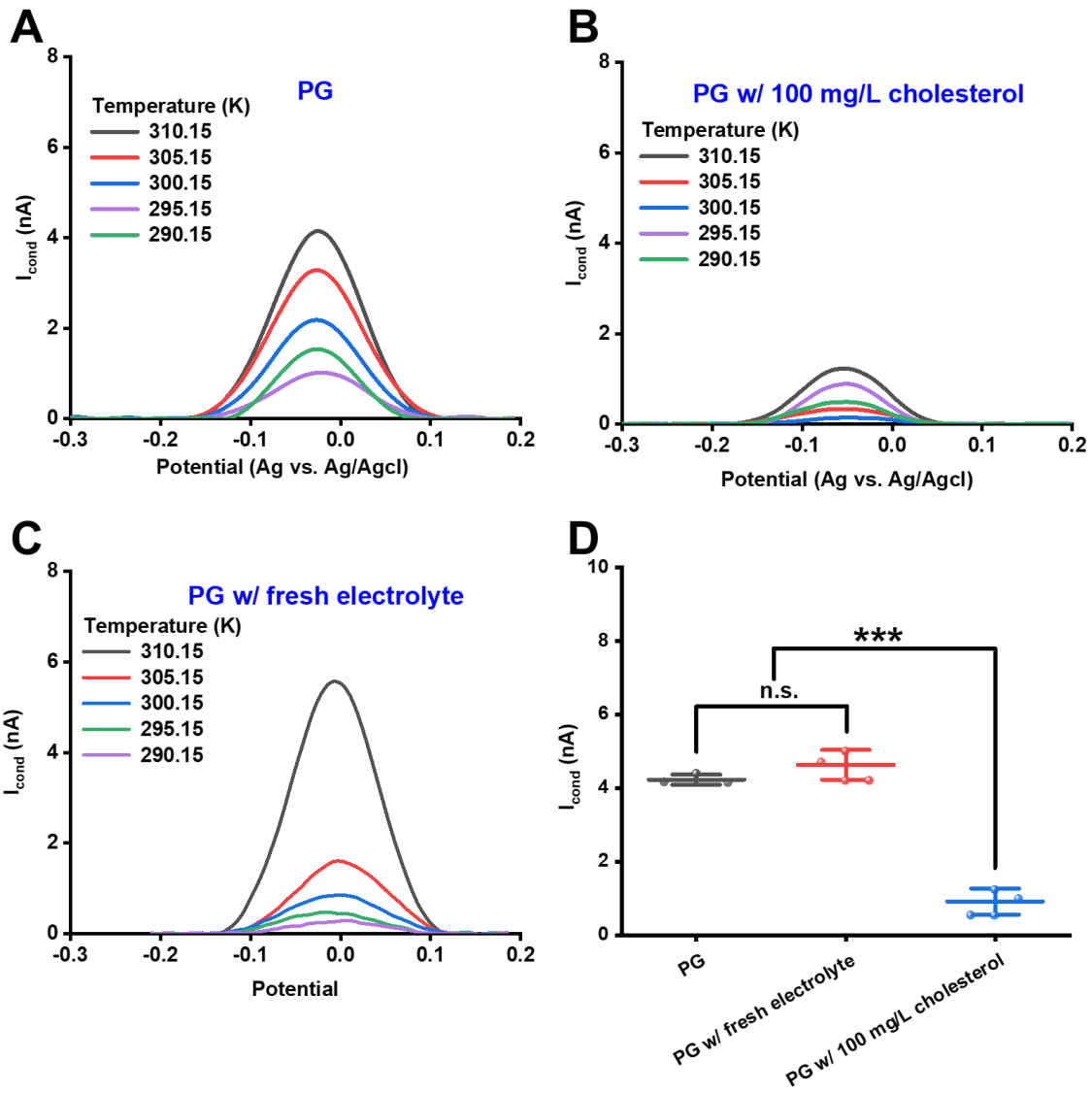

Figure 3.3. The representative PG (A), PG w/ fresh electrolyte (B) and PG w/ 100 mg/L cholesterol (C) Biofilm conduction current (I_{cond}) versus the gate potential under each temperature, calculated by subtracting the source from the drain current in the absence of an electron donor (offset voltage = 20 mV, scan rate and ν = 1 $mV \cdot s^{-1}$). The same tendency was observed in three independent assays. (D) I_{cond} comparison for PG (black), PG with fresh electrolyte (red), and PG with 100 mg/L cholesterol (blue). Data in panel D are presented as means ± s.d. (n = 3). n.s., not significant, and ***, $p < 0.001$ (n = 3).

This insight was further supported by E_a for the electron conduction through the PG biofilm. Lowering the reactor temperature from 37°C to 17°C revealed a linear correlation between ln (I_{cond}) and 1000/T for the untreated PG biofilms, PG w/ fresh electrolyte and cholesterol-treated biofilm (**Figure 2.4.A**), which inhibits membrane fluidity (Eaton et al., 1981). Based on previous studies (Equation 2) (Xu et al., 2018), we used the Arrhenius equation to estimate the higher energy barrier, calculating a semi-empirical thermal E_a of 0.47 ± 0.08 eV and 0.44 ± 0.07 eV for the untreated PG biofilms and the washed biofilm than 0.79 ± 0.04 eV for the cholesterol-treated biofilm (**Figure 2.4.B**). These results highlight the critical role of membrane-bound enzymes in PG biofilms for I_{cond}, suggesting that a low-energy barrier pathway exists when membrane fluidity is not suppressed by cholesterol. These results are aligned with our hypothesis that MVs mediate electron conduction through the biofilm.

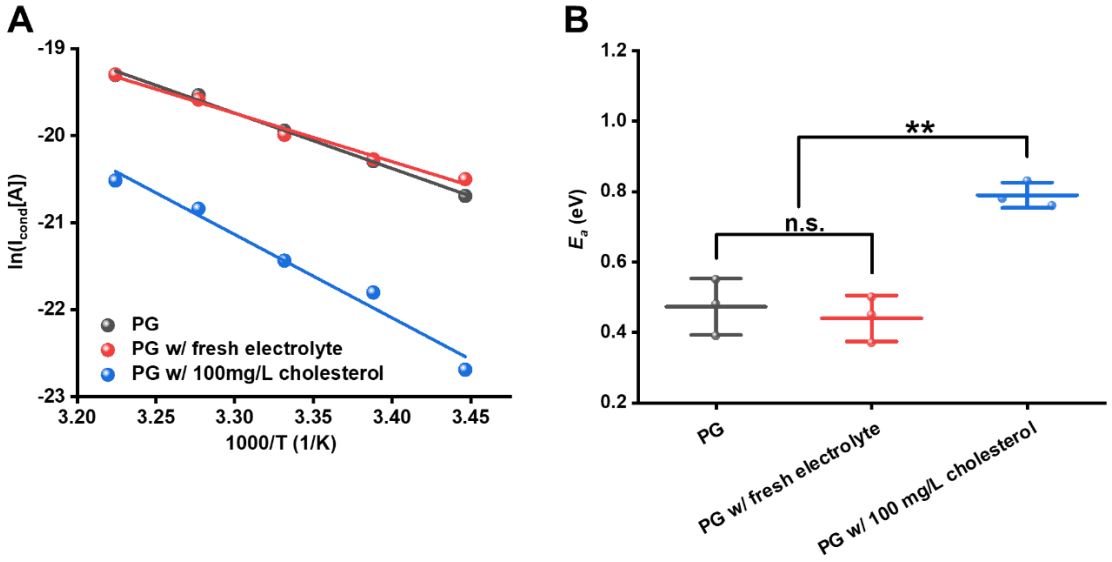

Figure 3.4. (A) Representative Arrhenius-style plots of PG, PG w/ fresh electrolyte and PG w/ 100 mg/L cholesterol. (B) The semi-empirical thermal activation energy (E_a) of PG, PG w/ fresh electrolyte and PG w/ 100 mg/L cholesterol. Data in panel B is presented as means ± s.d. (n = 3). n.s., not significant and **, $p < 0.01$ (n = 3).

3.3.2 PG biofilms electron conduction enhancement via OMVs

Next, to examine the contribution of OMVs for LDET in PG biofilms, we added OMVs isolated from culture medium to evaluate the I_{cond} of PG biofilm. OMVs were isolated using ultracentrifugation (**Figure 3.5.A**), and further purification was not performed. Transmission electron microscopy (TEM) confirmed that the isolated OMVs fraction has negligible cell debris (**Figure 3.5.B**). Upon staining the lipid with DID staining (1, 1'-Dioctadecyl-3,3,3',3'-Tetramethylindodicarbocyanine Perchlorate) (Blachutzik et al., 2012; Lai et al., 2013), the particle size and concentration of the OMVs were characterized using nanoflow cytometry (nanoFCM) (Han et al., 2023; Li et al., 2025). The size of OMVs primarily ranged between 50 and 180 nm, consistent with previous studies(Gui et al., 2016), with a concentration of approximately 2.46 × 10^{10} particles/mL (**Figure 3.5.C**).

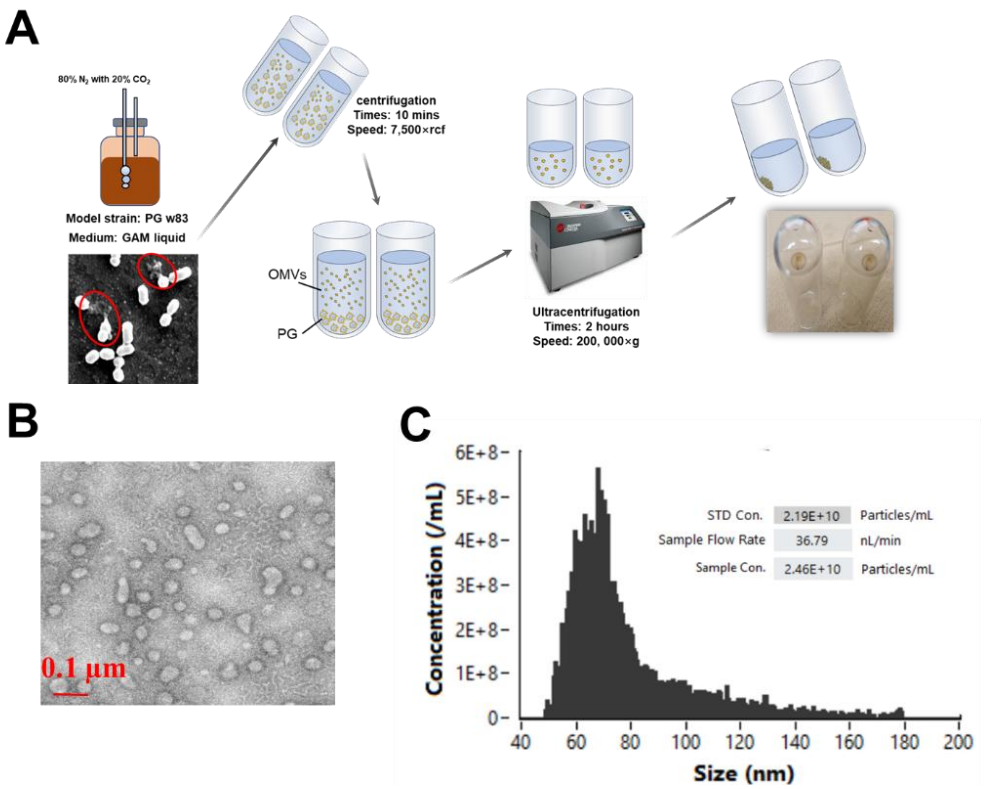

Figure 3.5. Isolation and characterization of OMVs from PG culture. (A) Schematic diagram of OMVs isolation from PG cultures using ultracentrifugation. (B)

Transmission electron microscopy image for isolated OMVs (scale bar = 0.1 μm). (C) Nanoflow cytometry analysis of lipid-stained OMVs.

We mixed 0.5 mL of OMVs and PG cells with a final OD_{600} of 0.5, where the cell versus MVs ratio is 1:100. Electrochemically incubated at + 0.2 V for twenty-four hours. The increased concentration of OMVs in the PG biofilms resulted in a notable enhancement of I_{cond} (**Figure 3.6.A**), generating currents exceeding 15 nA compared to native PG biofilms (**Figure 3.6.B**), associated with a ten-fold increase in the colony-forming unit from biofilm on the electrode (**Figure 3.6.C**). While the more viable cell accumulation is explainable as OMVs enhance intercellular attachment, the I_{cond} increase clearly suggests the electron conduction enhancement rather than facilitating the cellular attachment.

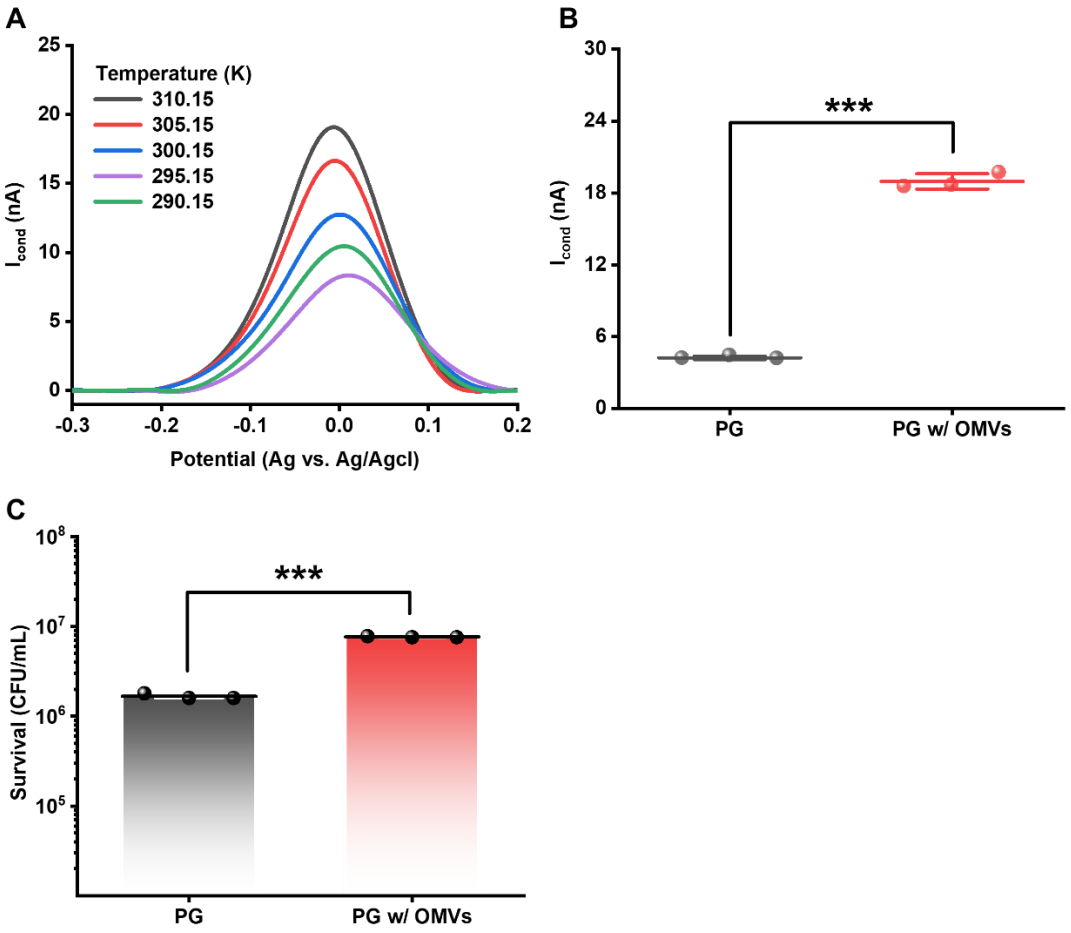

Figure 3.6. (A) The representative PG w/ OMVs for I_{cond} versus the gate potential under

each temperature, calculated by subtracting the source from the drain current without an electron donor (offset voltage = 20 mV, scan rate and ν = 1 mV s^{-1}). The same tendency was observed in three independent assays. (B) I_{cond} comparison for PG (black) and PG w/ OMVs (red). Data in panel B are presented as means ± s.d. (n = 3). ***, $p < 0.001$ (n = 3). (C) Cell survival for PG and PG w/ OMVs by measuring the colony-forming units (CFUs) from the biofilm on the electrode. Data in panel C are presented as means ± s.d. (n = 3). ***, $p < 0.001$ (n = 3).

Furthermore, E_a of PG biofilms significantly decreased by 0.15 eV upon incubation with OMVs, as shown in **Figure 3.7.A and 3.7.B**, indicating that OMVs provided an alternative electron pathway (**Figure 3.7.C**).

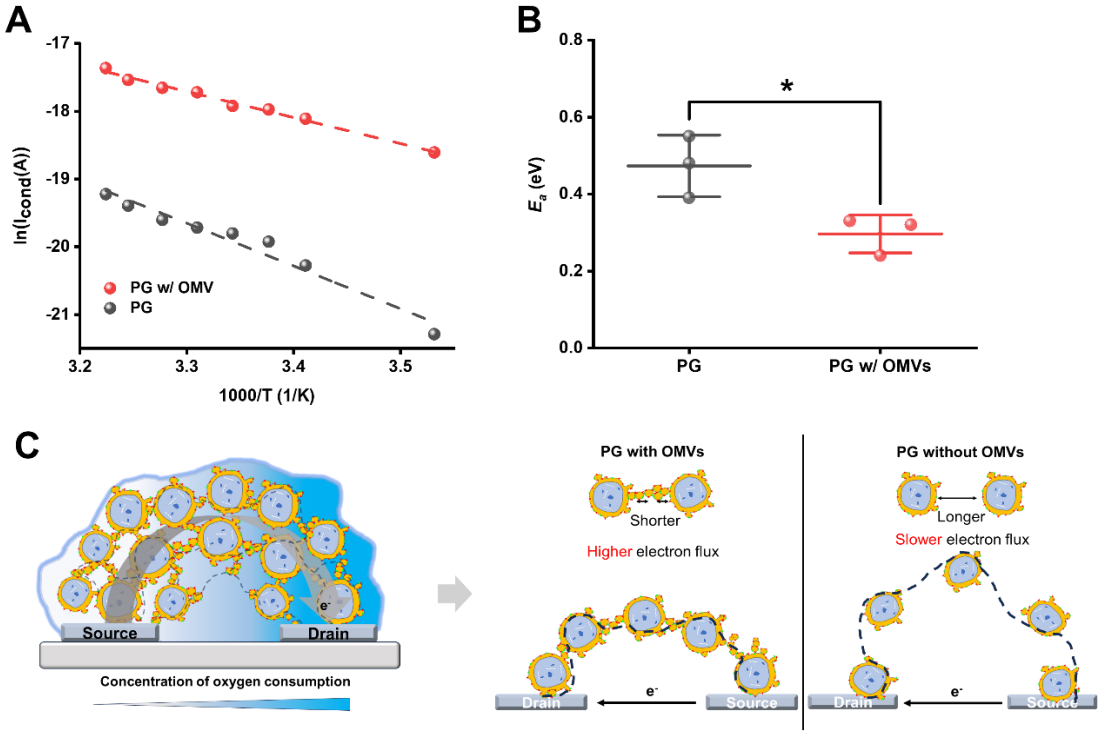

Figure 3.7. (A) Representative Arrhenius-style plots of PG and PG w/ OMVs. (B) The semi-empirical thermal E_a of PG and PG w/ OMVs. Data in panel B is presented as means ± s.d. (n = 3). *, $p < 0.05$ (n = 3). (C) Schematic illustration of OMV-mediated enhancement of PG biofilm electron pathway.

3.3.3 Peptidylarginine deiminase (PPAD) enzyme in OMVs mediates PG biofilm electron conduction

To identify key factors involved in biofilm electron conduction, particularly in OMVs, we conducted a series of assays. The TMBZ-H_2O_2 catalytic assay (Vargas et al., 1993) showed an absorbance of 0.23 at 450 nm, comparable to that of 1 μM cytochrome (**Figure 3.8.A**), suggesting the presence of significant redox-active cargo within OMVs. SDS-PAGE with TMBZ staining revealed a protein band at 27 kDa (**Figure 3.8.B**), indicating a potential redox-active candidate (Thomas et al., 1976; Miller et al., 1984). Subsequent LC-MS analysis identified the protein (**Figure 3.8.C**), and UniProt database analysis ("UniProt: the universal protein knowledgebase," 2017) (**Table 3.1**) indicated that Flavin mononucleotide (FMN) was a cofactor for PPAD, suggesting it may impart redox properties to PPAD, as FMN is a known redox cofactor (Lin et al., 2015) capable of reacting with oxidants (e.g., H_2O_2) in semiquinone or reduced states. No redox-active function was predicted for the other proteins analyzed.

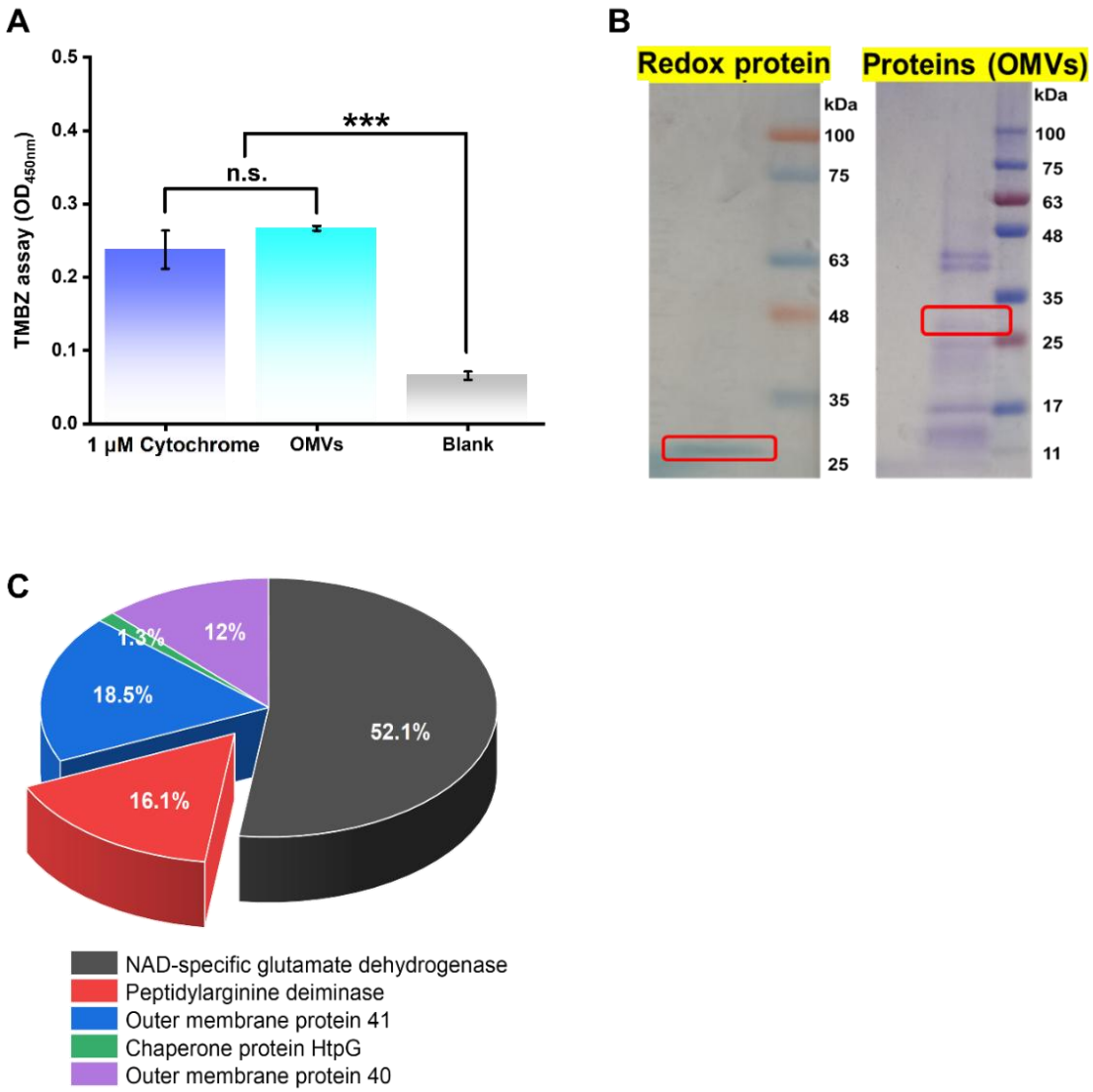

Figure 3.8. Identification of redox-active proteins in OMVs from PG biofilms. (A) TMBZ-H_2O_2 oxidation assay indicates the presence of redox-active substances in OMVs. (B) SDS-PAGE analysis with TMBZ staining (left) and Coomassie blue staining (right) of OMV proteins. (C) LC-MS proteomic analysis of the TMBZ-stained gel band from OMV-associated proteins. n = 5.

Table 3.1. Predicted functions of potential redox proteins based on UniProt database analysis.

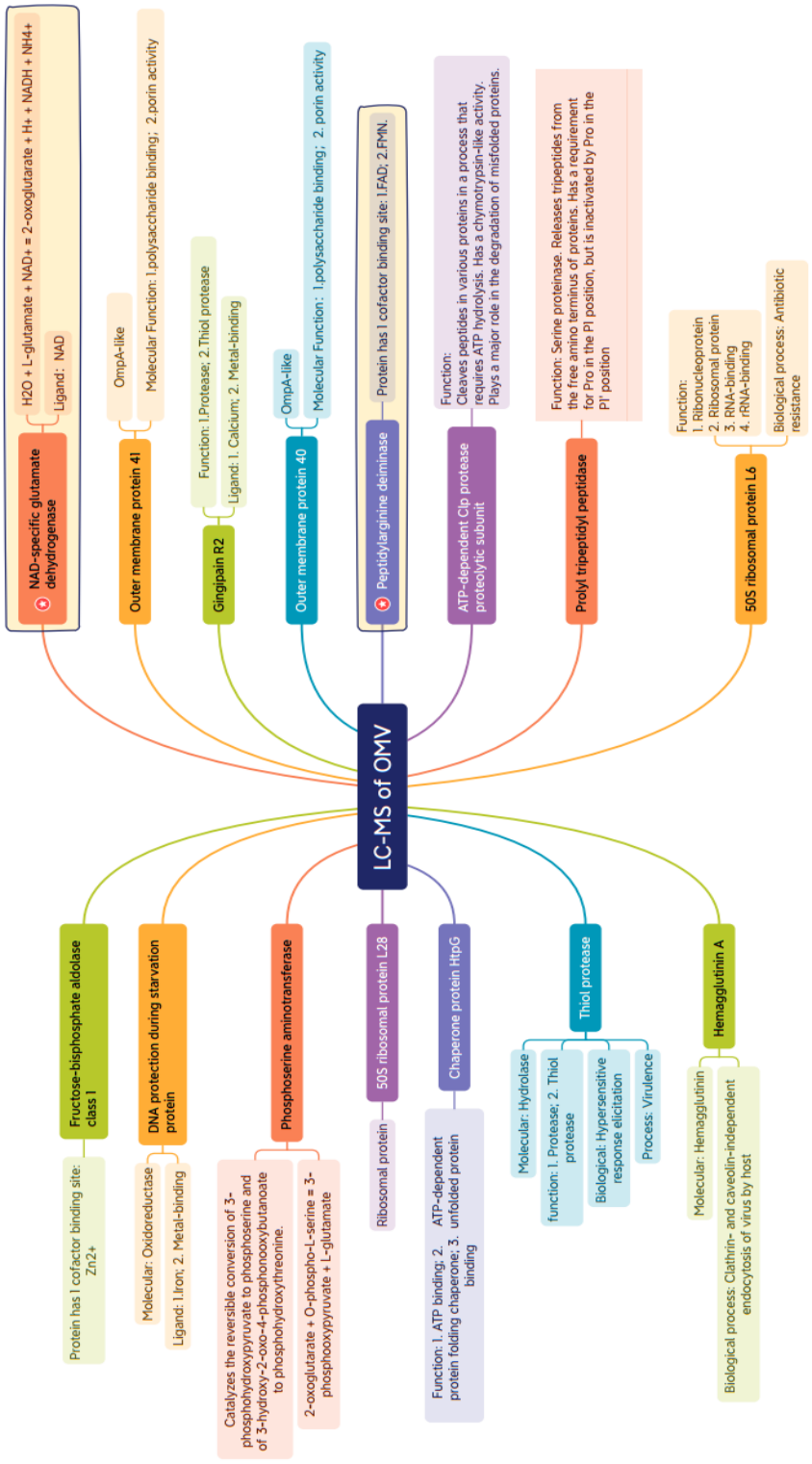

To examine the role of PPAD, we first performed I_{cond} measurement upon the addition FMN to the reactor with biofilm electrochemically incubated for 1 hour. Increasing the added FMN concentration with an hour interval, the I_{cond} increased with added FMN concentration, and twice higher current was observed at 10 μM FMN (**Figure 3.9A**). This effect of FMN was not a transcriptional factor by the presence of FMN, because addition of 10 μM FMN immediately increased to a similar extent of I_{cond} enhancement and significantly decreased E_a (**Figure 3.9**). In contrast, when we used riboflavin (RF), a similar redox cofactor but with a different structure (Pinto et al., 2016; Wakchaure et al., 2020), we did not see the I_{cond} enhancement (**Figure 3.9.B**). These data suggest that the electron transfer reaction mediated by FMN limits the I_{cond}, supporting that PPAD is mediating electron transfer, and the cofactor is a limiting factor.

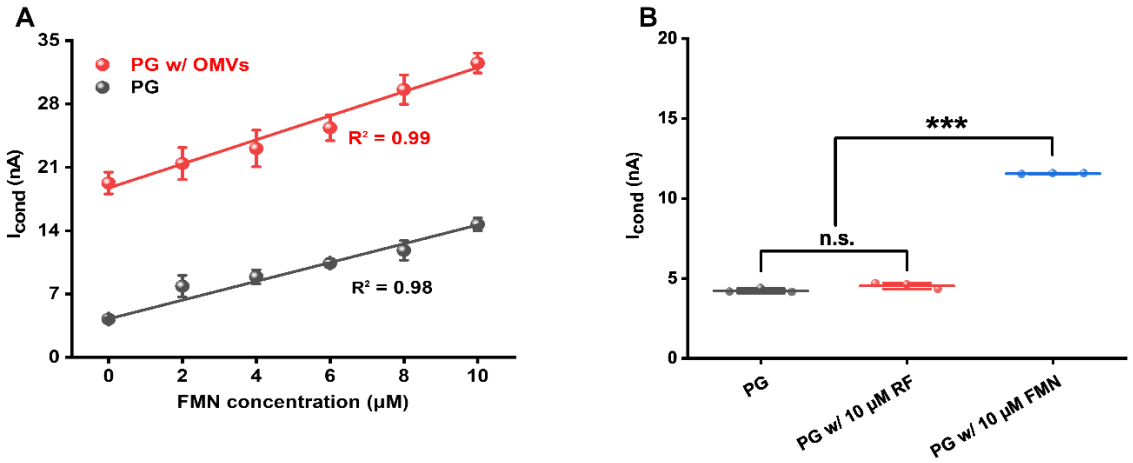

Figure 3.9. (A) I_{cond} changes in PG and PG w/ OMVs upon increasing Flavin mononucleotide (FMN) concentrations. (B) Comparison of I_{cond} between PG (black), PG w/ 10 μM Riboflavin (RF) (red) and PG w/ 10 μM FMN (blue). Data in panel B is presented as means ± s.d. (n = 3). n.s., not significant; ***, $p < 0.001$ (n = 3).

3.3.4 Flavin mononucleotide as the cofactor of PPAD enzyme in OMVs mediates PG biofilm electron conduction

To further elucidate the idea, we further examined the impact of FMN addition with the PPAD gene deletion mutant (*ΔPPAD*). *ΔPPAD* is known to form less biofilm (Karkowska et al., 2018). We also observed a decrease in I_{cond} compared with wild type (WT) biofilm in our electrode system (**Figure 3.10.A**). The presence of 10 µM FMN resulted in a significant but only 20-30% increase for I_{cond} (**Figure 3.10.A**) and increased E_a (**Figure 3.10.B**) in Δ*PPAD*, indicating that FMN does not have a positive effect on the electron transport process in Δ*PPAD*. These results strongly suggest that PPAD mediates I_{cond} via FMN cofactor in PG biofilms. This highlights PPAD as essential for facilitating LDET in PG biofilms.

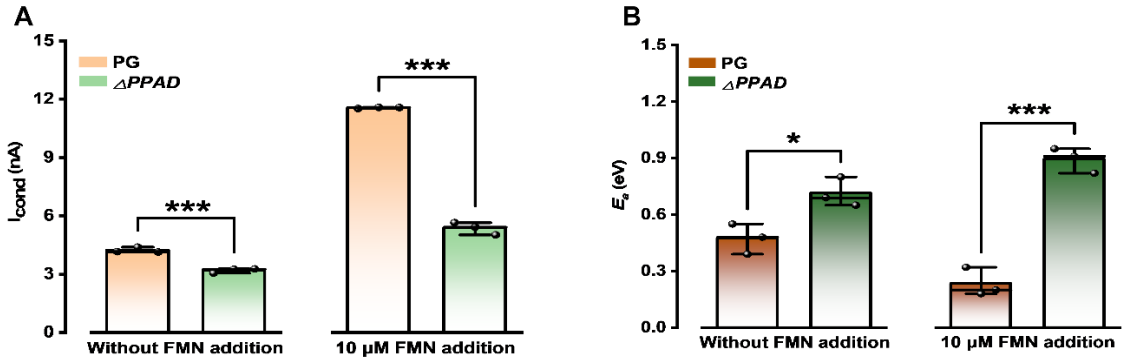

Figure 3.10. (A) I_{cond} comparison for PG and Δ*PPAD* with and without 10 µM FMN addition. (B) The semi-empirical thermal E_a of PG and Δ*PPAD* with and without 10 µM FMN addition. Data in panels A and B are presented as means ± s.d. (n = 3). *, $p < 0.05$ (n = 3), ***, $p < 0.001$ (n = 3).

To examine the contribution of PPAD on the OMV, we performed I_{cond} measurement with OMV isolated from the *ΔPPAD* culture. When WT was incubated with OMVs for 24 hours, I_{cond} decreased threefold with *ΔPPAD* OMVs compared with WT w/ OMVs (**Figure 3.11.A**). A similar significant decrease was observed in the presence of WT w/ OMVs treated with Cl-amidine (**Figure 3.11.A**), a PPAD inhibitor (Chumanevich et al., 2011; Uysal-Onganer et al., 2021), strongly suggesting the role of OMVs in mediating

LDET via membrane-bound PPAD. Consistently, after incubating WT w/ OMVs with FMN, the I_{cond} showed a further increase compared with WT biofilm with native OMVs (**Figure 3.11.A**). In contrast, I_{cond} decreased with ΔPPAD OMVs with FMN incubation (**Figure 3.11.A**), indicating that the concentration of active electron carrier on the OMVs is critical for the I_{cond}. An alternative electron pathway is suggested because the deletion of PPAD does not diminish the I_{cond}. By Temperature-dependent conduction analyses, we estimated the E_a of PG biofilms in various conditions (**Figure 3.11.B**). When biofilm is treated with FMN, E_a decreased twofold, as biofilm is co-incubated with WT w/ OMVs treated with FMN.

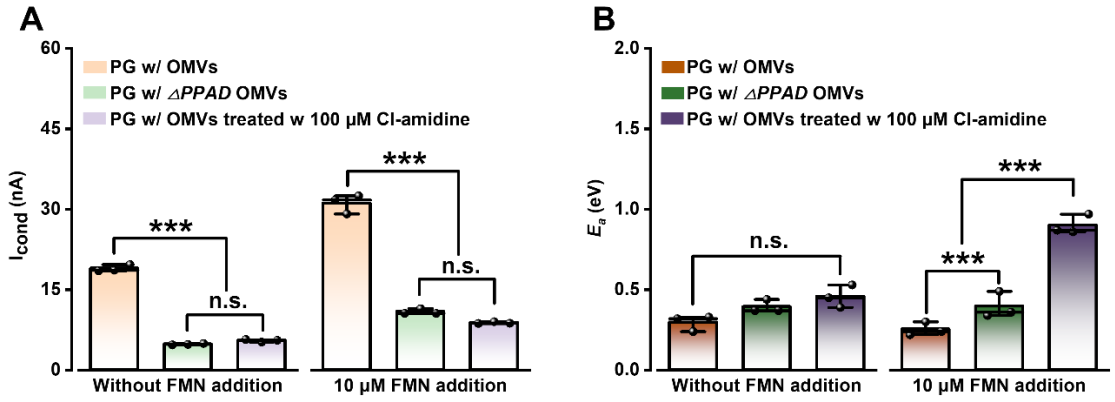

Figure 3.11. (A) Comparison of I_{cond} in PG biofilms supplemented with OMVs, *ΔPPAD* OMVs, or OMVs treated with 100 μM Cl-amidine, with or without the addition of 10 μM FMN. (B) Semi-empirical thermal E_a of the corresponding groups shown in (A). Data in panels A and B are presented as means ± s.d. (n = 3). n.s., not significant; ***, $p < 0.001$ (n = 3).

Meanwhile, we also quantified the PPAD enzyme content in OMVs, which corresponded to approximately 150 μM citrulline, indicating a substantial secretion of PPAD via OMVs (**Figure 3.12**). This value was higher than PG, suggesting that PPAD is enriched on the OMVs. These results indicate the critical role of OMVs in enhancing the biofilm activity and virulence factor. The importance of PPAD on the OMVs is consistent with the predominant localization of PPAD on OMVs in the natural oral

environment (Gabarrini et al., 2018; Vermilyea et al., 2021).

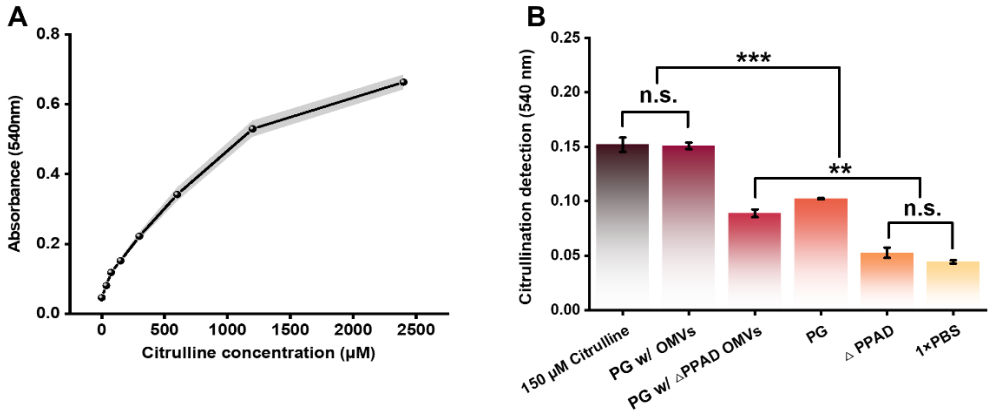

Figure 3.12. Comparison of PPAD activity in PG biofilm among PG with OMVs, PG with ΔPPAD OMVs, PG alone, ΔPPAD alone, and 1×PBS control.

3.3.5 Electroactive OMVs enhance PG biofilm formation

To further explore the vital role of OMVs for biofilm formation, PG suspensions were applied to calcium discs soaked in saline solution, simulating a dental environment conducive to biofilm development (**Figure 3.13**) (Jaffar et al., 2016). Calcium disc surfaces (**Figure 3.13**) confirmed biofilm formation on the discs after 24 hours of incubation. As shown in **Figure 3.14**, showed that three times more absorption in wild-type PG than Δ*PPAD*, suggesting that biofilm formation on the hydroxyapatite disk would require LDET more than the IDE system. The presence of FMN enhanced biofilm formation further in the WT. Furthermore, the presence of 100 mg/L cholesterol suppressed the biofilm formation as with *ΔPPAD*. This large suppression of biofilm formation is aligned with the factors lowering I_{cond}, indicating the significance of electron conduction in biofilm formation.

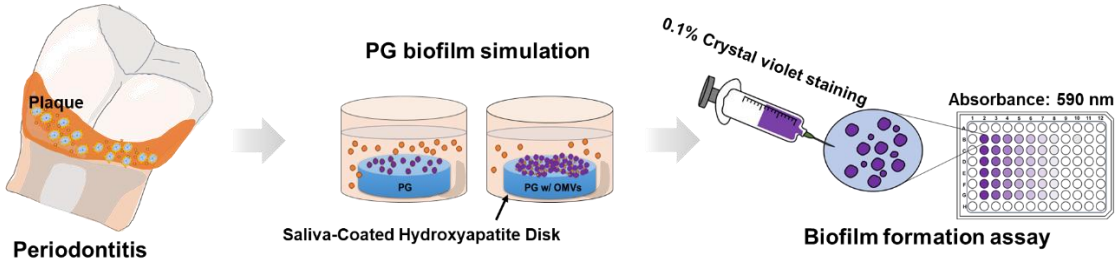

Figure 3.13. Schematic illustration of PG biofilm formation on saliva-coated hydroxyapatite disks.

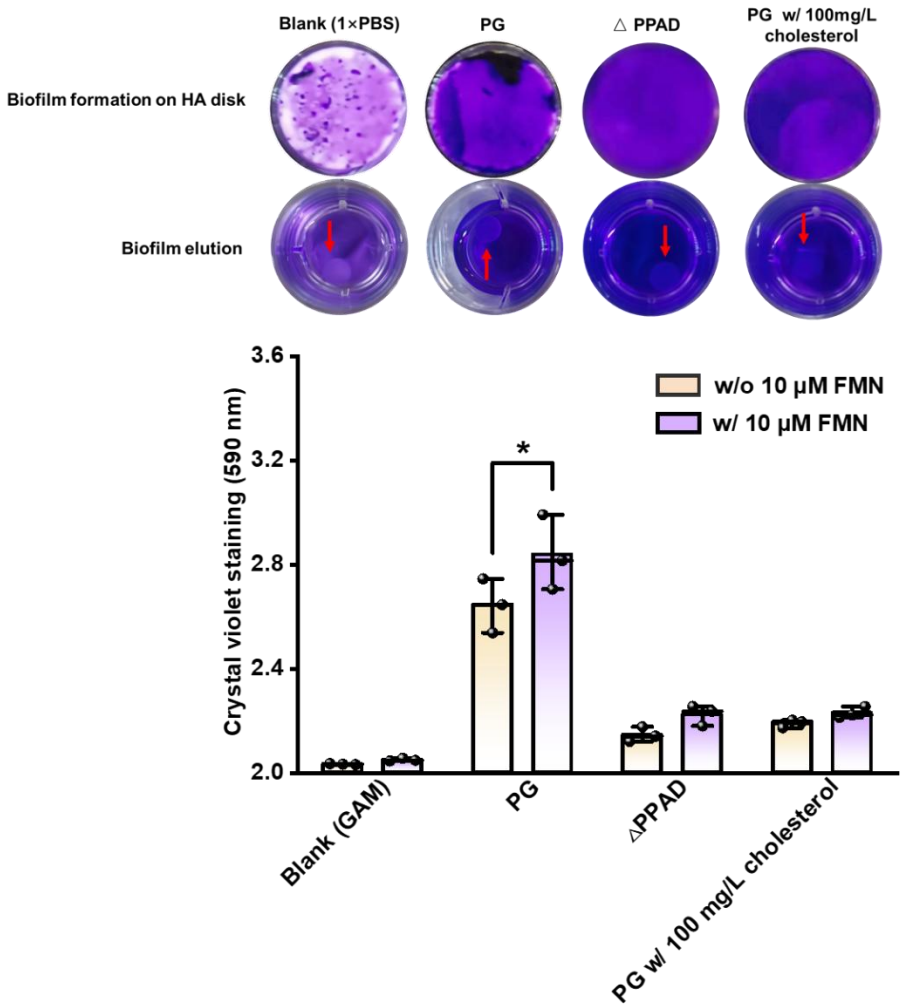

Figure 3.14. Quantification of PG biofilm formation on saliva-coated hydroxyapatite disks using 0.1% crystal violet staining. Data is presented as means ± s.d. (n = 3). *, $p < 0.05$.

We next confirmed the role of OMVs in the PG biofilm formation on the hydroxyapatite disk. The presence of OMVs enhanced biofilm formation, and the addition of FMN further increased biofilm formation (**Figure 3.15**). In contrast, the addition of OMVs from the mutant strain or those treated with Cl-amidine showed the biofilm formation enhancement by neither OMVs nor FMN addition (**Figure 3.15**). These results indicate that electron transfer via PPAD on the OMVs plays a critical role in PG biofilm formation. This highlights the role of OMVs mediating LDET in PG

biofilm, demonstrating that OMVs are integral to biofilm physiology. Targeting OMVs-facilitated LDET offers a promising therapeutic approach for managing oral pathogens.

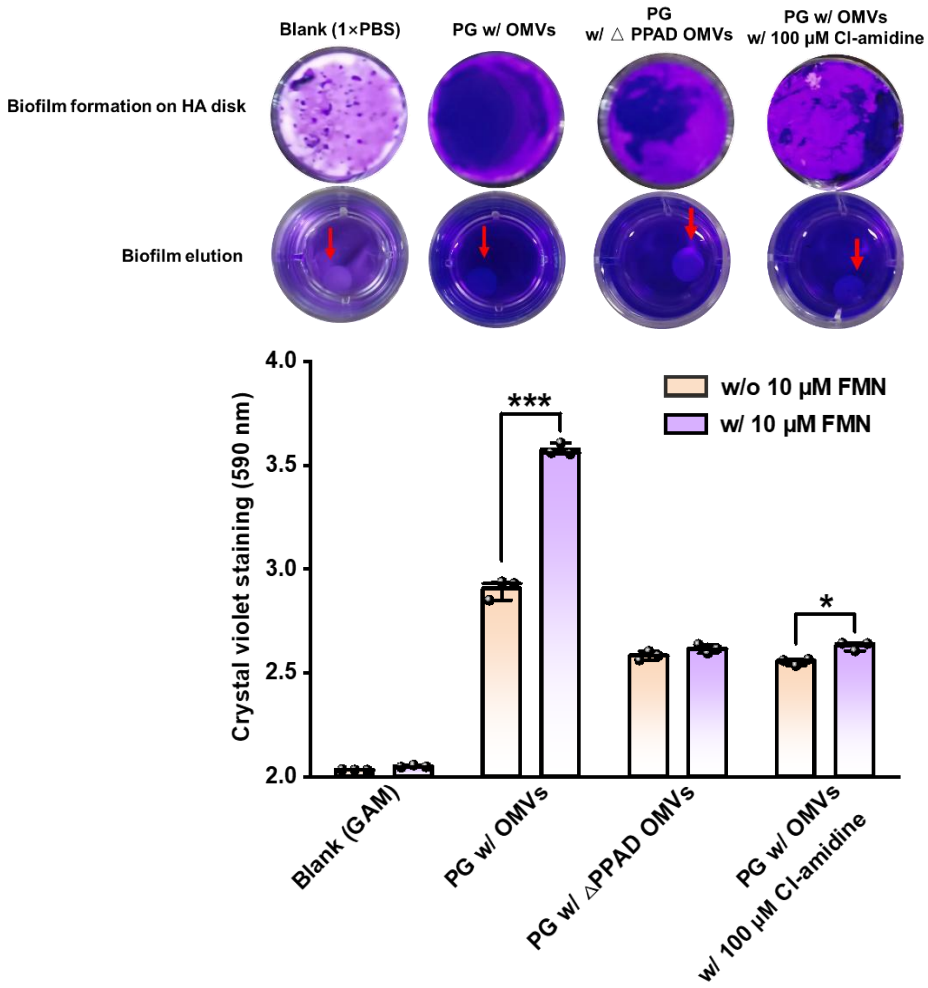

Figure 3.15. Quantification of PG biofilm formation on saliva-coated hydroxyapatite disks using 0.1% crystal violet staining. Data is presented as means ± s.d. (n = 3). *, $p < 0.05$; ***, $p < 0.001$.

3.4 Discussion

This study demonstrates that PPAD, traditionally recognized as a deiminase rather than a redox enzyme (Abdullah et al., 2013), indirectly contributes to the LDET process within PG biofilms. This contribution is mediated by FMN as a cofactor and facilitated by the structural environment provided by OMVs. The findings indicate that PPAD, in association with FMN, enhances LDET in PG biofilms, which is an unconventional function for typical deiminases. This study elucidates the mechanisms through which PPAD participates in LDET and discusses the broader significance of these findings.

FMN is a well-known redox-active molecule that undergoes reversible oxidation and reduction (Deller et al., 2008; Durchschein et al., 2013; Okamoto et al., 2013). This study shows that when FMN is associated with PPAD in OMVs, it acts as a cofactor, enabling PPAD to indirectly participate in electron transfer. The observed enhancement in biofilm electron conduction with FMN addition suggests that PPAD serves as an auxiliary platform, stabilizing the redox state of FMN and facilitating FMN-mediated electron transport. This interaction effectively imparts redox functionality to PPAD, allowing it to contribute to electron flow within the biofilm. Without FMN, PPAD lacks the intrinsic capacity for redox reactions, indicating that this activity depends entirely on FMN's presence and interaction with PPAD. Experimental results support this cofactor-dependent role of PPAD. Comparisons between wild-type PG biofilms and *ΔPPAD* mutants, as well as FMN-treated versus untreated conditions, underscore the importance of FMN-PPAD complexes in maintaining LDET. The addition of FMN significantly enhances I_{cond}, particularly in wild-type biofilms, suggesting that FMN amplifies the role of PPAD in the LDET network. This observation is consistent with previous research highlighting FMN in electron transfer in *S.* MR-1 systems (Xu et al., 2018), although its role as a cofactor for PPAD is a novel finding.

OMVs secreted by PG provide a structural basis (Thoma et al., 2018; Rocha et al., 2020 and 2021) for LDET by encapsulating PPAD and FMN. These vesicles are rich in

outer membrane proteins and create a favorable environment for stabilizing redox-active molecules that would otherwise be unstable in extracellular conditions (Bonnington et al., 2014). By incorporating PPAD and FMN, OMVs act as conduits for electron transfer, bridging spatial gaps within the biofilm and enabling more efficient electron flow. This study demonstrates that OMVs enhance biofilm electron conduction and reduce E_a required for electron conduction, suggesting that OMVs not only shorten electron diffusion paths but also facilitate LDET thermodynamically within the biofilm matrix. The structural role of OMVs is further evidenced by experiments showing a marked decrease in I_{cond} upon inhibition of Cl-amidine or deletion of the PPAD gene. This decrease suggests that the OMV-associated PPAD-FMN complex is a critical component of the biofilm electron conduction network. Additionally, the high concentration of PPAD in OMVs, as indicated by citrulline quantification, confirms its abundance and underscores its functional significance. OMVs thus provide a unique microenvironment that allows PPAD to indirectly support LDET, a function it would not demonstrate in isolation.

While PPAD's primary enzymatic function involves deimination, its association with FMN in OMVs reveals an additional, non-canonical redox role (Rosen et al., 2020; Weusthuis et al., 2020). This study shows that the FMN-PPAD complex exhibits redox activity, facilitating LDET within the PG biofilm. Although PPAD lacks intrinsic redox-active centers typical of redox enzymes, binding with FMN appears to enable pseudo-redox behavior, wherein PPAD stabilizes FMN's redox transitions without directly participating in electron exchange. This non-canonical redox role of PPAD can be described as surface-mediated electron transfer (SMET). In this model, PPAD functions as a passive mediator of electron transfer, while FMN performs the actual redox reaction. The OMVs' microenvironment supports this process by stabilizing the interactions between PPAD and FMN, allowing efficient electron transfer across the biofilm. Such SMET functionality is advantageous in anoxic environments, where PG typically resides, as it facilitates energy transfer without requiring oxygen as a terminal

electron acceptor (Naradasu et al., 2022).

To confirm the role of PPAD in the biofilm LDET process, we utilized various inhibitory and comparative approaches. Inhibition of PPAD with Cl-amidine and deletion of the PPAD gene both led to significant reductions in I_{cond}, indicating that PPAD is integral to the electron transfer of the biofilm network. Moreover, the addition of cholesterol, which increases membrane rigidity (Eaton et al., 1981), similarly decreased I_{cond}, suggesting that membrane fluidity and OMVs dynamics are crucial for efficient electron flow. These findings underscore that, while PPAD is not a conventional redox enzyme, its interaction with FMN and encapsulation within OMVs enable it to mediate biofilm electron conduction. Temperature-dependent conduction measurements provided further insight into the mechanism by which PPAD contributes to LDET. Arrhenius analysis revealed a lower E_a for I_{cond} in biofilms containing OMVs with PPAD, indicating that the FMN-PPAD complex thermodynamically favors LDET. The reduction in E_a reflects increased efficiency of electron flow, further confirming PPAD's supportive role in LDET.

In conclusion, while PPAD is not a conventional redox enzyme, this study shows that it can contribute to PG biofilm electron conduction through its interaction with FMN and association with OMVs. The FMN-PPAD complex enables a pseudo-redox activity that is crucial for facilitating electron conduction across the biofilm matrix. OMVs provide both structural and thermodynamic support for this process, enhancing LDET, promoting anaerobic survival, and increasing antibiotic resistance. Although this study verifies the atypical redox activity of PPAD, particularly in the formation of a stable complex between FMN and PPAD in OMVs, is needed to elucidation of the precise molecular mechanism. Nevertheless, this study reveals a novel, indirect redox role for PPAD and highlights the importance of OMVs in PG biofilm physiology. By expanding our understanding of LDET in PG biofilm, this research suggests potential therapeutic strategies targeting OMVs-mediated electron transfer to manage PG-related infections and biofilm-associated antibiotic resistance.

3.5 References

Abdullah, S.-N., Farmer, E.-A., Spargo, L., Logan, R., & Gully, N. (2013). *Porphyromonas gingivalis* peptidylarginine deiminase substrate specificity. *Anaerobe*, 23, 102-108.

Begić, M., & Josić, D. (2020). Biofilm formation and extracellular microvesicles-The way of foodborne pathogens toward resistance. *Electrophoresis*, 41(20), 1718-1739.

Blachutzik, J. O., Demir, F., Kreuzer, I., Hedrich, R., & Harms, G. S. (2012). Methods of staining and visualization of sphingolipid enriched and non-enriched plasma membrane regions of *Arabidopsis thaliana* with fluorescent dyes and lipid analogues. *Plant Methods*, 8, 1-18.

Bonnington, K., & Kuehn, M. (2014). Protein selection and export via outer membrane vesicles. *Biochimica et Biophysica Acta (BBA)-Molecular Cell Research*, 1843(8), 1612-1619.

Camussi, G., Deregibus, M. C., Bruno, S., Cantaluppi, V., & Biancone, L. (2010). Exosomes/microvesicles as a mechanism of cell-to-cell communication. *Kidney international,* 78(9), 838-848.

Ceriotti, F., Zakowski, J., Sine, H., Altaie, S., Horowitz, G., Pesce, A. J., Boyd, J., Horn, P., Gard, U., & Horowitz, G. (2012). Clinical and Laboratory Standards Institute (CLSI).

Chumanevich, A. A., Causey, C. P., Knuckley, B. A., Jones, J. E., Poudyal, D., Chumanevich, A. P., Davis, T., Matesic, L. E., Thompson, P. R., & Hofseth, L. J. (2011). Suppression of colitis in mice by Cl-amidine: a novel peptidylarginine deiminase inhibitor. *American Journal of Physiology-Gastrointestinal and Liver Physiology*, 300(6), G929-G938.

Dahl, P. J., Yi, S. M., Gu, Y., Acharya, A., Shipps, C., Neu, J., O'Brien, J. P., Morzan, U. N., Chaudhuri, S., & Guberman-Pfeffer, M. J. (2022). A 300-fold conductivity increase in microbial cytochrome nanowires due to temperature-induced restructuring of hydrogen bonding networks. *Science Advances*, 8(19), eabm7193.

Damgaard, D., Senolt, L., Nielsen, M. F., Pruijn, G. J., & Nielsen, C. H. (2014). Demonstration of extracellular peptidylarginine deiminase (PAD) activity in synovial fluid of patients with rheumatoid arthritis using a novel assay for

citrullination of fibrinogen. *Arthritis research & therapy,* 16, 1-7.

Deller, S., Macheroux, P., & Sollner, S. (2008). Flavin-dependent quinone reductases. *Cellular and Molecular Life Sciences*, 65, 141-160.

Deng, X., Dohmae, N., Nealson, K. H., Hashimoto, K., & Okamoto, A. (2018). Multi-heme cytochromes provide a pathway for survival in energy-limited environments. *Science Advances*, 4(2), eaao5682.

Durchschein, K., Hall, M., & Faber, K. (2013). Unusual reactions mediated by FMN-dependent ene- and nitro-reductases. *Green chemistry*, 15(7), 1764-1772.

Džunková, M., Martinez-Martinez, D., Gardlík, R., Behuliak, M., Janšáková, K., Jiménez, N., Vázquez-Castellanos, J. F., Martí, J. M., D'Auria, G., & Bandara, H. (2018). Oxidative stress in the oral cavity is driven by individual-specific bacterial communities. *NPJ biofilms and microbiomes*, 4(1), 29.

Eaton, L., Erdos, G., Vreeland, N., & Ingram, L. (1981). Failure of *Escherichia coli* to alter its fatty acid composition in response to cholesterol-induced changes in membrane fluidity. *Journal of bacteriology*, 146(3), 1151-1153.

Flemming, H.-C. (2002). Biofouling in water systems-cases, causes and countermeasures. *Applied microbiology and biotechnology*, 59(6), 629-640.

Gabarrini, G., Palma Medina, L. M., Stobernack, T., Prins, R. C., du Teil Espina, M., Kuipers, J., Chlebowicz, M. A., Rossen, J. W., van Winkelhoff, A. J., & van Dijl, J. M. (2018). There's no place like OM: Vesicular sorting and secretion of the peptidylarginine deiminase of *Porphyromonas gingivalis*. *Virulence*, 9(1), 459-467.

Glasser, N. R., Saunders, S. H., & Newman, D. K. (2017). The colorful world of extracellular electron shuttles. *Annual review of microbiology*, 71, 731-751.

Gray, H. B., & Winkler, J. R. (2005). Long-range electron transfer. *Proceedings of the National Academy of Sciences*, 102(10), 3534-3539.

Gui, M., Dashper, S., Slakeski, N., Chen, Y. Y., & Reynolds, E. (2016). Spheres of influence: *Porphyromonas gingivalis* outer membrane vesicles. *Molecular Oral Microbiology*, 31(5), 365-378.

Hall-Stoodley, L., Costerton, J. W., & Stoodley, P. (2004). Bacterial biofilms: from the natural environment to infectious diseases. *Nature Reviews Microbiology*, 2(2), 95-108.

Han, D., Wang, F., Ma, Y., Zhao, Y., Zhang, W., Zhang, Z., Liu, H., Yang, X., Zhang, C.,

& Zhang, J. (2023). Redirecting antigens by engineered photosynthetic bacteria and derived outer membrane vesicles for enhanced cancer immunotherapy. *ACS nano*, 17(19), 18716-18731.

Hasegawa, Y., Futamata, H., & Tashiro, Y. (2015). Complexities of cell-to-cell communication through membrane vesicles: implications for selective interaction of membrane vesicles with microbial cells. *Frontiers Media*, SA. 6, 633.

Hensen, S. M., & Pruijn, G. J. (2014). Methods for the detection of peptidylarginine deiminase (PAD) activity and protein citrullination. *Molecular & Cellular Proteomics*, 13(2), 388-396.

Jaffar, N., Miyazaki, T., & Maeda, T. (2016). Biofilm formation of periodontal pathogens on hydroxyapatite surfaces: Implications for periodontium damage. J*ournal of Biomedical Materials Research*, Part A, 104(11), 2873-2880.

Jeong, G.-J., Khan, F., Tabassum, N., Cho, K.-J., & Kim, Y.-M. (2024). Bacterial extracellular vesicles: modulation of biofilm formation and virulence. *Acta Biomaterialia*.

Karkowska-Kuleta, J., Bartnicka, D., Zawrotniak, M., Zielinska, G., Kierońska, A., Bochenska, O., Ciaston, I., Koziel, J., Potempa, J., & Baster, Z. (2018). The activity of bacterial peptidylarginine deiminase is important during formation of dual-species biofilm by periodontal pathogen *Porphyromonas gingivalis* and opportunistic fungus *Candida albicans*. *Pathogens and disease*, 76(4), fty033.

Kesarwala, A. H., Krishna, M. C., & Mitchell, J. B. (2016). Oxidative stress in oral diseases. *Oral diseases*, 22(1), 9-18.

Lai, R. C., Yeo, R. W. Y., Tan, K. H., & Lim, S. K. (2013). Exosomes for drug delivery-a novel application for the mesenchymal stem cell. *Biotechnology advances*, 31(5), 543-551.

Lee, A. R., Park, S. B., Kim, S. W., Jung, J. W., Chun, J. H., Kim, J., Kim, Y. R., Lazarte, J. M. S., Jang, H. B., & Thompson, K. D. (2022). Membrane vesicles from antibiotic-resistant *Staphylococcus aureus* transfer antibiotic resistance to antibiotic‐susceptible *Escherichia coli*. *Journal of Applied Microbiology*, 132(4), 2746-2759.

Li, Q., Ou, Z., Lin, J., Tang, D., He, B., Wu, Y., Huang, X., Huang, X., Ru, B., & Wang, Q. (2025). Specific labeling of outer membrane vesicles with antibiotic-conjugated

probe reveals early bacterial infections in blood. *Nature Communications*, 16(1), 3535.

Light, S. H., Su, L., Rivera-Lugo, R., Cornejo, J. A., Louie, A., Iavarone, A. T., Ajo-Franklin, C. M., & Portnoy, D. A. (2018). A flavin-based extracellular electron transfer mechanism in diverse Gram-positive bacteria. *Nature*, 562(7725), 140-144.

Lin, F., Ferguson, K. L., Boyer, D. R., Lin, X. N., & Marsh, E. N. G. (2015). Isofunctional enzymes PAD1 and UbiX catalyze formation of a novel cofactor required by ferulic acid decarboxylase and 4-hydroxy-3-polyprenylbenzoic acid decarboxylase. *ACS chemical biology*, 10(4), 1137-1144.

Liu, X., Jing, X., Ye, Y., Zhan, J., Ye, J., & Zhou, S. (2019). Bacterial vesicles mediate extracellular electron transfer. *Environmental Science & Technology Letters*, 7(1), 27-34.

Marquis, R. (1995). Oxygen metabolism, oxidative stress and acid-base physiology of dental plaque biofilms. *Journal of industrial microbiology and biotechnology*, 15(3), 198-207.

Miller, D. J., & Nicholas, D. (1984). 3, 3′, 5, 5′-Tetramethylbenzidine/H2O2 staining is not specific for heme proteins separated by gel electrophoresis. *Analytical biochemistry*, 140(2), 577-580.

Naradasu, D. (2022). Extracellular electron transfer capability of oral pathogens *Aggregatibacter actinomycetemcomitans* and *Porphyromonas gingivalis*. *In: Microbiology Society*.

Naradasu, D., Miran, W., Sakamoto, M., & Okamoto, A. (2019). Isolation and characterization of human gut bacteria capable of extracellular electron transport by electrochemical techniques. *Frontiers in Microbiology*, 9, 3267.

Naradasu, D., Miran, W., Sharma, S., Takenawa, S., Soma, T., Nomura, N., Toyofuku, M., & Okamoto, A. (2021). Biogenesis of outer membrane vesicles concentrates the unsaturated fatty acid of phosphatidylinositol in *Capnocytophaga ochracea*. *Frontiers in Microbiology*, 12, 682685.

Okamoto, A., Hashimoto, K., & Nakamura, R. (2012). Long-range electron conduction of *Shewanella* biofilms mediated by outer membrane C-type cytochromes. *Bioelectrochemistry*, 85, 61-65.

Okamoto, A., Hashimoto, K., Nealson, K. H., & Nakamura, R. (2013). Rate enhancement of bacterial extracellular electron transport involves bound flavin semiquinones. *Proceedings of the National Academy of Sciences*, 110(19), 7856-7861.

Okamoto, A., Nakamura, R., Nealson, K. H., & Hashimoto, K. (2014). Bound flavin model suggests similar electron - transfer mechanisms in *Shewanella* and *Geobacter*. *ChemElectroChem*, 1(11), 1808-1812.

Pinto, J. T., & Zempleni, J. (2016). Riboflavin. *Advances in nutrition*, 7(5), 973-975.

Poole, K. (2012). Bacterial stress responses as determinants of antimicrobial resistance. *Journal of Antimicrobial Chemotherapy*, 67(9), 2069-2089.

Reguera, G., McCarthy, K. D., Mehta, T., Nicoll, J. S., Tuominen, M. T., & Lovley, D. R. (2005). Extracellular electron transfer via microbial nanowires. *Nature*, 435(7045), 1098-1101.

Rocha, F. G., Ottenberg, G., Eure, Z. G., Davey, M. E., & Gibson III, F. C. (2020). Sphingolipid Containing Outer Membrane Vesicles Serve as a Delivery Vehicle to Limit Host Immune Response to *Porphyromonas gingivalis*. *bioRxiv*, 2020.2010. 2005.327544.

Rocha, F. G., Ottenberg, G., Eure, Z. G., Davey, M. E., & Gibson III, F. C. (2021). Sphingolipid-containing outer membrane vesicles serve as a delivery vehicle to limit macrophage immune response to *Porphyromonas gingivalis*. *Infection and Immunity*, 89(4), 10.1128/iai. 00614-00620.

Rosen, J., Jakobs, P., Ale-Agha, N., Altschmied, J., & Haendeler, J. (2020). Non-canonical functions of Telomerase Reverse Transcriptase-Impact on redox homeostasis. *Redox Biology*, 34, 101543.

Saunders, S. H., Edmund, C., Yates, M. D., Otero, F. J., Trammell, S. A., Stemp, E. D., Barton, J. K., Tender, L. M., & Newman, D. K. (2020). Extracellular DNA promotes efficient extracellular electron transfer by pyocyanin in Pseudomonas aeruginosa biofilms. *Cell*, 182(4), 919-932. e919.

Schooling, S. R., & Beveridge, T. J. (2006). Membrane vesicles: an overlooked component of the matrices of biofilms. *Journal of Bacteriology*, 188(16), 5945-5957.

Schwechheimer, C., & Kuehn, M. J. (2015). Outer-membrane vesicles from Gram-negative bacteria: biogenesis and functions. *Nature Reviews Microbiology*, 13(10), 605-619.

Shi, L., Dong, H., Reguera, G., Beyenal, H., Lu, A., Liu, J., Yu, H.-Q., & Fredrickson, J. K. (2016). Extracellular electron transfer mechanisms between microorganisms and minerals. *Nature Reviews Microbiology*, 14(10), 651-662.

Steeves, C. H., Potrykus, J., Barnett, D. A., & Bearne, S. L. (2011). Oxidative stress response in the opportunistic oral pathogen *Fusobacterium nucleatum*. *Proteomics*, 11(10), 2027-2037.

Stewart, P. S., & Franklin, M. J. (2008). Physiological heterogeneity in biofilms. *Nature Reviews Microbiology*, 6(3), 199-210.

Thoma, J., Manioglu, S., Kalbermatter, D., Bosshart, P. D., Fotiadis, D., & Müller, D. J. (2018). Protein-enriched outer membrane vesicles as a native platform for outer membrane protein studies. *Communications biology*, 1(1), 23.

Thomas, P. E., Ryan, D., & Levin, W. (1976). An improved staining procedure for the detection of the peroxidase activity of cytochrome P-450 on sodium dodecyl sulfate polyacrylamide gels. *Analytical biochemistry*, 75(1), 168-176.

UniProt: the universal protein knowledgebase. (2017). *Nucleic Acids Research*, 45(D1), D158-D169.

Uysal-Onganer, P., D'Alessio, S., Mortoglou, M., Kraev, I., & Lange, S. (2021). Peptidylarginine deiminase inhibitor application, using Cl-amidine, PAD2, PAD3 and PAD4 isozyme-specific inhibitors in pancreatic cancer cells, reveals roles for PAD2 and PAD3 in cancer invasion and modulation of extracellular vesicle signatures. *International Journal of Molecular Sciences*, 22(3), 1396.

Vargas, C., McEwan, A., & Downie, J. (1993). Detection of c-type cytochromes using enhanced chemiluminescence. *Analytical biochemistry*, 209(2), 323-326.

Vermilyea, D. M., Moradali, M. F., Kim, H.-M., & Davey, M. E. (2021). PPAD activity promotes outer membrane vesicle biogenesis and surface translocation by *Porphyromonas gingivalis*. *Journal of Bacteriology*, 203(4), 10.1128/jb. 00343-00320.

Wakchaure, P. D., Jana, K., & Ganguly, B. (2020). Structural insights into the interactions of flavin mononucleotide (FMN) and riboflavin with FMN riboswitch:

A molecular dynamics simulation study. *Journal of Biomolecular Structure and Dynamics*, 38(13), 3856-3866.

Walters III, M. C., Roe, F., Bugnicourt, A., Franklin, M. J., & Stewart, P. S. (2003). Contributions of antibiotic penetration, oxygen limitation, and low metabolic activity to tolerance of *Pseudomonas aeruginosa* biofilms to ciprofloxacin and tobramycin. *Antimicrobial Agents and Chemotherapy*, 47(1), 317-323.

Wang, W., Chanda, W., & Zhong, M. (2015). The relationship between biofilm and outer membrane vesicles: a novel therapy overview. *FEMS microbiology letters*, 362(15), fnv117.

Weusthuis, R. A., Folch, P. L., Pozo-Rodríguez, A., & Paul, C. E. (2020). Applying non-canonical redox cofactors in fermentation processes. *Iscience*, 23(9).

Xu, S., Barrozo, A., Tender, L. M., Krylov, A. I., & El-Naggar, M. Y. (2018). Multiheme cytochrome mediated redox conduction through *Shewanella oneidensis* MR-1 cells. *Journal of the American Chemical Society*, 140(32), 10085-10089.

Yu, H., Lu, Y., Lan, F., Wang, Y., Hu, C., Mao, L., Wu, D., Li, F., & Song, H. (2023). Engineering Outer Membrane Vesicles to Increase Extracellular Electron Transfer of *Shewanella oneidensis*. *ACS Synthetic Biology*, 12(6), 1645-1656.

Chapter 4. Targeting biofilm electron transfer to overcome antibiotic tolerance

4.1 Introduction

Bacterial biofilms represent one of the most formidable barriers to successful antimicrobial therapy, contributing significantly to chronic infections, treatment failure, and relapse (Costerton et al., 1999; Hall-Stoodley et al., 2004; Zhang et al., 2020). Characterized by multicellular aggregates encased in a self-produced extracellular polymeric substance (EPS), biofilms enable bacteria to persist in hostile environments, resist immune clearance, and tolerate a wide range of antibiotics (Flemming et al., 2010; Singh et al., 2021; Shree et al., 2023). Among the pathogens known for their biofilm-forming ability, *Porphyromonas gingivalis* (PG), a Gram-negative, obligate anaerobe, stands out due to its dual role in localized periodontal disease and systemic pathologies such as atherosclerosis, Alzheimer's disease, diabetes, and colorectal cancer (Kanagasingam et al., 2020; Mei et al., 2020; Sharaf et al., 2022; Rajasekaran et al., 2024).

Conventional antibiotics, including β-lactams, fluoroquinolones, and macrolides, are primarily designed to act on metabolically active, planktonic bacterial cells. However, their effectiveness against sessile populations within biofilms is substantially compromised (Simoes et al., 2011; Lebeaux et al., 2014; Sahli et al., 2022). The multifactorial nature of biofilm-associated resistance encompasses limited antibiotic penetration, altered microenvironments (e.g., hypoxia, low pH), efflux pump upregulation, and the presence of metabolically dormant persister cells (Sadiq et al., 2017; Benz et al., 2020; Azeem et al., 2025; Mahdizade Ari et al., 2025). Notably, PG has evolved additional defense strategies through the secretion of outer membrane vesicles (OMVs), nanoscale lipid bilayer vesicles loaded with virulence factors and enzymes such as peptidylarginine deiminase (PPAD) (Ma et al., 2021; Zhang et al., 2021; Wu et al., 2025). OMVs not only serve as delivery vehicles for bioactive molecules but also contribute to biofilm stability, immune evasion, and interspecies communication (Caruana et al., 2020; Jeong et al., 2024; Xiu et al., 2024).

PPAD, a unique bacterial member of the peptidylarginine deiminase family, catalyzes the post-translational conversion of arginine residues to citrulline in bacterial and host proteins (Wang et al., 2013; Goulas et al., 2015; Vermilyea, 2019). Its expression has been strongly linked to periodontal disease severity and is implicated in systemic autoimmune conditions like rheumatoid arthritis due to the generation of neoepitopes (Koziel et al., 2014; Gabarrini et al., 2018). Despite these immunopathological associations, the role of PPAD in modulating biofilm structural integrity and antibiotic resistance has remained largely unexplored (Aliko et al., 2018; Vermilyea et al., 2019; Vermilyea et al., 2021).

Parallel to structural and enzymatic defenses, targeting bacterial metabolism, particularly anaerobic energy production, has emerged as a promising strategy for disrupting biofilm persistence (Koo et al., 2017; Ahmad et al., 2025). Compounds such as nitazoxanide and tizoxanide are known to impair microbial ATP synthesis by disrupting pyruvate: ferredoxin oxidoreductase and oxidative phosphorylation pathways (Ragsdale et al., 2003; Pankuch et al., 2006). These agents may circumvent traditional resistance mechanisms by collapsing the proton motive force, thereby sensitizing biofilms to antibiotic action or directly inducing bacterial death.

In this study, we sought to unravel the interplay between OMVs, PPAD, and antibiotic tolerance in PG biofilms. Specifically, we investigated (1) the contribution of OMVs to broad-spectrum antibiotic resistance, (2) the protective role of PPAD in OMVs-enriched biofilms, and (3) the potential of energy-targeting agents to overcome these resistance mechanisms. Through a combination of Colony Forming Units (CFUs) assays, 50% Minimum Inhibitory Concentration (MIC_{50}) analysis, and pharmacological inhibition studies, we delineate the biofilm-specific adaptations that underlie PG persistence and highlight new avenues for therapeutic intervention.

4.2 Methods

4.2.1 The microbe culture conditions

PG and its isogenic PPAD-deficient mutant (*ΔPPAD*) were employed in this study. PG and *ΔPPAD* grew anaerobically in 20 mL GAM for 48 hours at 37 °C. To maintain microbial circumstances anaerobically, GAM was purged with CO2: N2 (20:80 v/v) mixed gas for 30 min before cell cultivation. Cell suspensions were centrifuged at 7500 rpm and 4°C for 5 min, then cell aggregations were washed two times with 1×phosphate-buffered saline (1×PBS) under the same centrifugal conditions, resulting in an OD_{600} of 1.

4.2.2 Outer membrane vesicles (OMVs) preparation and quantification

PG solution was cultured using the method previously described (Naradasu et al., 2021). Cell suspensions were centrifuged at 7800 rpm and 4°C for 10 min, then the cell supernatants were filtered through a 0.22 μm filter to remove cell debris. The filtrates were ultracentrifuged at 210,000 × g and 4°C for 2 h. After the ultracentrifugation, the supernatants gradually drained away, and the inner surface of the tube was softly cleansed using 1×PBS. Subsequently, the aggregated pellets adhered to the tube were collected using 1×PBS through pipetting, resulting in OMV solutions, and stored at 4°C until further use. OMV's solutions underwent a fourfold dilution, following which the dimensions and concentration of the nanoparticles were quantified utilizing the nanoparticle flow cytometry (NanoAnalyzer, NanoFCM Co. Ltd.).

4.2.3 Biofilm formation

To simulate a tooth-like environment for biofilm formation, sterile calcium phosphate-coated disks were used as substrata. PG cultures were adjusted to $OD_{600} = 1.0$, and bacterial suspensions were incubated with the disks in 48-well plates under anaerobic conditions at 37 °C for 24 hours to allow initial biofilm establishment.

4.2.4 Antimicrobial assay based on Colony Forming Units (CFUs) enumeration

After biofilm formation on the disks, the Disks were subsequently transferred to

1×PBS to perform the antibacterial assay. For treatment, biofilm-bearing disks were incubated with antibiotics (amoxicillin, metronidazole, clindamycin hydrochloride, nitazoxanide, or tizoxanide) at concentrations ranging from 0 to 256 μM for 6 hours. Where indicated, Cl-amidine (100 μM) was applied to inhibit PPAD enzymatic activity. Control groups received an equivalent volume of 1×PBS. Biofilms were maintained under anaerobic conditions throughout the treatment period (**Figure 4.1**).

Following treatment, the calcium disks were transferred into sterile 1.5 mL tubes containing 1 mL of 1×PBS, gently vortexed, and subjected to bath sonication for 10 minutes to disrupt residual aggregates and detach the biofilm. The disks were then discarded, and the suspensions were centrifuged at 7500 rpm for 5 minutes at room temperature.

Serial 10-fold dilutions (10^{0} to 10^{-8}) were prepared in sterile 96-well plates, and 5 μL of each dilution was spot-plated onto anaerobic blood agar plates. The plates consisted of brain heart infusion (BHI) agar supplemented with 5 μg/mL hemin and 1 μg/mL menadione and were incubated under a gas mixture of 85% N_2, 10% H_2, and 5% CO_2 (Karkowska-Kuleta et al., 2018 and 2020). Plates were incubated anaerobically for over three days, after which CFUs were enumerated to determine bacterial load. Colony morphology was used to confirm the identity of PG.

4.2.5 Determination of 50% Minimum Inhibitory Concentration (MIC_{50})

MIC_{50} values of the tested antibiotics were determined by CFU enumeration following the broth microdilution method, by Clinical and Laboratory Standards Institute (CLSI) guidelines (Kassim et al., 2016).

4.2.6 Statistical analysis

All data are presented as mean ± standard deviation (SD). Statistical analyses were conducted using Origin software. Group comparisons were performed using either unpaired Student's t-tests or one-way ANOVA followed by Tukey's multiple comparisons test.

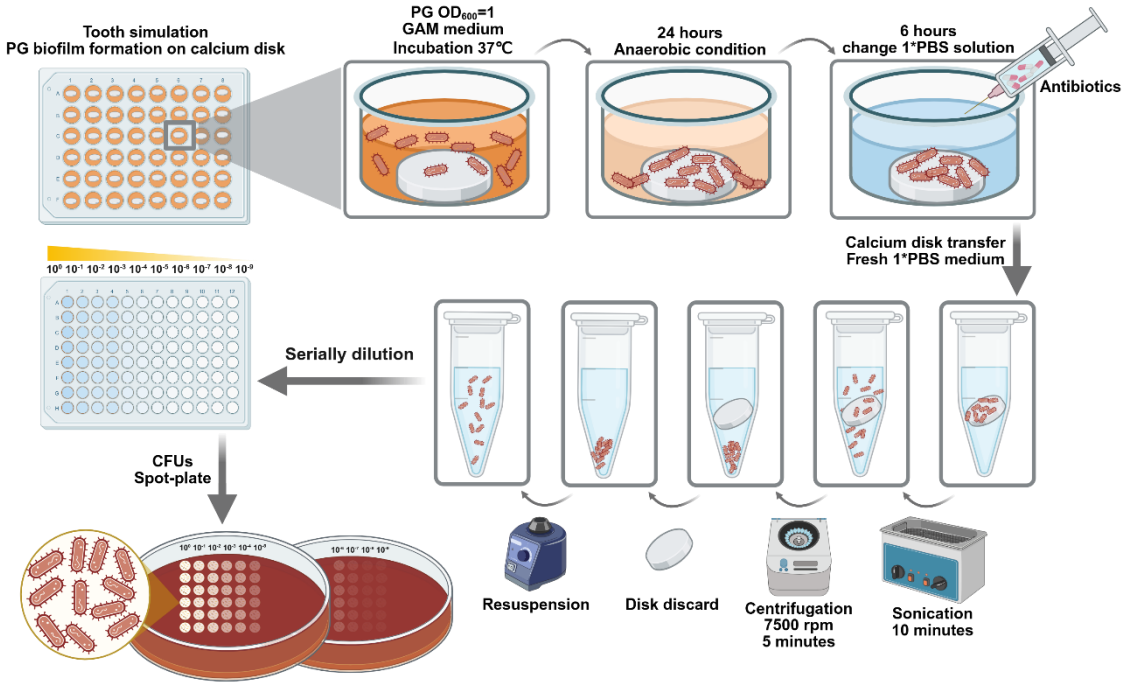

Figure 4.1. Experimental workflow for assessing PG cell survival after antibiotic treatment via microplate dilution and CFUs enumeration.

4.3 Results

4.3.1 OMVs-associated *Porphyromonas gingivalis* (PG) biofilm displays broad-spectrum resistance to conventional antibiotics

To elucidate the role of OMVs and the OMV-associated enzyme PPAD in antibiotic tolerance, we systematically examined the susceptibility of PG biofilms to three widely used antibiotics: amoxicillin, metronidazole, and clindamycin hydrochloride. Each compound represents a distinct antimicrobial class: β-lactams, nitroimidazoles, and lincosamides, respectively. And these targets essential bacterial processes including cell wall synthesis, DNA integrity, and protein translation (Gordon et al., 1990; Kaur et al., 2011; Dingsdag et al., 2018).

In OMVs-enriched PG biofilms, all three conventional antibiotics demonstrated markedly reduced bactericidal efficacy. Specifically, when treated with amoxicillin at concentrations up to 256 μM, PG biofilms incorporating OMVs maintained bacterial viability at approximately 8×10^5 CFU/mL, while the ΔPPAD mutant and PG treated with ΔPPAD-derived OMVs exhibited a sharp decline in viability, underscoring PPAD's contribution to OMVs-mediated resistance (**Figure 4.2.A**).

A comparable pattern was observed with metronidazole. Despite its known efficacy under anaerobic conditions through the induction of DNA strand breaks, OMVs-associated PG biofilms retained survival at 9×10^5 CFU/mL, while the absence of PPAD substantially enhanced susceptibility (**Figure 4.2.B**). This suggests that OMVs and PPAD not only serve as structural barriers but may also modulate intracellular redox responses that mitigate DNA damage.

Clindamycin hydrochloride, a potent inhibitor of the 50S ribosomal subunit, also failed to significantly suppress growth in OMVs-containing PG biofilms, with bacterial counts remaining at 7×10^5 CFU/mL even at maximum tested concentrations. Again, both ΔPPAD mutants and OMVs lacking PPAD markedly sensitized the biofilms (**Figure 4.2.C**).

These findings collectively indicate that OMVs play a multifaceted role in biofilm-associated drug tolerance, likely through a combination of physical shielding, biochemical modification of the microenvironment, and functional support by virulence factors such as PPAD. The differential outcomes between wild-type and *ΔPPAD*-associated conditions strongly implicate PPAD as a central effector in this protective mechanism, corroborating recent literature that links OMVs-derived enzymes to enhanced survival in hostile conditions (Veith et al., 2014; Kosgodage et al., 2019; Vermilyea et al., 2021).

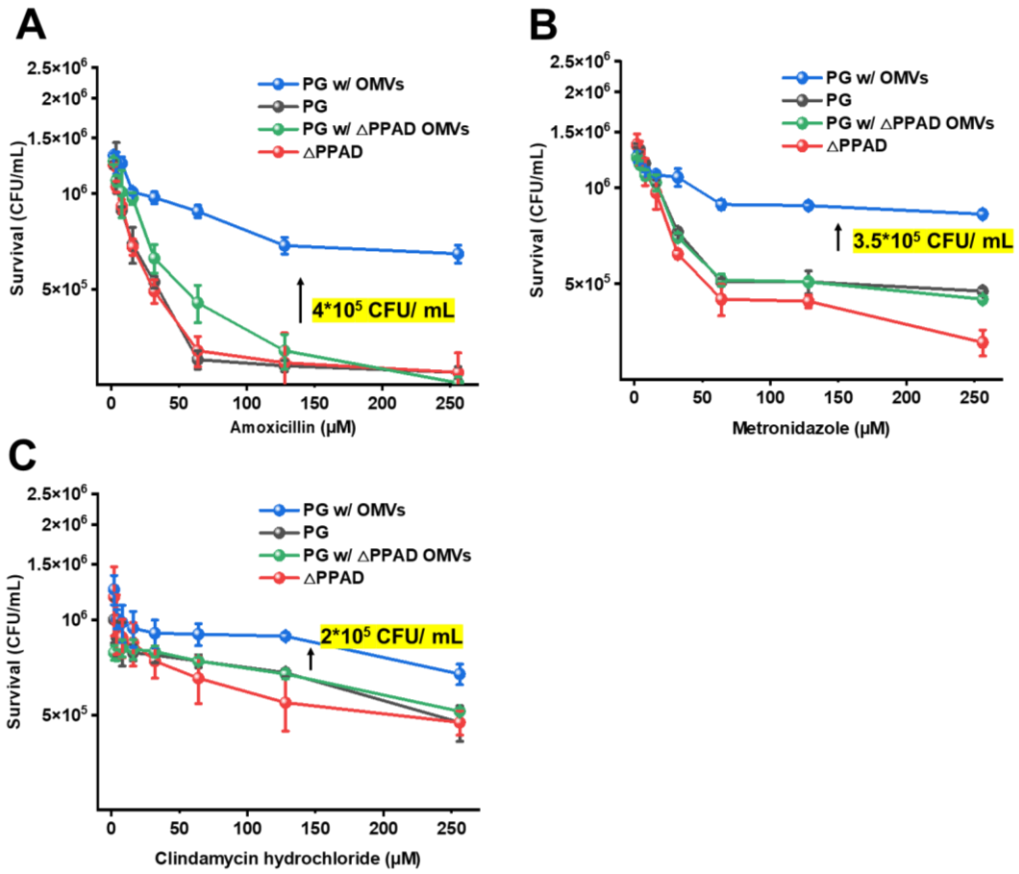

Figure 4.2. Viability of PG biofilms following 6 hours treatment with increasing concentrations (0-256 μM) of amoxicillin (A), metronidazole (B), or clindamycin hydrochloride (C). Four conditions were tested (Blue: PG biofilm + OMVs; Green: PG biofilm + ΔPPAD OMVs; Gray: PG biofilm; Red: ΔPPAD biofilm). CFU values at the different drug concentrations are annotated. Data are expressed as mean ± SD from three independent biological replicates.

4.3.2 Bioenergetic inhibitors retain antimicrobial efficacy against OMVs-protected biofilm

To investigate whether targeting bacterial energy metabolism offers a viable strategy for overcoming OMVs-associated antibiotic tolerance, we examined the efficacy of nitazoxanide and its active metabolite tizoxanide against PG biofilm. These agents are known to interfere with anaerobic energy metabolism by inhibiting the pyruvate: ferredoxin oxidoreductase complex within the anaerobic respiratory chain (Dubreuil et al., 1996; Yamamoto et al., 1999; Hoffman et al., 2007).

Strikingly, both compounds maintained potent antibacterial activity across all tested PG strains and biofilm conditions, including OMVs-enriched biofilms. When treated with nitazoxanide at concentrations up to 256 μM, the survival rate of PG biofilms with OMVs was reduced to levels comparable with PG lacking OMVs or the PPAD-deficient strains, with final counts approaching 5×10^5 CFU/mL (**Figure 4.3.A**). A similar pattern was observed with tizoxanide, which demonstrated slightly higher potency across the concentration gradient and consistently suppressed biofilm viability irrespective of OMV presence or PPAD expression (**Figure 4.3.B**).

These results indicate that nitazoxanide and tizoxanide act independently of OMVs-mediated resistance mechanisms and likely target fundamental metabolic processes essential for bacterial viability within biofilms. Notably, OMVs-associated tolerance observed with traditional antibiotics did not manifest when these bioenergetic inhibitors were applied, suggesting a distinct therapeutic advantage.

Our data align with prior studies reporting the broad-spectrum efficacy of nitazoxanide against anaerobic pathogens, including *Clostridium difficile*, *Helicobacter pylori*, and oral biofilm-forming species (Yamamoto et al., 1999; Rossignol, 2014). Its ability to bypass membrane-associated resistance elements and disrupt energy conservation pathways underscores its potential utility in recalcitrant biofilm infections. Furthermore, this energy-targeting mechanism may synergize with other therapeutic approaches aimed at sensitizing dormant or metabolically quiescent biofilm populations

(Farha et al., 2013; Murima et al., 2014; Hards et al., 2018; Ciemniecki et al., 2024).

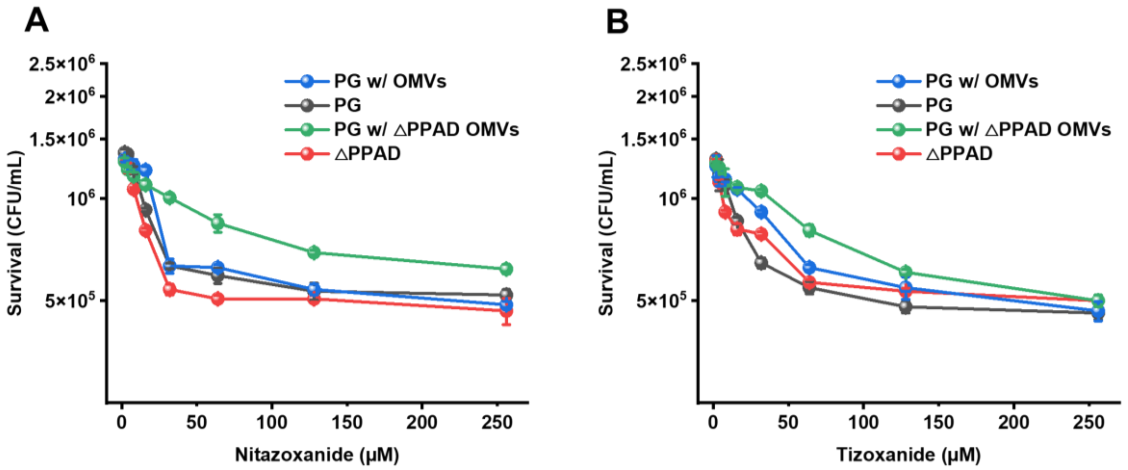

Figure 4.3. Viability of PG biofilms following 6 hours treatment with increasing concentrations (0-256 μM) of nitazoxanide (A) and tizoxanide (B). Four conditions were tested (Blue: PG biofilm + OMVs; Green: PG biofilm + ΔPPAD OMVs; Gray: PG biofilm; Red: ΔPPAD biofilm). CFU values at the different drug concentrations are annotated. Data are expressed as mean ± SD from three independent biological replicates.

4.3.3 OMVs increase the MIC_{50} of conventional antibiotics but not that of energy metabolism inhibitors

To quantitatively assess the protective impact of OMVs on antibiotic efficacy, we measured MIC_{50} for selected antibiotics against PG with and without OMVs supplementation (**Table 4.1**). The MIC_{50} assay provides a robust metric for evaluating drug potency under standardized in vitro conditions.

For conventional antibiotics, including amoxicillin, metronidazole, and clindamycin, the presence of OMVs resulted in a significant increase in MIC_{50} values, indicating diminished susceptibility. Amoxicillin exhibited an eightfold increase (from 32 to 256 μM), metronidazole showed a shift from 64 to >256 μM, and clindamycin likewise surpassed the measurable range (>256 μM). These data reflect a consistent trend of OMV-mediated attenuation of antibiotic potency.

In sharp contrast, the MIC_{50} values for nitazoxanide and its metabolite tizoxanide remained unchanged at 32 μM, regardless of OMVs presence. This suggests that these agents bypass OMVs-related defense mechanisms, possibly by targeting conserved intracellular processes essential for energy metabolism, such as the pyruvate: ferredoxin oxidoreductase system or components of the proton motive force (Buckel et al., 2021).

These observations further substantiate our findings from survival assays (**Figures 4.2 and 4.3**), reinforcing that conventional antibiotics are compromised by OMVs shielding, while bioenergetic inhibitors remain effective. The MIC_{50} stability in the face of OMVs highlights the therapeutic potential of targeting core metabolic pathways to overcome biofilm-associated resistance.

Table 4.1. MIC_{50} values of antibiotics against PG with and without OMVs (n = 3)

Antibiotic	**PG**	**PG w/ OMVs**	**MIC_{50} trend**
Amoxicillin	32 μM	256 μM	MIC_{50} rise
Metronidazole	64 μM	>256 μM	MIC_{50} rise
Clidamycin	256 μM	>256 μM	MIC_{50} rise
Nitazoxanide	32 μM	32 μM	Stay sensitive
Tizoxanide	32 μM	32 μM	Stay sensitive

4.3.4 Cl-amidine inhibits Peptidylarginine deiminase (PPAD) activity and sensitizes OMVs-associated PG Biofilm

To validate the functional contribution of PPAD to OMVs-mediated antibiotic tolerance, we examined the effect of pharmacological inhibition using Cl-amidine, an irreversible pan-PAD inhibitor known to modify active site cysteines in PPAD homologs covalently (Mondal et al., 2019).

Colony formation assays revealed a marked decrease in bacterial viability in PG biofilms treated with 100 μM Cl-amidine in the presence of OMVs. Representative images (**Figure 4.4.A**) show a reduction in visible colonies from 38 CFUs in the untreated PG + OMVs group to 26 CFUs following Cl-amidine treatment.

Quantitative CFUs enumeration corroborated these results. As shown in Figure 4B, PG cultures supplemented with OMVs and treated with Cl-amidine exhibited significantly lower survival, with a nearly 10-fold reduction in CFUs/mL compared to untreated controls ($p < 0.001$) (**Figure 4.4.B**). The statistical significance and consistent directional change across replicates affirm the role of PPAD in promoting biofilm resilience.

These findings suggest that PPAD is not only implicated in immune modulation and protein citrullination (Wang eet al., 2013; Stobernack et al., 2018) but also plays a direct role in maintaining bacterial survival under stress conditions (Aliko et al., 2018), likely through stabilization of OMVs-associated structures or modulation of extracellular matrix proteins. As such, PPAD inhibition represents a viable adjunctive strategy to sensitize PG biofilms to conventional and metabolism-targeted antibiotics.

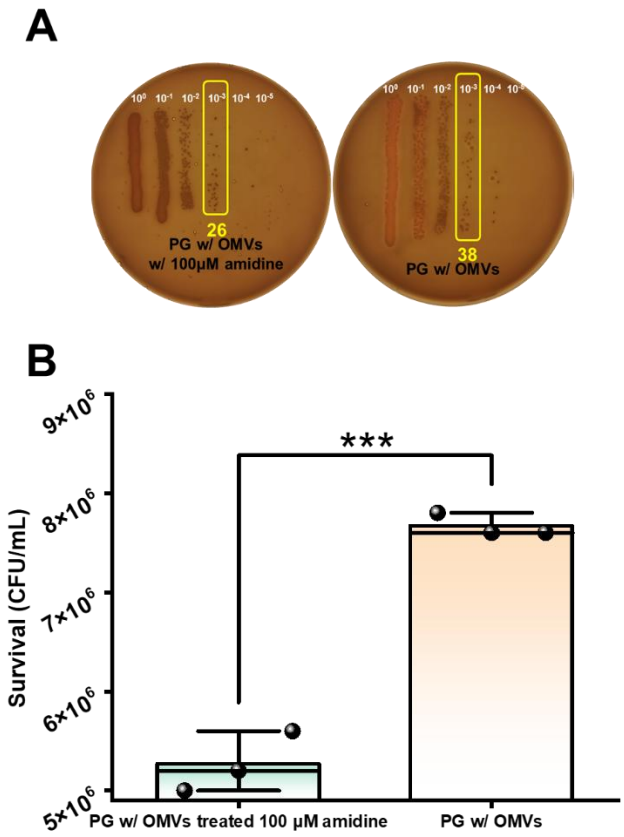

Figure 4.4. Inhibition of PPAD by Cl-amidine reduces PG biofilm viability in OMVs-enriched environments. (A) Representative colony counting plates showing reduced CFU formation in PG biofilms treated with Cl-amidine (100 μM) compared to OMV-only controls. Yellow boxes indicate 10^{-3} dilution levels. (B) Quantitative CFU analysis shows a statistically significant reduction in survival in Cl-amidine-treated. Data in panel B is presented as means ± s.d. (n = 3). ***, $p < 0.001$.

4.3 Discussion

The persistence of PG biofilm communities represents a major clinical challenge, particularly due to its inherent resistance to conventional antibiotics and its association with systemic inflammatory conditions such as cardiovascular disease, rheumatoid arthritis, and Alzheimer's pathology (Liao et al., 2009; Dominy et al., 2019; Olsen et al., 2019). The present study elucidates several interlinked mechanisms by which PG enhances its antibiotic tolerance within biofilms, chiefly through the structural and enzymatic functions of OMVs and the virulence enzyme PPAD. Additionally, we demonstrate that targeting bacterial energy metabolism remains a viable strategy for circumventing such biofilm-mediated defenses.

Our findings clearly show that OMVs enhance the survival of PG biofilms when challenged with antibiotics of diverse functional classes, including amoxicillin, metronidazole, and clindamycin. These antibiotics, which target bacterial cell wall synthesis, DNA replication, and protein translation, respectively, were significantly less effective in OMVs-rich environments (**Figure 4.2**). Such protection likely stems from a combination of OMVs-mediated drug sequestration, limited penetration, and enzymatic modification within the extracellular matrix, consistent with previously described mechanisms in gram-negative pathogens (Manning et al., 2011; Kulkarni et al., 2015; Toyofuku et al., 2019).

In contrast to conventional agents, nitazoxanide and tizoxanide retained their antimicrobial efficacy regardless of OMVs' presence or PPAD expression (**Figure 4.3**). This highlights the strategic advantage of targeting metabolic pathways rather than biosynthetic or structural processes. Nitazoxanide is known to collapse proton motive force (PMF), inhibit pyruvate: ferredoxin oxidoreductase, and suppress ATP production under anaerobic conditions (Shakya et al., 2018). Such disruptions impair the energetic viability of biofilm-embedded bacteria, including metabolically quiescent subpopulations often protected from traditional drugs (Bald et al., 2017; Hards et al.,

2018). Our MIC_{50} data further confirmed that OMVs-associated resistance mechanisms did not alter the potency of these agents (**Table 4.1**), supporting their translational potential in recalcitrant infections.

OMVs have been increasingly recognized as extracellular carriers of redox-active components, including multiheme cytochromes and small molecule cofactors such as FMN, which facilitate long-distance electron transfer between bacteria. Our results demonstrate that the collapse of the proton motive force (PMF), a key driver of cellular energy metabolism, attenuates the electron transfer function of OMVs without substantially affecting their release. This functional loss appears to result from impaired synthesis or export of redox-active proteins and cofactors, both of which rely on intact PMF for optimal expression and transport across the membrane. In particular, new studies have shown that electron flux through the respiratory chain and the generation of flavin molecules are tightly linked to the energy state of the cell. Thus, uncoupling PMF not only inhibits intracellular respiration but also limits the assembly of electron-conducting machinery within OMVs. Given that OMVs may serve as intercellular conduits for electron transfer in anaerobic or biofilm environments, our findings suggest that PMF-targeting antibiotics such as nitazoxanide may hold potential for selectively disrupting microbial electron exchange networks, thereby reducing biofilm resilience or metabolic cooperation in multispecies communities.

Beyond structural contributions, we identified PPAD as a critical effector of OMVs-mediated resistance. Pharmacological inhibition via Cl-amidine significantly impaired bacterial survival in OMVs-rich conditions (**Figure 4.4**). These results suggest that PPAD supports biofilm fitness through mechanisms that may include citrullination of matrix proteins, modulation of host immune evasion pathways, or stabilization of OMVs integrity (Goulas et al., 2015; Aliko et al., 2018; Vermilyea et al., 2021). Cl-amidine's inhibition of PPAD enzymes has been explored in inflammatory and autoimmune contexts (Yang et al., 2021), but this study extends its potential to microbial applications. The observed reduction in CFUs after Cl-amidine treatment

highlights a promising strategy for weakening OMVs-based defenses and restoring antibiotic efficacy.

Collectively, these findings advance our understanding of the multifaceted resistance mechanisms in PG biofilms and propose two novel therapeutic targets: (1) bioenergetic disruption and (2) enzymatic neutralization of OMVs-resident virulence factors such as PPAD. The combination of metabolic inhibitors with PPAD-targeting agents may yield synergistic outcomes and warrants further investigation in vivo models and polymicrobial settings. Additionally, this study emphasizes the importance of moving beyond traditional drug classes toward therapies that address bacterial physiology and biofilm-specific adaptations. Future work should explore the spatial distribution of OMVs within biofilms using advanced imaging techniques such as cryo-electron tomography and assess PPAD's contribution to extracellular matrix remodeling. Multi-omics approaches, including transcriptomics and proteomics under energy-deprived conditions, may also elucidate compensatory pathways activated upon PPAD inhibition. Moreover, investigations into host-pathogen crosstalk in the presence of Cl-amidine will be crucial for assessing immunological side effects and therapeutic viability.

4.4 References

Ahmad, M., Aduru, S. V., Smith, R. P., Zhao, Z., & Lopatkin, A. J. (2025). The role of bacterial metabolism in antimicrobial resistance. *Nature Reviews Microbiology*, 1-16.

Aliko, A., Kamińska, M., Bergum, B., Gawron, K., Benedyk, M., Lamont, R. J., Malicki, S., Delaleu, N., Potempa, J., & Mydel, P. (2018). Impact of *Porphyromonas gingivalis* peptidylarginine deiminase on bacterial biofilm formation, epithelial cell invasion, and epithelial cell transcriptional landscape. *Scientific Reports*, *8*(1), 14144.

Azeem, K., Fatima, S., Ali, A., Ubaid, A., Husain, F. M., & Abid, M. (2025). Biochemistry of Bacterial Biofilm: Insights into Antibiotic Resistance Mechanisms and Therapeutic Intervention. *Life*, *15*(1), 49.

Bald, D., Villellas, C., Lu, P., & Koul, A. (2017). Targeting energy metabolism in Mycobacterium tuberculosis, a new paradigm in antimycobacterial drug discovery. *MBio*, *8*(2), 10.1128/mbio. 00272-00217.

Benz, C., Kassa, E., Tjärnhage, E., Lind, S. B., & Ivarsson, Y. (2020). Identification of Cellular Protein–Protein Interactions. In A. Tavassoli (Ed.), *Inhibitors of Protein–Protein Interactions* (pp. 0). The Royal Society of Chemistry.

Buckel, W. (2021). Energy conservation in fermentations of anaerobic bacteria. *Frontiers in Microbiology*, *12*, 703525.

Caruana, J. C., & Walper, S. A. (2020). Bacterial membrane vesicles as mediators of microbe-microbe and microbe–host community interactions. *Frontiers in Microbiology*, *11*, 432.

Ciemniecki, J. A., Ho, C.-L., Horak, R. D., Okamoto, A., & Newman, D. K. (2024). Mechanistic study of a low-power bacterial maintenance state using high-throughput electrochemistry. *Cell*, *187*(24), 6882-6895. e6888.

Costerton, J. W., Stewart, P. S., & Greenberg, E. P. (1999). Bacterial biofilms: a common cause of persistent infections. *Science*, *284*(5418), 1318-1322.

Dingsdag, S. A., & Hunter, N. (2018). Metronidazole: an update on metabolism, structure-cytotoxicity and resistance mechanisms. *Journal of Antimicrobial Chemotherapy*, *73*(2), 265-279.

Dominy, S. S., Lynch, C., Ermini, F., Benedyk, M., Marczyk, A., Konradi, A., Nguyen, M., Haditsch, U., Raha, D., & Griffin, C. (2019). *Porphyromonas gingivalis* in Alzheimer's disease brains: Evidence for disease causation and treatment with small-molecule inhibitors. *Science Advances*, *5*(1), eaau3333.

Dubreuil, L., Houcke, I., Mouton, Y., & Rossignol, J.-F. (1996). In vitro evaluation of activities of nitazoxanide and tizoxanide against anaerobes and aerobic organisms. *Antimicrobial Agents and Chemotherapy*, *40*(10), 2266-2270.

Farha, M. A., Verschoor, C. P., Bowdish, D., & Brown, E. D. (2013). Collapsing the proton motive force to identify synergistic combinations against *Staphylococcus aureus*. *Chemistry & biology*, *20*(9), 1168-1178.

Flemming, H.-C., & Wingender, J. (2010). The biofilm matrix. *Nature Reviews Microbiology*, *8*(9), 623-633.

Gabarrini, G. (2018). *Porphyromonas gingivalis*, the beast with two heads: A bacterial role in the etiology of rheumatoid arthritis.

Gabarrini, G., Palma Medina, L. M., Stobernack, T., Prins, R. C., du Teil Espina, M., Kuipers, J., Chlebowicz, M. A., Rossen, J. W., van Winkelhoff, A. J., & van Dijl, J. M. (2018). There's no place like OM: Vesicular sorting and secretion of the peptidylarginine deiminase of *Porphyromonas gingivalis*. *Virulence*, *9*(1), 459-467.

Gordon, J., Walker, C., Hovliaras, C., & Socransky, S. (1990). Efficacy of clindamycin hydrochloride in refractory periodontitis: 24-month results. *Journal of periodontology*, *61*(11), 686-691.

Goulas, T., Mizgalska, D., Garcia-Ferrer, I., Kantyka, T., Guevara, T., Szmigielski, B., Sroka, A., Millán, C., Usón, I., & Veillard, F. (2015). Structure and mechanism of a bacterial host-protein citrullinating virulence factor, *Porphyromonas*

gingivalis peptidylarginine deiminase. *Scientific Reports*, *5*(1), 11969.

Hall-Stoodley, L., Costerton, J. W., & Stoodley, P. (2004). Bacterial biofilms: from the natural environment to infectious diseases. *Nature Reviews Microbiology*, *2*(2), 95-108.

Hards, K., & Cook, G. M. (2018). Targeting bacterial energetics to produce new antimicrobials. *Drug Resistance Updates*, *36*, 1-12.

Hoffman, P. S., Sisson, G., Croxen, M. A., Welch, K., Harman, W. D., Cremades, N., & Morash, M. G. (2007). Antiparasitic drug nitazoxanide inhibits the pyruvate oxidoreductases of *Helicobacter pylori*, selected anaerobic bacteria and parasites, and Campylobacter jejuni. *Antimicrobial Agents and Chemotherapy*, *51*(3), 868-876.

Jeong, G.-J., Khan, F., Tabassum, N., Cho, K.-J., & Kim, Y.-M. (2024). Bacterial extracellular vesicles: modulation of biofilm formation and virulence. *Acta Biomaterialia*.

Kanagasingam, S., Chukkapalli, S. S., Welbury, R., & Singhrao, S. K. (2020). *Porphyromonas gingivalis* is a strong risk factor for Alzheimer's disease. *Journal of Alzheimer's disease reports*, *4*(1), 501-511.

Karkowska-Kuleta, J., Bartnicka, D., Zawrotniak, M., Zielinska, G., Kierońska, A., Bochenska, O., Ciaston, I., Koziel, J., Potempa, J., & Baster, Z. (2018). The activity of bacterial peptidylarginine deiminase is important during formation of dual-species biofilm by periodontal pathogen *Porphyromonas gingivalis* and opportunistic fungus *Candida albicans*. *Pathogens and disease*, *76*(4), fty033.

Karkowska-Kuleta, J., Surowiec, M., Gogol, M., Koziel, J., Potempa, B., Potempa, J., Kozik, A., & Rapala-Kozik, M. (2020). Peptidylarginine deiminase of *Porphyromonas gingivalis* modulates the interactions between *Candida albicans* biofilm and human plasminogen and high-molecular-mass kininogen. *International Journal of Molecular Sciences*, *21*(7), 2495.

Kassim, A., Omuse, G., Premji, Z., & Revathi, G. (2016). Comparison of Clinical

Laboratory Standards Institute and European Committee on Antimicrobial Susceptibility Testing guidelines for the interpretation of antibiotic susceptibility at a University teaching hospital in Nairobi, Kenya: a cross-sectional study. *Annals of clinical microbiology and antimicrobials*, *15*, 1-7.

Kaur, S. P., Rao, R., & Nanda, S. (2011). Amoxicillin: a broad spectrum antibiotic. *Int J Pharm Pharm Sci*, *3*(3), 30-37.

Koo, H., Allan, R. N., Howlin, R. P., Stoodley, P., & Hall-Stoodley, L. (2017). Targeting microbial biofilms: current and prospective therapeutic strategies. *Nature Reviews Microbiology*, *15*(12), 740-755.

Kosgodage, U. S., Matewele, P., Mastroianni, G., Kraev, I., Brotherton, D., Awamaria, B., Nicholas, A. P., Lange, S., & Inal, J. M. (2019). Peptidylarginine deiminase inhibitors reduce bacterial membrane vesicle release and sensitize bacteria to antibiotic treatment. *Frontiers in cellular and infection microbiology*, *9*, 227.

Koziel, J., Mydel, P., & Potempa, J. (2014). The link between periodontal disease and rheumatoid arthritis: an updated review. *Current rheumatology reports*, *16*, 1-7.

Kulkarni, H. M., Nagaraj, R., & Jagannadham, M. V. (2015). Protective role of *E. coli* outer membrane vesicles against antibiotics. *Microbiological research*, *181*, 1-7.

Lebeaux, D., Ghigo, J.-M., & Beloin, C. (2014). Biofilm-related infections: bridging the gap between clinical management and fundamental aspects of recalcitrance toward antibiotics. *Microbiology and Molecular Biology Reviews*, *78*(3), 510-543.

Liao, F., Li, Z., Wang, Y., Shi, B., Gong, Z., & Cheng, X. (2009). *Porphyromonas gingivalis* may play an important role in the pathogenesis of periodontitis-associated rheumatoid arthritis. *Medical hypotheses*, *72*(6), 732-735.

Ma, L., & Cao, Z. (2021). Membrane vesicles from periodontal pathogens and their potential roles in periodontal disease and systemic illnesses. *Journal of periodontal research*, *56*(4), 646-655.

Mahdizade Ari, M., Scholz, K. J., Cieplik, F., & Al-Ahmad, A. (2025). Viable but non-

cultivable state in oral microbiota: a critical review of an underexplored microbial survival strategy. *Frontiers in cellular and infection microbiology*, *15*, 1533768.

Manning, A. J., & Kuehn, M. J. (2011). Contribution of bacterial outer membrane vesicles to innate bacterial defense. *BMC microbiology*, *11*, 1-15.

Mei, F., Xie, M., Huang, X., Long, Y., Lu, X., Wang, X., & Chen, L. (2020). *Porphyromonas gingivalis* and its systemic impact: current status. *Pathogens*, *9*(11), 944.

Mondal, S., & Thompson, P. R. (2019). Protein arginine deiminases (PADs): biochemistry and chemical biology of protein citrullination. *Accounts of chemical research*, *52*(3), 818-832.

Murima, P., McKinney, J. D., & Pethe, K. (2014). Targeting bacterial central metabolism for drug development. *Chemistry & biology*, *21*(11), 1423-1432.

Naradasu, D., Miran, W., Sharma, S., Takenawa, S., Soma, T., Nomura, N., Toyofuku, M., & Okamoto, A. (2021). Biogenesis of outer membrane vesicles concentrates the unsaturated fatty acid of phosphatidylinositol in *Capnocytophaga ochracea*. *Frontiers in Microbiology*, *12*, 682685.

Olsen, I., & Yilmaz, Ö. (2019). Possible role of *Porphyromonas gingivalis* in orodigestive cancers. *Journal of oral microbiology*, *11*(1), 1563410.

Pankuch, G. A., & Appelbaum, P. C. (2006). Activities of tizoxanide and nitazoxanide compared to those of five other thiazolides and three other agents against anaerobic species. *Antimicrobial Agents and Chemotherapy*, *50*(3), 1112-1117.

Ragsdale, S. W. (2003). Pyruvate ferredoxin oxidoreductase and its radical intermediate. *Chemical Reviews*, *103*(6), 2333-2346.

Rajasekaran, J. J., Krishnamurthy, H. K., Bosco, J., Jayaraman, V., Krishna, K., Wang, T., & Bei, K. (2024). Oral microbiome: a review of its impact on oral and systemic health. *Microorganisms*, *12*(9), 1797.

Rossignol, J.-F. (2014). Nitazoxanide: a first-in-class broad-spectrum antiviral agent.

Antiviral research, *110*, 94-103.

Sadiq, F. A., Flint, S., Li, Y., Ou, K., Yuan, L., & He, G. Q. (2017). Phenotypic and genetic heterogeneity within biofilms with particular emphasis on persistence and antimicrobial tolerance. *Future Microbiology*, *12*(12), 1087-1107.

Sahli, C., Moya, S. E., Lomas, J. S., Gravier-Pelletier, C., Briandet, R., & Hémadi, M. (2022). Recent advances in nanotechnology for eradicating bacterial biofilm. *Theranostics*, *12*(5), 2383.

Shakya, A., Bhat, H. R., & Ghosh, S. K. (2018). Update on nitazoxanide: a multifunctional chemotherapeutic agent. *Current drug discovery technologies*, *15*(3), 201-213.

Sharaf, S., & Hijazi, K. (2022). Modulatory mechanisms of pathogenicity in *porphyromonas gingivalis* and other periodontal pathobionts. *Microorganisms*, *11*(1), 15.

Shree, P., Singh, C. K., Sodhi, K. K., Surya, J. N., & Singh, D. K. (2023). Biofilms: Understanding the structure and contribution towards bacterial resistance in antibiotics. *Medicine in Microecology*, *16*, 100084.

Simoes, M. (2011). Antimicrobial strategies effective against infectious bacterial biofilms. *Current medicinal chemistry*, *18*(14), 2129-2145.

Singh, S., Datta, S., Narayanan, K. B., & Rajnish, K. N. (2021). Bacterial exo-polysaccharides in biofilms: role in antimicrobial resistance and treatments. *Journal of Genetic Engineering and Biotechnology*, *19*, 1-19.

Stobernack, T., du Teil Espina, M., Mulder, L. M., Palma Medina, L. M., Piebenga, D. R., Gabarrini, G., Zhao, X., Janssen, K. M., Hulzebos, J., & Brouwer, E. (2018). A secreted bacterial peptidylarginine deiminase can neutralize human innate immune defenses. *MBio*, *9*(5), 10.1128/mbio. 01704-01718.

Toyofuku, M., Nomura, N., & Eberl, L. (2019). Types and origins of bacterial membrane vesicles. *Nature Reviews Microbiology*, *17*(1), 13-24.

Veith, P. D., Chen, Y.-Y., Gorasia, D. G., Chen, D., Glew, M. D., O'Brien-Simpson, N.

M., Cecil, J. D., Holden, J. A., & Reynolds, E. C. (2014). *Porphyromonas gingivalis* outer membrane vesicles exclusively contain outer membrane and periplasmic proteins and carry a cargo enriched with virulence factors. *Journal of Proteome Research*, *13*(5), 2420-2432.

Vermilyea, D. M., Moradali, M. F., Kim, H.-M., & Davey, M. E. (2021). PPAD activity promotes outer membrane vesicle biogenesis and surface translocation by *Porphyromonas gingivalis*. *Journal of bacteriology*, *203*(4), 10.1128/jb. 00343-00320.

Vermilyea, D. M., Ottenberg, G. K., & Davey, M. E. (2019). Citrullination mediated by PPAD constrains biofilm formation in *P. gingivalis* strain 381. *NPJ biofilms and microbiomes*, *5*(1), 7.

Wang, S., & Wang, Y. (2013). Peptidylarginine deiminases in citrullination, gene regulation, health and pathogenesis. *Biochimica et Biophysica Acta (BBA)-Gene Regulatory Mechanisms*, *1829*(10), 1126-1135.

Wu, Z., Long, W., Yin, Y., Tan, B., Liu, C., Li, H., & Ge, S. (2025). Outer membrane vesicles of *Porphyromonas gingivalis*: recent advances in pathogenicity and associated mechanisms. *Frontiers in Microbiology*, *16*, 1555868.

Xiu, L., Wu, Y., Lin, G., Zhang, Y., & Huang, L. (2024). Bacterial membrane vesicles: orchestrators of interkingdom interactions in microbial communities for environmental adaptation and pathogenic dynamics. *Frontiers in Immunology*, *15*, 1371317.

Yamamoto, Y., Hakki, A., Friedman, H., Okubo, S., Shimamura, T., Hoffman, P. S., & Rossignol, J.-F. (1999). Nitazoxanide, a nitrothiazolide antiparasitic drug, is an anti-Helicobacter pylori agent with anti-vacuolating toxin activity. *Chemotherapy*, *45*(4), 303-312.

Yang, C., Dong, Z.-Z., Zhang, J., Teng, D., Luo, X., Li, D., & Zhou, Y. (2021). Peptidylarginine deiminases 4 as a promising target in drug discovery. *European journal of medicinal chemistry*, *226*, 113840.

Zhang, K., Li, X., Yu, C., & Wang, Y. (2020). Promising therapeutic strategies against microbial biofilm challenges. *Frontiers in cellular and infection microbiology*, *10*, 359.

Zhang, Z., Liu, D., Liu, S., Zhang, S., & Pan, Y. (2021). The role of *Porphyromonas gingivalis* outer membrane vesicles in periodontal disease and related systemic diseases. *Frontiers in cellular and infection microbiology*, *10*, 585917.

Chapter 5: Conclusion and prospects

5.1 General summary and key findings

This dissertation systematically investigated the molecular, biophysical, and electrochemical mechanisms that underpin biofilm-associated electron transfer in both the electroactive model bacterium *Shewanella oneidensis* MR-1 (*S.* MR-1) and the pathogenic anaerobe *Porphyromonas gingivalis* (PG). The interdisciplinary approach, combining high-resolution electrochemical techniques, spectroscopic analysis, and genetic manipulation, has yielded novel insights into long-distance electron transfer (LDET) within microbial communities. These findings contribute substantially to our understanding of microbial respiration, microbial electrogenicity and biofilm resilience in both natural and clinical settings.

In **Chapter 2**, we demonstrated that the lateral electron flow within the stratified biofilms of *S.* MR-1 is limited by inter-cytochrome electron transfer between outer membrane cytochromes (OMCs), particularly MtrC and OmcA. Using a temperature-variable interdigitated electrode (IDE) array, we calculated E_a associated with various mutant strains and conditions, revealing that the disruption of OMCs mobility, either through genetic deletion or cholesterol-mediated membrane rigidification, substantially impedes electron flow. Our results not only corroborate previous computational models suggesting that redox center proximity and protein diffusion are vital for efficient LDET (Xu et al., 2018) but also provide direct experimental evidence for the kinetic role of protein-protein interactions in cytochrome networks. Moreover, we found that the binding of flavin cofactors (e.g., flavin mononucleotide (FMN) and riboflavin), non-covalent to specific heme centers (notably hemes 2 and 7), selectively enhanced conduction, with a notable decrease in E_a. Circular dichroism spectroscopy further confirmed that flavin binding did not disturb heme alignment, implying that electron relay through cofactors is functionally superior in energetics without structurally compromising OMCs.

In **Chapter 3**, we translated these principles into a pathogenic context by analyzing

conductive behavior in PG biofilms. Our data revealed that OMVs function as electrical mediators by forming conductive pathways that integrate redox-active enzymes, primarily PPAD. OMVs-enriched biofilms displayed significantly enhanced electron conduction and lower E_a values compared to OMV-depleted or cholesterol-rigidified counterparts. Through a combination of SDS-PAGE of TMBZ staining and LC-MS, we confirmed the presence of redox-active PPAD in OMVs. Interestingly, while this enzyme has been primarily studied for its immunomodulatory and citrullination functions, our study revealed its FMN-dependent redox activity, implicating it in electron transfer across the biofilm. The specific enhancement of I_{cond} by FMN, and its abrogation in Δ*PPAD* strains or upon Cl-amidine treatment, underscores the cofactor-dependent bio-electrochemical function of PPAD.

In **Chapter 4**, we investigated the implications of redox-enabled biofilms for antimicrobial resistance. PG biofilms enriched with OMVs demonstrated substantial resistance to diverse antibiotics, including amoxicillin, metronidazole and clindamycin. However, bioenergetic inhibitors such as nitazoxanide and its active metabolite tizoxanide effectively disrupted biofilm viability across all conditions, regardless of OMVs and PPAD presence. These results reveal that while redox-based resilience may shield biofilms from traditional antibiotics, targeting fundamental metabolic functions, such as anaerobic ATP generation, can bypass OMVs-mediated tolerance. These findings align with current trends in antimicrobial development that emphasize metabolic and respiratory disruption over classical cell wall targeting (Caño-Muñiz et al., 2018; Virolle et al., 2020).

5.2 Future prospects

First, high-resolution structural elucidation using advanced tools such as cryo-electron microscopy or solid-state NMR is essential to visualize OMC-flavin complexes and PPAD-FMN interactions within OMVs. These approaches will refine our atomic-level understanding of electron tunneling and cofactor positioning (Nagel & Klinman, 2006; Moser et al., 2010; Winkler & Gray, 2014). Second, synthetic biology and engineering applications offer exciting possibilities; artificial biofilm systems or engineered OMVs with tunable redox activity could be developed for use in microbial fuel cells, biosensors, or the targeted disruption of pathogenic biofilms (Yu et al., 2023; Fang et al., 2024). These systems can be rationally designed based on the redox scaffolds validated in this study. Third, pharmacological targeting of redox proteins represents a viable strategy(Hards & Cook, 2018); future efforts should focus on identifying inhibitors that bind to redox-active sites on PPAD or OMCs. Combining high-throughput screening with structure-guided design may yield adjuvants that impair electron transfer and sensitize biofilms to antibiotics (Ciemniecki et al., 2024; Tokunou et al., 2025). Fourth, host–biofilm interaction studies are crucial, particularly the immunomodulatory effects of PPAD-containing OMVs (Gabarrini et al., 2018; Stobernack et al., 2018). Understanding how redox states influence host inflammation, T-cell activation, and chronic systemic diseases could bridge immunology and bioelectrochemistry to inform holistic therapeutic strategies (Kesarwani et al., 2013; Schieber & Chandel, 2014; Forrester et al., 2018; Weyand et al., 2018). Finally, integrating multi-omics platforms, including transcriptomics, proteomics, and metabolomics, with dynamic electrochemical readouts will facilitate the development of system-level models capturing energy flow, redox balance, and resistance phenotypes within biofilms (Van et al., 2010; Zhou et al., 2011).

5.3 Final remarks

In summary, this dissertation provides a detailed, multi-scale dissection of extracellular electron transfer processes within microbial biofilms, bridging fundamental microbiology with applied biomedical and energy research. By establishing that redox protein dynamics and cofactor interactions are central to LDET, by uncovering their implications for pathogenicity and drug resistance, we pave the way for new paradigms in microbial biotechnology and infection control. The findings not only enrich our mechanistic understanding of microbial respiration and biofilm resilience but also offer translational insights for developing anti-biofilm therapeutics and bioelectronic innovations.

5.4 References

Caño-Muñiz, S., Anthony, R., Niemann, S., & Alffenaar, J.-W. C. (2018). New approaches and therapeutic options for *Mycobacterium tuberculosis* in a dormant state. Clinical microbiology reviews, 31(1), 10.1128/cmr. 00060-00017.

Ciemniecki, J. A., Ho, C.-L., Horak, R. D., Okamoto, A., & Newman, D. K. (2024). Mechanistic study of a low-power bacterial maintenance state using high-throughput electrochemistry. *Cell*, *187*(24), 6882-6895. e6888.

Fang, Y., Yang, G., Wu, X., Lin, C., Qin, B., & Zhuang, L. (2024). A genetic engineering strategy to enhance outer membrane vesicle-mediated extracellular electron transfer of *Geobacter sulfurreducens*. *Biosensors and Bioelectronics*, *250*, 116068.

Forrester, S. J., Kikuchi, D. S., Hernandes, M. S., Xu, Q., & Griendling, K. K. (2018). Reactive oxygen species in metabolic and inflammatory signaling. *Circulation research*, *122*(6), 877-902.

Gabarrini, G., Palma Medina, L. M., Stobernack, T., Prins, R. C., du Teil Espina, M., Kuipers, J., Chlebowicz, M. A., Rossen, J. W., van Winkelhoff, A. J., & van Dijl, J. M. (2018). There's no place like OM: Vesicular sorting and secretion of the peptidylarginine deiminase of *Porphyromonas gingivalis*. *Virulence*, *9*(1), 459-467.

Hards, K., & Cook, G. M. (2018). Targeting bacterial energetics to produce new antimicrobials. *Drug Resistance Updates*, *36*, 1-12.

Kesarwani, P., Murali, A. K., Al-Khami, A. A., & Mehrotra, S. (2013). Redox regulation of T-cell function: from molecular mechanisms to significance in human health and disease. *Antioxidants & redox signaling*, *18*(12), 1497-1534.

Moser, C. C., Anderson, J. R., & Dutton, P. L. (2010). Guidelines for tunneling in enzymes. *Biochimica et Biophysica Acta (BBA)-Bioenergetics*, *1797*(9), 1573-1586.

Nagel, Z. D., & Klinman, J. P. (2006). Tunneling and dynamics in enzymatic hydride transfer. *Chemical Reviews*, *106*(8), 3095-3118.

Schieber, M., & Chandel, N. S. (2014). ROS function in redox signaling and oxidative stress. *Current biology*, *24*(10), R453-R462.

Stobernack, T., du Teil Espina, M., Mulder, L. M., Palma Medina, L. M., Piebenga, D. R., Gabarrini, G., Zhao, X., Janssen, K. M., Hulzebos, J., & Brouwer, E. (2018). A secreted bacterial peptidylarginine deiminase can neutralize human innate immune defenses. *MBio*, *9*(5), 10.1128/mbio. 01704-01718.

Tokunou, Y., Yamazaki, T., Fujikawa, T., & Okamoto, A. (2025). Decoding in-cell respiratory enzyme dynamics by label-free in situ electrochemistry. *Proceedings of the National Academy of Sciences*, *122*(12), e2418926122.

Van Der Meer, J. R., & Belkin, S. (2010). Where microbiology meets microengineering: design and applications of reporter bacteria. *Nature Reviews Microbiology*, *8*(7), 511-522.

Virolle, M.-J. (2020). A challenging view: antibiotics play a role in the regulation of the energetic metabolism of the producing bacteria. Antibiotics, 9(2), 83.

Weyand, C. M., Shen, Y., & Goronzy, J. J. (2018). Redox-sensitive signaling in inflammatory T cells and in autoimmune disease. *Free Radical Biology and Medicine*, *125*, 36-43.

Winkler, J. R., & Gray, H. B. (2014). Long-range electron tunneling. *Journal of the American Chemical Society*, *136*(8), 2930-2939.

Xu, S., Barrozo, A., Tender, L. M., Krylov, A. I., & El-Naggar, M. Y. (2018). Multiheme cytochrome mediated redox conduction through *Shewanella oneidensis* MR-1 cells. *Journal of the American Chemical Society*, *140*(32), 10085-10089.

Yu, H., Lu, Y., Lan, F., Wang, Y., Hu, C., Mao, L., Wu, D., Li, F., & Song, H. (2023). Engineering Outer Membrane Vesicles to Increase Extracellular Electron Transfer of *Shewanella oneidensis*. *ACS Synthetic Biology*, *12*(6), 1645-1656.

Zhou, M., & Dong, S. (2011). Bioelectrochemical interface engineering: toward the

fabrication of electrochemical biosensors, biofuel cells, and self-powered logic biosensors. *Accounts of chemical research*, *44*(11), 1232-1243.

List of publications

This thesis is based on the following publications.

1. Scientific papers

1. **Wen, X.X.**, Long, X.Z., Huang, W.Y and Okamoto, A., *2025.* Cell-surface Inter-Cytochrome Electron Transfer Limits Biofilm Electron Conduction Kinetics in *Shewanella oneidensis* MR-1. J. Am. Chem. Soc.

2. **Wen, X.X.**, Takanawa, S., Okamoto, A., *2025.* Outer membrane vesicle facilitates biofilm development by enhancing electron conduction in *Porphyromonas gingivalis* biofilm. **(Manuscript completed)**

3. Sotaro Takano, Satoshi Takenawa, Naradasu Divya, Kangmin Yan, **Wen, X.X.**, Tomoko Maehara, Nobuhiko Nomura, Nozomu Obana, Masanori Toyofuku, Michihiko Usui, Wataru Ariyoshi, Akihiro Okamoto, Enrichment of Horizontally Transferred Gene Clusters in Bacterial Extracellular Vesicles via Non-Lytic Mechanisms, *The ISME Journal*, 2025; wraf193.

2. Presentation

Xinxin Wen and Akihiro Okamoto, “Membrane vesicle enhances the electron conduction within PG biofilm”. The Conference of the International Society of Electrochemistry (ISE) in Montreal, Canada (August 13-24, 2024). Oral presentation.

Acknowledgement

At this significant milestone of my doctoral graduation, I would like to express my deepest gratitude to all those who have supported and guided me throughout the past three years of my Ph.D. journey.

First and foremost, I am profoundly thankful to my supervisor, Professor Akihiro Okamoto, for granting me the invaluable opportunity to pursue my doctoral studies in Japan. His patient and insightful mentorship has been instrumental in helping me overcome research challenges, develop scientific writing skills, and cultivate independent thinking. More importantly, his rigorous approach to science, tireless dedication to research, and optimistic outlook in the face of difficulties have profoundly shaped my academic perspective and personal growth. Studying under his guidance has been one of the most rewarding and unforgettable experiences of my life.

I am also sincerely grateful to many colleagues and friends who generously offered their support during my time in the lab. As a newcomer to bio-electrochemical experimentation, I greatly benefited from the expertise and guidance of Ms. Dan Luo, Dr. Wenyuan Huang, Dr. Xizhi Long, and Dr. Satoshi Takenawa, whose advice and encouragement helped me navigate new technical challenges. I am equally thankful for the thoughtful assistance and warm encouragement provided by Ms. Chiharu Yamaguchi, Ms. Sayaka Morita, and our former secretary Ms. Miwa Uematsu, as well as the support I received from Ms. Kangmin Yan, Ms. Xiao Deng, Ms. Chialun Ho and Mr. Sota Ihara, your kindness made a lasting difference. I would also like to acknowledge the contributions and camaraderie of my fellow team members, including Dr. Takashi Fujikawa, Dr. Sotaro Takano, Dr. Mohammed Emran, Dr. Duyen Minh Pham, Dr. Silvia Sato, Dr. Arpit Goyal, Ms. Yuriko Naito, and all the technical staff and colleagues whose efforts and friendship enriched my experience.

To each one of you, I offer my heartfelt thanks. I would not be who I am today without your generous support, and I will always cherish the memories we created together.